# Molecular and Physiological function of the mammalian CCR4-NOT subunit CNOT9

Okinawa Institute of Science and Technology
Graduate University

Thesis submitted for the degree

Doctor of Philosophy

# Molecular and Physiological function of the mammalian CCR4-NOT subunit CNOT9

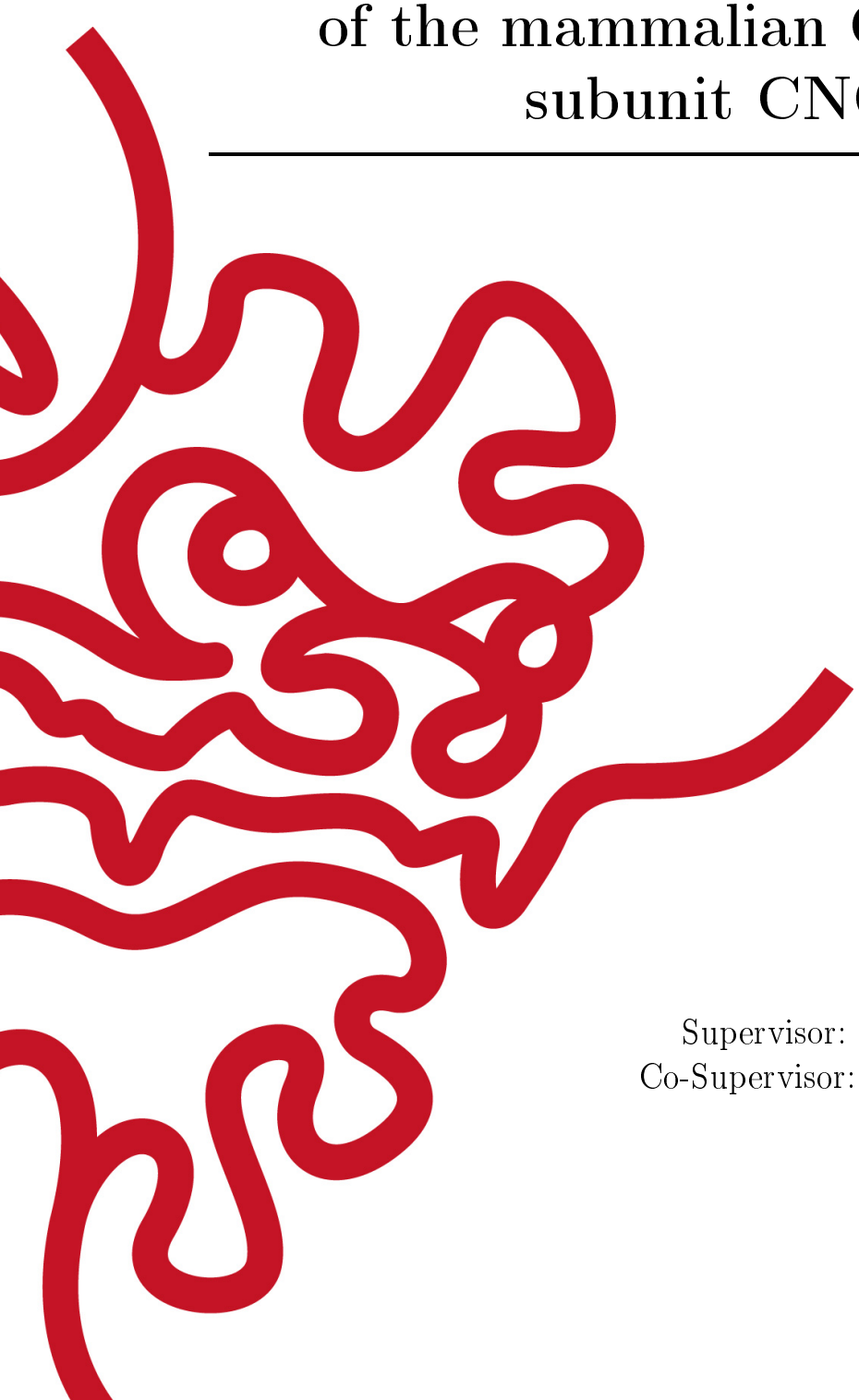

by

**Hemanta Sarmah**

Supervisor: **Prof. Tadashi Yamamoto**
Co-Supervisor: **Prof. Yohei Yokobayashi**

May 2020

# Declaration of Original and Sole Authorship

I, Hemanta Sarmah, declare that this thesis entitled "*Molecular and Physiological function of the mammalian CCR4-NOT subunit CNOT9*", and the data presented in it are original and my own work.

I confirm that:

- This work was done solely while being a candidate for the research degree at the Okinawa Institute of Science and Technology Graduate University, Japan.
- No part of this work has previously been submitted for a degree at this or any other university.
- References to the work of others have been clearly attributed. Quotations from the work of others have been clearly indicated and attributed to them.
- In cases where others have contributed to part of this work, such contribution has been clearly acknowledged and distinguished from my own work.
- None of this work has been previously published elsewhere

Date: May 21, 2020

Signature: 

# Abstract


## Molecular and Physiological function of the mammalian CCR4-NOT subunit CNOT9

Messenger RNA (mRNA) decay is an indisputable component of gene expression regulation. In higher eukaryotes such as humans and mice, this process is mainly governed by a multi-subunit protein assemblage known as the CCR4-NOT complex. The complex is composed of a central scaffold CNOT1, regulatory subunits CNOT2 and CNOT3, a catalytic core consisting of CNOT6, CNOT6L, CNOT7, and CNOT8 proteins, and additional three subunits CNOT9, CNOT10, and CNOT11. In this study, I analyzed the role of subunit CNOT9 in target mRNA decay in the context of mouse embryonic development. CNOT9 knockout mice appear normal during onset of gastrulation, yet exhibit severe growth and differentiation defects during mid-late gastrulation stages (E8.5 to E9.5), accompanied by extensive cell death. Similar nature of phenotype was also observed in epiblast specific CNOT9 deletion mutants, suggesting major contribution of epiblast lineage cells in determining knockout embryo phenotype. At the molecular level, CNOT9 is primarily localized within the cytoplasm and bridges interactions between the CCR4-NOT complex and the miRNA-RISC complex. Transcriptomic analysis identified key determinants of gastrulation such as *Nodal, Lefty1/2, Cfc-1* to be significantly upregulated in CNOT9 KO embryos relative to controls. Among these targets, *Lefty2* mRNA expression was found to be post-transcriptionally regulated by CNOT9. Reporter mRNA containing *Lefty2* 3'-UTR element had higher stability in cells expressing CNOT1-binding-mutant form of CNOT9, compared to cells expressing wild-type CNOT9. Finally, in-vitro experiments with CNOT9 KO embryonic stem (ES) cells further substantiated the importance of gastrulation regulation via CNOT9.

# Acknowledgment

I would like to convey my sincere thanks and appreciation to many people who helped me produce this piece of work.

My PhD advisor, Prof. Tadashi Yamamoto, showed his immense support and encouragement to help me pursue an innovative and challenging project. He also provided me an excellent research environment that promotes independent thinking and collaborative exchange of ideas. Most important of all, his curiosity, persistence, and dedication towards learning has been ever inspiring.

I would like to thank all previous and current lab members for their enthusiastic and kind support during the entire course of my thesis. I am grateful for the guidance and feedback provided by Dr. Ken Matsuura and Dr. Akinori Takahashi on matters directly related to my research project. I would like to convey special thanks to our lab technicians, Ms. Atsuko Sato and Dr. Saori Nishijima, for their assistance and support in experiments involving cell-culture. I also had the privilege to learn from experiences with rotation student Mrs. Swathy Babu on topics not closely connected to my research.

I am grateful to Ms. Yuki Nakagawa and Ms. Kaori Yamashiro for taking care of all administrative responsibilities related to my work. Without your tireless efforts the process would not have been as smooth.

I am also extremely grateful to Dr. Daiki Sasaki and Ms. Mio Miyagi at Immune Signal Unit (OIST), and Dr. Narae Kim at Nucleic Acid Chemistry and Engineering Unit (OIST), for sharing their expertise and technical knowhow on a variety of topics ranging from embryo manipulation and transplantation, to methods involving culture of mouse embryonic stem cells. You were very approachable, and your enthusiasm and support improved my research by leaps and bounds. I would also like to thank Prof. Ichiro Masai and other lab members of Developmental Neurobiology Unit (OIST), for training and insights on histological techniques.

My sincere thanks to Prof. Hiroshi Hamada and Dr. Katsura Minegishi at RIKEN Kobe for providing me an opportunity to perform RNA in-situ hybridization experiments. I also thank Prof. Masahito Ikawa at RIMD, Osaka University for training and guidance in experiments involving lentivirus-based embryo manipulation.

A large section of my experiments would not have been possible without concerted efforts of scientists and staff working for the Animal Resources Section (ARS) as well as Sequencing section (SQC) at OIST. Special thanks to Ms. Tomomi Miyamoto for dedicating her time and efforts towards my training on procedures related to animal handling and surgery.

I thank the OIST Graduate University, and in particular the Graduate School for providing the opportunity and funding for my PhD.

I find it extremely hard to comprehend the past few years without the love and support of many friends within and beyond the OIST community. I would like to thank all members of the OIST Cricket Club, the OIST Football Club, the Indian Cultural Club, and Foodie OISTERs for numerous fun and recreational experiences beyond the workplace. Special thanks to my friend Vivek Pareek for his immense contribution in helping me compile this thesis in LaTeX.

Finally, I would like to thank my parents, siblings and other members of my family for their continued support, encouragement, and understanding. My fiancé, Nishtha, has been extremely supporting and caring. To say the least, without her support, this would not have been possible.

The journey so far has been thoroughly enjoyable and truly memorable!

**Hemanta Sarmah**

# Abbreviations

All abbreviations used in the thesis are be listed here, with their definitions, in alphabetical order. This includes trivial and commonly used abbreviations, but not words that have entered into general English usage (such as laser or DNA). In particular, non-standard abbreviations have also been included.

| | |
|---|---|
| 2-ME | $\beta$-mercaptoethanol |
| AREs | AU-rich elements |
| ARM | armadillo repeat motif |
| ATF2 | Activating Transcription factor 2 |
| ATP | Adenosine Triphosphate |
| BCA | bicinchoninic acid |
| CBB | Coomassie Brilliant Blue |
| CCR4-NOT | Carbon Catabolite Repression 4 Negative on TATA-less |
| cDNA | complementary DNA |
| CDS | coding sequence |
| CIAP | Calf Intestinal Alkaline Phosphatase |
| CNOT9 | CCR4-NOT complex subunit 9 |
| Co-IP | Co-immunoprecipitation |
| CRISPR | clustered regularly interspaced short palindromic repeats |
| DMEM | Dulbecco's Modified Eagle Medium |
| DMSO | Dimethyl sulfoxide |
| dNTP | Deoxynucleotide triphosphates |
| DRE | Differentiation-specific enhancer |
| DTT | Dithiothreitol |
| DUF3819 | Domain of unknown function 3819 |
| *E. coli* | Escherichia coli |
| EBs | embryoid bodies |
| EDTA | Ethylenediaminetetraacetic acid |
| EGFP | Enhanced Green Fluorescent Protein |
| EGTA | Ethylene glycol tetraacetic acid |
| ELISA | enzyme-linked immunosorbent assay |
| EP | Embryo proper |
| EPC | ectoplacental cone |
| EPO | erythropoietin |
| ERK | extracellular signal-regulated kinases |
| Ext-Em | extra embryonic |

| | |
|---|---|
| FBS | Fetal Bovine Serum |
| Fgf | Fibroblast growth factor |
| Fgfr | Fibroblast growth factor receptor |
| FP | Forward primer |
| FPKM | Fragments per kilo base per million mapped reads |
| GAPDH | Glyceraldehyde 3-phosphate dehydrogenase |
| GSEA | Gene set enrichment analysis |
| GSK3$\beta$ | Glycogen synthase kinase 3$\beta$ |
| HCG | human chorionic gonadotropin |
| HE | heterozygous |
| H-E | Hematoxylin-Eosin |
| HEK293T | Human Embryonic kidney 293 (transformed) |
| HeLa | Henrietta Lacks |
| HhR | hammerhead ribozyme sequence |
| HMG | high mobility group |
| HRP | horseradish peroxidase |
| ICM | inner cell mass |
| IgG | Immunoglobulin G |
| IL2 | Interleukin2 |
| kDA | kilo Daltons |
| KO | knockout |
| KSR | KnockOut Serum Replacement |
| lacZ | $\beta$-galactosidase |
| LDS | Lithium dodecyl sulfate |
| LIF | leukemia inhibitory factor |
| MEFs | mouse embryonic fibroblasts |
| mESCs | Mouse embryonic stem cells |
| miRNA | microRNA |
| MOPS | 3-(N-morpholino) propanesulfonic acid |
| MQ | Milli-Q grade |
| mRNA | messenger RNA |
| PARP | poly ADP ribose polymerase |
| PBS | Phosphate buffer saline |
| PCR | polymerase chain reaction |
| PFA | Paraformaldehyde |
| PL | placenta |
| PMSF | Phenylmethylsulfonyl fluoride |
| PMSG | pregnant mare serum gonadotropin |
| PVDF | polyvinylidene difluoride |
| qRT-PCR | quantitative real-time PCR |
| RA | Retinoic acid |
| RAR | Retinoic acid receptor |
| RBPs | RNA binding proteins |
| RISC | RNA induced silencing complex |
| RP | Reverse Primer |
| RqCD1/Rcd1 | Required for cell diffeentiation1 |

| | |
|---|---|
| RT | room temperature |
| SD | silencing domain |
| SDS-PAGE | sodium dodecyl sulfate polyacrylamide gel electrophoresis |
| siRNA | Small interfering RNA |
| TBST | tris-buffered saline + Tween 20 |
| Tris | tris(hydroxymethyl)aminomethane |
| TTP | Tristetraprolin |
| UTR | untranslated region |
| WT | wild type |
| X-Gal | 5-bromo-4-chloro-3-indolyl-$\beta$-D-galactopyranoside |
| YS | Yolk sac |

Dedicated to my beloved teachers

# Contents

# List of Figures

# List of Tables

# Chapter 1

# Introduction and Literature Review

## 1.1 RNA metabolism and the CCR4-NOT complex

Eukaryotic gene expression is fundamentally perpetuated via regulation of messenger RNA (mRNA) expression. Typically, mRNA is synthesized within the nucleus by a process known as transcription, followed by translocation into cytoplasm for synthesis of proteins, and eventually undergoes degradation. In addition to these, a majority of cellular mRNAs undergo post-transcriptional regulation that influence mRNA length, half-life, localization, and translation. Examples of post-transcriptional changes include splicing of pre-mRNAs, 5' end capping, polyadenylation, and most importantly interactions with RNA binding proteins (RBPs). Further complexity emerges with the influence of internal or external stimuli such as nutrients, chemical and morphogen gradients, ligand-receptor interactions, stress etc.

RNA metabolism refers to the entire scheme of events starting from biogenesis to turnover of RNA, including incumbent steps of regulation. A large body of cellular machines mainly consisting of multimeric protein complexes help in orchestrating these processes. One such cellular machinery is the cytoplasmic CCR4-NOT complex that is primarily known to stimulate decay of target mRNAs via deadenylation of polyA tail. In humans and mice, the core complex is composed of a central scaffold protein CNOT1, regulatory subunits CNOT2 and CNOT3, a catalytic core consisting of CNOT6, CNOT6L, CNOT7, and CNOT8 proteins, and additional three subunits CNOT9, CNOT10, and CNOT11. Combinations of these subunits have been classified into four modules – the NOT module, the catalytic module, the CAF40 module, and the NOT10-NOT11 module, based on their ability to associate with independently folding $\alpha$-helical domains on CNOT1 (Wahle and Winkler, 2013). The NOT module consists of subunits CNOT2 and CNOT3 as a heterodimer bound to the superfamily homology domain (SHD) of CNOT1 at the C-terminal end (Bhaskar et al., 2013, Boland et al., 2013). The catalytic module is typically composed of two deadenylase subunits – CNOT7/8 and CNOT6/6L. CNOT7/8 interacts with middle portion of eIF4G (MIF4G) domain of CNOT1 and in return also serves as a docking site for leucine-rich repeat domains (LRR) of CNOT6/6L proteins (Basquin et al., 2012, Petit et al., 2012, Draper et al., 1994, Dupressoir et al., 2001). The CAF40 module consists of CNOT9 bound to domain of unknown function 3819 (DUF3819) domain of CNOT1 protein

(Chen et al., 2014, Mathys et al., 2014). Lastly, the NOT10-NOT11 module consists of proteins CNOT10 and CNOT11 bound to N-terminal end of CNOT1 (Bawankar et al., 2013, Mauxion et al., 2013). A schematic representing the architecture and assembly of various subunits of the mammalian CCR4-NOT complex is depicted in Figure 1.1.

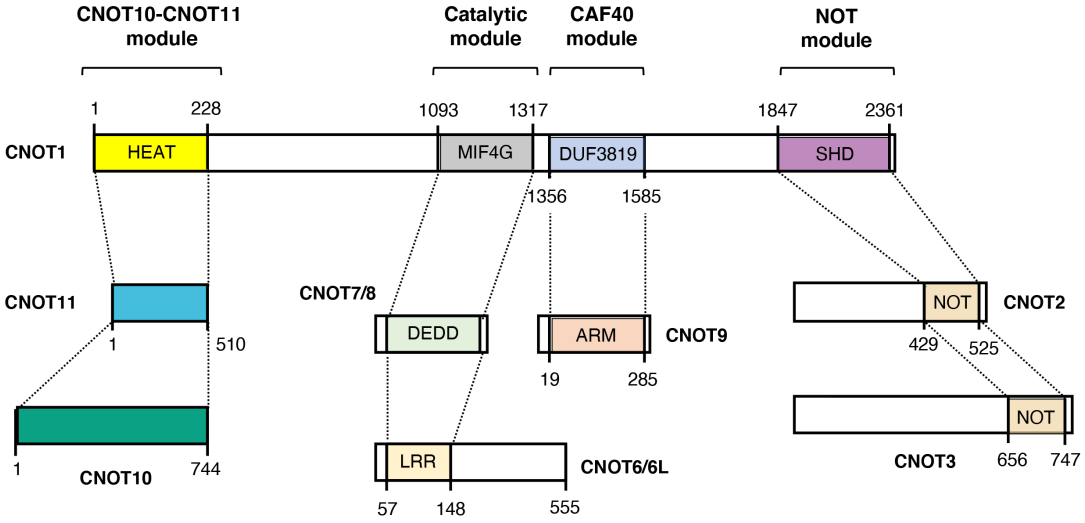


**Figure 1.1: Architecture and assembly of the mammalian CCR4-NOT complex.** Protein-protein interactions allow assembly of subunits on different domains of the central scaffolding subunit CNOT1. The N-terminal HEAT domain contributes to formation of NOT10-NOT11 module, central MIF4G and DUF3819 domains assemble the catalytic module and the CAF40 module respectively, while C-terminal SHD domain forms the NOT module.

The complex is expressed in various cell types and tissues from early developmental stages to adult life (Chen et al., 2011). Mechanisms behind recruitment of this ubiquitously expressed complex to its targets has been extensively investigated. Based on the current understanding, under homeostatic conditions, the basal activity of the complex involves bulk non-specific deadenylation. Tob/BTG family of proteins play and important role in guiding such processes. Tob interacts with CNOT7 subunit of the complex via its N-terminal antiproliferative domain (Xu et al., 2014). Tob also contains PAM2 (Poly(A)-binding-protein-interacting Motif 2) element at its C-terminal, that allows interaction with cytoplasmic Poly(A)-binding protein (PABPC), thereby facilitating turnover of bound mRNA (Okochi et al., 2005, Ezzeddine et al., 2007, Funakoshi et al., 2007). Unlike Tob, BTG1 and BTG2 proteins that lack PAM2 elements, play their part by interacting with RRM1 domain of PABPC1 via their N-terminal antiproliferative domains (Stupfler et al., 2016). However, under stimulation, protein-protein interactions between RNA binding proteins and subunits of the CCR4-NOT complex lead to preferential recruitment of bound transcripts resulting in targeted mRNA decay. For instance, RNA binding protein Tristetraprolin (TTP) interacts with AREs (AU-rich elements) within 3'UTR of Tnf$\alpha$ mRNA and mediates rapid mRNA decay by

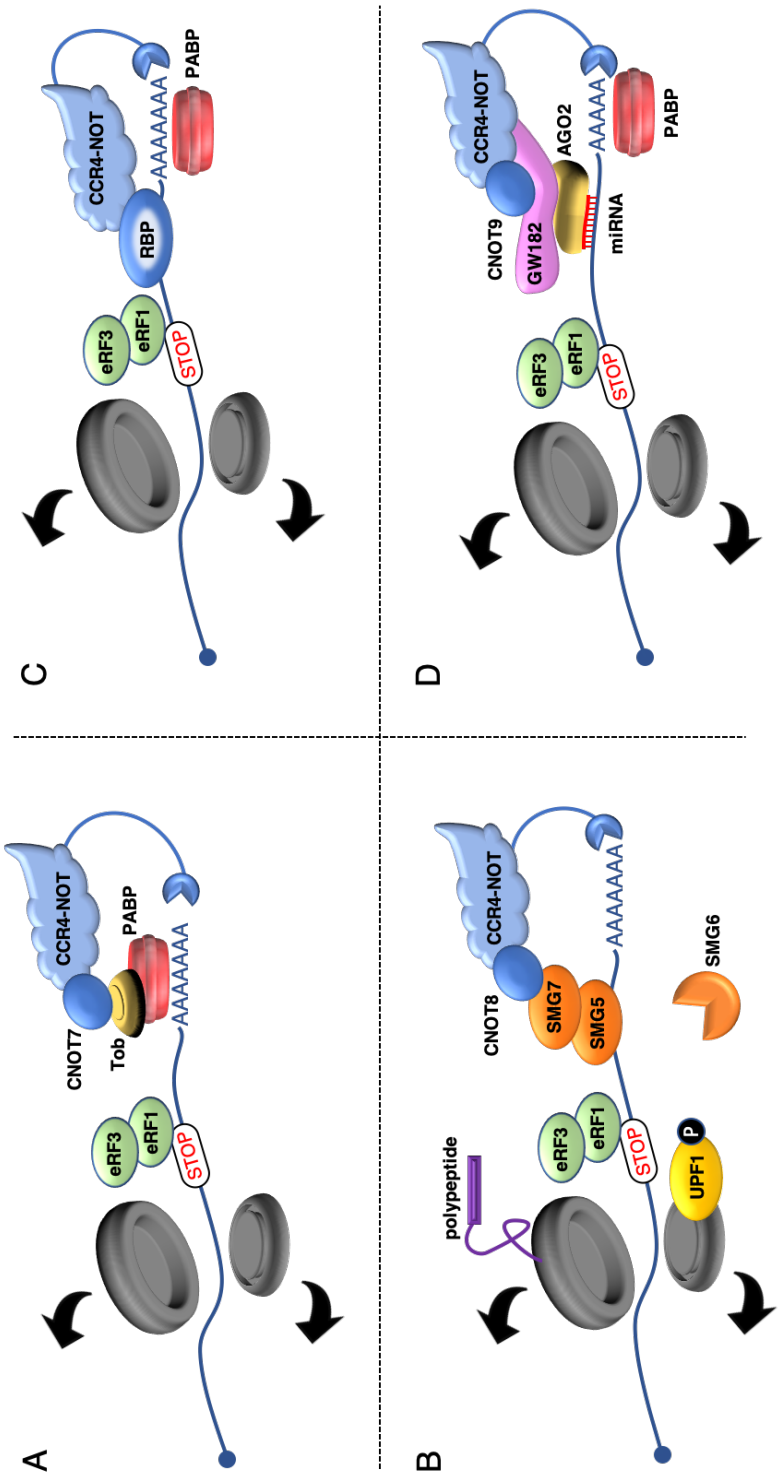


**Figure 1.2: Involvement of CCR4-NOT complex in various forms of mRNA decay** via interactions with: (A) TOB and PABP in generic RNA decay processes (B) SMG5-SMG7 heterodimer bound transcripts for nonsense mediated decay (C) tethered RNA Binding Proteins (RBPs) for targeted mRNA decay (D) miRNA bound to AGO2 and GW182

further interacting with decay complex subunit CNOT1 (Sandler et al., 2011, Fabian et al., 2013). Likewise, loss of CNOT7 and TOB proteins leads to post-transcriptional stabilization of *Ucp1* mRNA thereby protecting mice from diet induced obesity, despite being bound to RNA binding protein BRF1 (Takahashi et al., 2015). Other forms of stimulation may involve intracellular response to mutations leading to production of nonsense transcripts. In such scenarios, SMG5-SMG7 bound mRNAs get recruited to the complex via interactions with CNOT8 (Loh et al., 2013). Another common form of stimulation occurs via interactions between microRNA and target mRNAs leading to translation suppression followed by mRNA decay coordinated via Ago2 and GW182 family of proteins (Valencia-Sanchez et al., 2006, Behm-Ansmant et al., 2006, Chen et al., 2009). An example of this was observed in zebrafish embryos undergoing maternal to zygotic transition, wherein a sudden increase in miR-430 levels strongly correlated with decay of maternal mRNAs possessing miR-430-binding sites in 3'UTR regions (Giraldez et al., 2006). A schematic of CCR4-NOT complex driven mRNA decay mechanisms is shown in Figure 1.2.

Impact of the CCR4-NOT complex on RNA metabolism extends beyond the scope of deadenylation dependent mRNA decay. Subunits of the complex intervene in a variety of other cellular processes that include transcription initiation and elongation, mRNA quality control, mRNA export, translational quality control and protein turnover. (Chapat and Corbo, 2014, Collart, 2016, Shirai et al., 2014, Miller and Reese, 2012). In fact, NOT subunits (Not1, Not2, Not3, Not4) were first discovered as negative regulators of transcription in yeast (Collart and Struhl, 1994, Collart and Struhl, 1993). Mutant yeast showed preferential increase in HIS3 mRNA expression driven by TATA-less promoter element upon disruption of the canonical TATA-box containing promoter. Hence the name "Negative on TATA-less" was attributed to these proteins. This notion prevailed for many years until biochemical and mass spectrometric evidence emerged in support of a cytoplasmic protein complex constituted by Not proteins and other associated molecules such as CCR4 and CAF1, collectively contributing to mRNA deadenylation (Tucker et al., 2001, Chen et al., 2001). Soon, studies in Drosophila and mouse fibroblasts showed conserved nature of metazoan homologues of these proteins in accomplishing deadenylation dependent mRNA decay (Temme et al., 2004, Yamashita et al., 2005). These findings highlighted an intriguing new function to the complex, but also raised doubts over its true function in regulation of gene expression. Furthermore, in the case of yeast and other models used for characterization of CCR4-NOT subunits, an overall increase in mRNA levels or accumulation thereof, may have resulted from a cumulative effect of derepression of transcription as well as impairment of mRNA decay. Over time, research advances in the field of CCR4-NOT biology presented additional evidences of gene expression control. For instance, proteomics analysis in HeLa cells showed interactions between subunits of the CCR4-NOT complex and components of nuclear mRNA processing machinery that included nuclear pore complex proteins and splicing factors (Lau et al., 2009). In the context of translation repression, tethering of CAF1 (CNOT7) deadenylase to reporter mRNA was found to repress of cap-dependent translation in Xenopus oocytes (Cooke et al., 2010). This was a case of deadenylation independent translation repression as catalytically inactive form of CAF1 also showed translation repression. Other modes of inducing translation repression either involve

microRNAs or interactions between CNOT1 and DDX6, an activator of Dcp1-Dcp2 decapping factors (Meijer et al., 2013, Chen et al., 2014, Mathys et al., 2014). Despite major focus in the direction of post-transcriptional regulation, reports indicating direct role of CNOT subunits in transcription regulation also surfaced. In one such example, promoter occupancy of CNOT3 was shown to regulate transcription of pluripotency associated transcription factors such as c-Myc and ZFX in mouse embryonic stem cells (Hu et al., 2009). Direct involvement of CNOT7 in transcription driven by activity of nuclear hormone receptors have also been reported (Prevot et al., 2001, Nakamura et al., 2004).

Understanding the role of CCR4-NOT complex and its subunits in overall gene expression regulation, requires a systems prospective. The idea of transcription-coupled mRNA decay has recently been proposed in a study involving Snf1, the yeast ortholog of AMP-activated protein kinase (Braun and Young, 2014). In addition to this, mRNA degradation factor Xrn1 has been implicated in transcription-cum-translation of mRNAs encoding membrane proteins (Blasco-Moreno et al., 2019). Conversely, transcription factors have also been directly implicated in guiding targeted mRNA decay. In one such study, transcription factor ERG was reported to recruit CNOT2 to control decay of mRNAs to RNA-binding protein RBPMS, thereby facilitating mitotic progression (Rambout et al., 2016). In addition to these higher order interactions, further heterogeneity in complex activity is attributed to variability in subunit stoichiometry and structural composition of the complex. For instance, expression of key subunits, CNOT1 and CNOT3, is barely expressed in mouse kidney lysates compared to higher abundance in brain or thymus tissue (Chen et al., 2011). Also, CNOT6L has ubiquitous expression across tissues, while CNOT6 is selectively expressed in thymus, ovary and testis, and spleen (Chen et al., 2011). Finally, it is important to delineate functional contributions of individual subunits or a subset thereof, vs. collective function mediated by the complex. For instance, many studies attributing role of individual CCR4-NOT subunits within the nucleus, fail to provide comprehensive structural information of the complex within the context of study. Also, mammalian CNOT4, previously understood to be structurally and functionally disconnected from the complex, has recently been shown to have affinity with the core complex duly supported by biochemical and crystal structure based evidences (Keskeny et al., 2019, Yang et al., 2016). In summary, the CCR4-NOT complex acts as a guardian of gene expression control by directly or indirectly influencing various cellular machinery that are individually responsible for specific function.

## 1.2 Physiological relevance of the CCR4-NOT complex

Manifestation of molecular events at the physiological level has always been an intriguing field of research. In the past, many examples of functional redundancy were observed in case of protein kinases, initially characterized to have definitive molecular function (Saba-El-Leil et al., 2016, Voisin et al., 2010). Furthermore, complex multicellular eukaryotes exhibit higher order gene expression regulation with intra-organ

and inter-organ crosstalk between various cell types. It is therefore worth investigating, the importance of a given molecule (protein) or biochemical pathway in the context of physiology at various levels of organization – cells, tissues, organs, and organ systems.

In higher eukaryotes such as mice and humans, the CCR4-NOT complex and its subunits have been found to regulate gene expression across a variety of different physiological processes such as germ layer differentiation, nervous system development, spermatogenesis, immune regulation, adipose and cardiac tissue development, to name a few (Nakamura et al., 2004, Yamaguchi et al., 2018, Joly et al., 2013, Koch et al., 2014, Inoue et al., 2015, Takahashi et al., 2019, Sohn et al., 2015). This falls in agreement with the diversity of molecular activity the complex orchestrates at the cellular level. For example, mice deficient in CNOT7 show impairment in spermatogenesis due to defects in testicular somatic cells (Nakamura et al., 2004). Haploinsufficiency of CNOT3 in mice leads to enhanced metabolic rates resulting in high glucose tolerance and resistance against diet-induced obesity (Morita et al., 2011). In another example, conditional depletion of the CCR4-NOT complex components CNOT1 or CNOT3 results in cardiomyocyte death triggered by elongation of poly(A) tail of *Atg7* mRNA (autophagy regulator) and activation of p53 (Yamaguchi et al., 2018). Likewise, over the past two decades, many examples of physiological function have been attributed to mice and human subunits CNOT1, CNOT2, CNOT3, CNOT6, CNOT6L, CNOT7, and CNOT8. However, very limited information exits with regard to subunits CNOT9, 10 and 11. Our laboratory generated knockout (KO) mice for various subunits and observed phenotypes as listed in Table 1.1.

| **Gene** | **Phenotype** | **References** |
|---|---|---|
| *Cnot1* | Embryonic lethal<E6.5 | Unpublished |
| *Cnot2* | Embryonic lethal | Unpublished |
| *Cnot3* | Embryonic lethal<E6.5 | (Neely et al., 2010, Morita et al., 2011) |
| *Cnot6* | Normal at birth | (Dominick et al., 2017) |
| *Cnot6l* | Resistant to HFD induced obesity | (Morita et al., 2019) |
| *Cnot7* | Male sterility, increased bone mass | (Nakamura et al., 2004, Washio-Oikawa et al., 2007) |
| *Cnot8* | Embryonic lethal ≈ E8.5 | Unpublished |
| *Cnot4, 9, 10, 11* | Embryonic lethal | Unpublished |

**Table 1.1:** Phenotype exhibited by KO mice deficient of CCR4-NOT subunits

## 1.3 Development and RNA metabolism

A spectrum of different phenotypes exhibited by mice upon depletion of CCR4-NOT subunits (as shown in Table 1.1), which emphasizes the requirement of the complex during early developmental stages. Causes of lethality can be postulated in terms of disruption in RNA homeostasis resulting from impairment in complex structure and/or function. In fact, beyond direct purview of the CCR4-NOT complex a large body of evidence endorses the importance of RNA regulation during development. For instance, fission yeast selectively eliminates meiosis-specific transcripts during vegetative growth stages to prevent untimely entry into meiosis (Harigaya et al., 2006). In Drosophila oocytes, pre-zygotic anterior-posterior axis specification is primarily driven by cytoplasmic compartmentalization of *bicoid* and *nano*s mRNAs (Ferrandon et al., 1997, Macdonald and Kerr, 1998). Embryos lacking Bicoid protein cannot form the fly head, whereas ectopic expression of *bicoid* mRNA at the posterior end result in two-headed embryos (Driever et al., 1990). During late gastrulation stages of mice embryos, anterior-posterior patterning occurs as a result of *Fgf8* mRNA decay in anterior regions (Dubrulle and Pourquie, 2004). In one of the better-known examples, oscillations in levels of *cyclin* transcripts guide cell cycle kinetics in mitotically active cells, while lack of adequate induction directs post-mitotic cell fate (Pines and Hunter, 1989, Maity et al., 1995). These and many more examples emphasize the importance of regulated RNA synthesis, localization, transport, and decay across various stages of development and differentiation.

A few studies showcasing direct functional role of CCR4-NOT subunits during development have been reported. For instance, CNOT1, CNOT2, and CNOT3 have been shown to maintain mouse and human embryonic stem cell identity via inhibition of *Cdx2, Gata3, Eomes*, and *Krt8* transcripts that promote extraembryonic differentiation (Zheng et al., 2012). CNOT3 depletion in mouse embryonic fibroblasts (MEFs) has been shown to promote necroptosis via stabilization of cell-death related transcripts (Suzuki et al., 2015). Interaction between RNA binding protein NANOS2, and CNOT1 was found to be critical for development of male germ cells in mice (Suzuki et al., 2010, Suzuki et al., 2012). Loss of Caf1 (CNOT7) in worms, leads to impairment in larval development with defects in progression of gametogenesis in both males and hermaphrodites (Molin and Puisieux, 2005). CNOT8 mutant fish lacking majority of RNAse domain due to a point-nonsense mutation, show compromised development of dopaminergic neurons in caudal hypothalamus region of the brain due to stabilization of *Fgf3, Fgfr1/2/3/4* and their downstream effectors (Koch et al., 2014). CNOT3 post-transcriptionally regulates decay of *Cdkn2a* mRNA and other cyclin-dependent kinase inhibitors (CDKIs), thereby abetting proliferation of cardiomyocytes derived from human embryonic stem cells (Zhou et al., 2017). Lastly, deadenylase activity of the CCR4-NOT complex has recently been implicated in decay of *hairy*-related transcripts during zebrafish somitogenesis (Fujino et al., 2018). Beyond these handful set of examples, direct involvement of CCR4-NOT subunits in vertebrate development, has not been comprehensively demonstrated. Therefore, understanding the role of uncharacterized subunits such as CNOT9 having developmental phenotype was an ideal choice for study. In the following section, existing literature concerning CNOT9

shall be introduced, before stating the objectives of this study.

## 1.4 CNOT9 (Rcd1/Rqcd1/Caf40)

### Identification, Characterization, and Function

CNOT9 (or RQCD1 or RCD1 or CAF40) was first identified as a factor responsible for inducing sexual differentiation in the fission yeast *Schizosaccharomyces pombe*, under conditions of nitrogen starvation (Okazaki et al., 1998). Thereafter, using mass spectrometry, it was confirmed to be a part of yeast CCR4-NOT complex (Chen et al., 2001). The monomeric form is a 33 kilodalton (299 amino acids) polypeptide consisting of six armadillo repeat (ARM) domains, capable of binding single and double stranded oligonucleotides (Garces et al., 2007, Chen et al., 2014, Mathys et al., 2014). CNOT9 protein is highly conserved from yeast to humans with over 70% amino acid sequence identity (Okazaki et al., 1998, Garces et al., 2007).

Ste11 was one of the first downstream targets of CNOT9 identified in *Schizosaccharomyces pombe* (Okazaki et al., 1998). It codes for a transcription factor that controls sexual differentiation– conjugation followed by meiosis and sporulation, under nutrient stress conditions (Kelly et al., 1988, Sugimoto et al., 1991). In absence of CNOT9, yeast cells were sterile under nutrient stress conditions, whereas rescue of fertility occurred via ectopic expression of Ste11 (Okazaki et al., 1998). Yeast Ste11 contains N-terminal HMG box (high mobility group) characteristic of HMG boxes present on Tcf-1/Lef-1 proteins in higher eukaryotes (Okazaki et al., 1998, Yamamoto et al., 1999). Such structural and functional homology raises the odds for CNOT9 role in processes such as T-lymphocyte differentiation.

Mammalian CNOT9 was first reported as a nuclear co-factor involved in retinoic acid (RA) induced differentiation of F9 teratocarcinoma (testicular cancer) cells (Hiroi et al., 2002). Knockdown of CNOT9 using anti-sense oligomers, displayed an impairment in RA induced differentiation of F9 cells (Hiroi et al., 2002). This study also highlighted the role of CNOT9 in RA induced complex formation between Retinoic acid receptor (RAR) and Activating Transcription factor 2 (ATF-2) at differentiation-specific enhancer (DRE) elements of the *c-jun* promoter (Hiroi et al., 2002). DRE element occupancy by RAR-CNOT9-ATF-2 complex resulted in an increase in *c-jun* expression, thereby leading to differentiation of F9 cells to visceral endoderm cells (Hiroi et al., 2002). In a study conducted on human cell lines, CNOT9 was reported as a transcriptional repressor for C-MYB and AP-1 target genes (Haas et al., 2004). C-MYB and AP-1 are transcription factors that associate with RNA Polymerase II to form pre-initiation complexes at target promoters. Nuclear C-MYB protein, via physical interactions with CNOT9 was found to repress mim-1 promoter activity (Haas et al., 2004). In a later study, based on yeast-two hybrid assay, CNOT9 was reported to enhance transcriptional activity of nuclear hormone receptors such as TR$\alpha$, RAR$\alpha$, and RXR$\alpha$, via direct interactions with NIF-1 protein in HeLa cells (Garapaty et al., 2008). However, results presented by this study need further validation in physiologi-

cal contexts, since knockdown of CNOT9 didn't have a profound effect on endogenous targets of nuclear hormone receptors such as *Hoxa1* and *Sox9*.

In-vivo function of CNOT9 has been reported in RA dependent embryonic lung development (Hiroi et al., 2002). CNOT9 expression increased upon RA induction leading to inhibition of branching morphogenesis of alveolar lung, while its subsequent knockdown restored branching leading to formation of distal alveolar buds (Hiroi et al., 2002). A schematic of RA dependent lung development potentially involving CNOT9, is summarized in Figure 1.3.

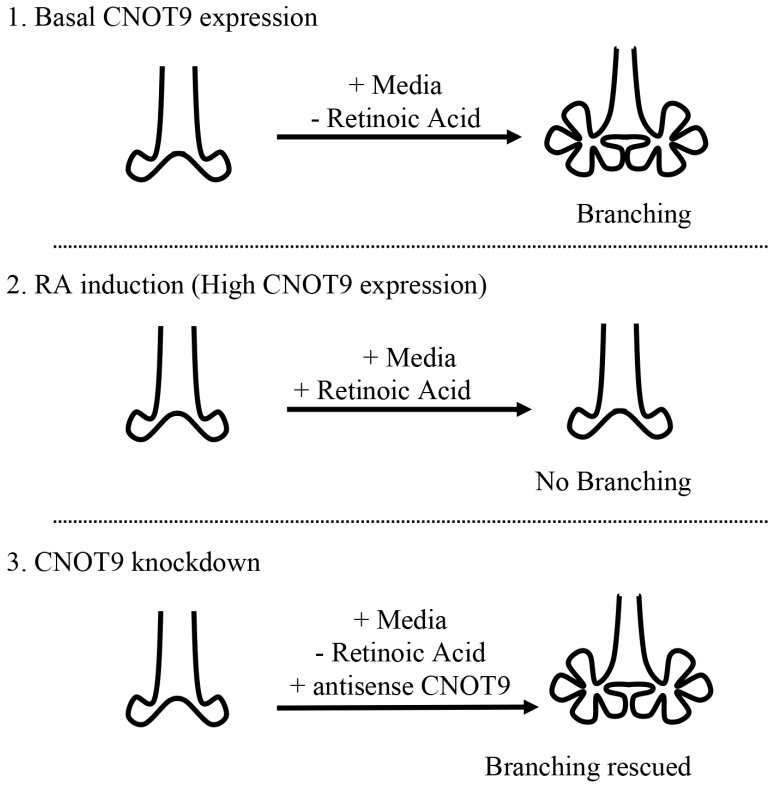


**Figure 1.3: Schematic of RA induced branching morphogenesis of embryonic lung**

In-vitro studies using human and Drosophila cell lines have identified CNOT9 to mediate stable protein - protein interactions between subunits of the CCR4-NOT complex and miRNA-RISC complex. Crystal structure analysis showed CNOT9 bound to DUF3819 domain of CNOT1 provided docking sites for W(tryptophan)-rich residues present on TNRC6 proteins (Mathys et al., 2014, Chen et al., 2014). These studies project possible contribution of CNOT9 in miRNA mediated translational repression and decay. In addition, human CNOT9 bound to CNOT1 was found to stimulate deadenylation driven by a nuclease module consisting of BTG2, CNOT6L, and CNOT7 (Pavanello et al., 2018). CNOT9 has also been found to recruit the complex to TTP

(Tristetraprolin) bound mRNAs, thereby contributing to decay of reporter RNA (Bulbrook et al., 2018). Drosophila Roquin was shown to interact with the CCR4-NOT complex via multiple and partially redundant interactions, one of which occurs via interaction with CNOT9 (Sgromo et al., 2017). A unique but poorly conserved short linear motif located at the c-terminal end of Roquin was deemed necessary and sufficient for interaction with CNOT9 (Sgromo et al., 2017). In another study, Drosophila Bag-of-marbles (Bam) protein has been shown to exclusively interact with CNOT9 subunit of the CCR4-NOT complex and facilitate both translation repression and decay of polyadenylated mRNAs, in-vitro (Sgromo et al., 2018). Human and Drosophila CNOT4 proteins have recently been found to possess a conserved motif that allows weak, yet direct interaction with CNOT9 protein (Keskeny et al., 2019). The study also revealed that both depletion of CNOT9 or disruption of CNOT4-CNOT9 interaction, leads to impairment in CNOT4 directed decay of tethered reporter RNA (Keskeny et al., 2019). Lastly, in a recent in-vitro reconstitution study, human CNOT9 was postulated to serve bipartite function in facilitating bulk nonspecific decay as well as targeted decay by interacting with substrate RNA or RNA binding proteins respectively (Raisch et al., 2019).

## CNOT9: Expression and Localization

Tissue wide expression studies showed a preferential expression of CNOT9 during embryonic stages over post-natal adult stage tissues (Hiroi et al., 2002). CNOT9 expression has been noted in embryonic rat tissues such as the brain, liver, lung, intestine, heart, kidney, thymus and spleen (Hiroi et al., 2002). However, its expression reduces considerably in adult rats with detectable levels found only in spleen, thymus, testis, bone marrow and lung (Hiroi et al., 2002). In humans, northern blotting analysis was used to detect CNOT9 expression in testis, prostate glands, thymus, ovaries, small intestine, mucosal lining of the colon, and peripheral blood leukocytes (Okazaki et al., 1998, Haas et al., 2004, Ajiro et al., 2009). In addition, a steep increase in mRNA expression was also noted in certain cases of breast cancer (Ajiro et al., 2009). These results suggest a correlation between CNOT9 expression and tissues undergoing or supporting active cellular differentiation.

Although it seems quite intuitive to predict CNOT9 localization, given its roles in nucleus and cytoplasm, certain reports have narrated biased inferences. CNOT9 was initially reported to be localized primarily within nuclei of COS-7 cells (Haas et al., 2004). This was in agreement with contemporary reports that identified its role in transcription repression. Later it was also identified as part of the cytosolic CCR4-NOT complex and yet another cytosolic complex containing GIGYF1/GIGYF2 proteins (Ajiro et al., 2009, Ajiro et al., 2010). Despite lacking a canonical nuclear localization signal sequence, CNOT9 localizes within the nucleus, by mechanisms that remain to be elucidated.

## 1.5 Research Objective

The purpose of this work is to investigate physiological role of mammalian CNOT9, using complete and conditional knockout mice models. Based on phenotype exhibited upon CNOT9 loss, molecular targets of CNOT9 at the level of transcription and/or mRNA decay, shall be identified. Furthermore, identified targets shall be validated using in-vitro cell culture-based assays. At the biochemical level, the degree of requirement for CNOT9 in terms of inter-complex and intra-complex interactions shall be investigated. In summary, novel perspectives of the CCR4-NOT complex in the context of RNA metabolism shall be investigated from the standpoint of subunit CNOT9 as listed below:

**Aim 1:** **Investigating phenotype of knockout mice to identify molecular targets and pathways regulated by CNOT9.**

**Aim 2:** **Understanding biochemical interactions of CNOT9, and role in translation repression and mRNA decay.**

**Aim 3:** **Identification of CNOT9 targets in mouse embryonic stem cells under conditions that promote self-renewal vs. lineage specific differentiation.**

The above three aims shall be addressed individually in Chapters 2, 3, and 4, respectively

# Chapter 2

# Role of CNOT9 in mouse embryonic development

## 2.1 Motivation

The relevance of a biochemical pathway, molecular mechanism, or a component thereof, can be best examined by studying its physiological significance. Over the past few decades, laboratory mouse has been serving as an excellent model to study genes and pathways related to human development and disease. This was largely facilitated by two techniques – gene trapping and gene targeting in mouse ES cells, that were developed during the late 1980s and gradually perfected over the next two decades (Stanford et al., 2001, van der Weyden et al., 2002). With the help of gene-targeting technique, a given locus in the mouse genome can be engineered to generate transgenic/knockout/knock-in mice. We used gene-targeting technique we could successfully disrupt the mouse CNOT9 locus and generate heterozygous (HE) mice.

Although CNOT9 has long been identified as part of the CCR4-NOT complex, there have been no reports suggesting direct targets of CNOT9 either at the level of translation repression, or mRNA decay. With our approach, we aimed to identify decay targets of CNOT9 that showed increased mRNA stability and expression in KO mice tissues. KO mouse also allows us to investigate indispensability or functional redundancy of CNOT9 in various processes of gene expression regulation that have previously been reported in literature. These include roles in mRNA decay either via the microRNA pathway or via interactions with RNA binding proteins.

In this chapter, we investigated the physiological function of CNOT9 by analyzing phenotype exhibited by KO mice. Results obtained from in-vivo studies were tested using in-vitro culture-based conditions to validate existing models and theories pertaining to gene expression control via CNOT9.

## 2.2 Materials and Methods

### 2.2.1 Animals (*Cnot9*$^{+/lacZ}$, *Cnot9*$^{+/loxP}$, and *Cnot9*$^{+/loxP}$ Sox2-Cre mice)

Both *Cnot9*$^{+/lacZ}$ and *Cnot9*$^{+/loxP}$ mice were generated and provided by from RIKEN Center for Developmental Biology, Japan. In the process of generating *Cnot9*$^{+/lacZ}$ mice, Exon 1 of the Cnot9 locus was targeted and replaced by LacZ and neomycin resistance gene via electroporation of TT2 ES cells (Yagi et al., 1993). Neomycin-resistant ES cell clones harboring homologous recombination were injected into ICR 8-cell-stage embryos to generate chimeric mice. Germline-transmitted male chimeras were crossed with C57BL/6J female mice to obtain heterozygous F1 offspring. Gene targeting strategy used to generate *Cnot9*$^{+/lacZ}$ mice is shown in Figure 2.1A and genotyping primers are listed in Table 2.1. *Cnot9* conditional (*Cnot9*$^{+/loxP}$) mice were also generated similarly by targeting TT2 ES cell lines. To generate conditional alleles (floxed alleles) from targeted alleles, mice with targeted alleles were crossed with transgenic mice expressing FLP enzyme. Gene targeting strategy used to generate *Cnot9*$^{+/loxP}$ mice is shown in Figure 2.1B and genotyping primers are listed in Table 2.1. Experiments were performed with mice that had been backcrossed successively to C57BL/6J mice for at least seven generations. *Cnot9*$^{+/loxP}$ Sox2-Cre mice were generated by crossing *Cnot9*$^{+/loxP}$ female mice with Sox2-Cre transgenic males. It is important to use CRE expressing male mice since maternal expression of Cre would lead to systemic depletion of floxed allele, leading to loss of cell-type specificity. Animals were maintained in 12-hour light dark-cycle within temperature-controlled (22$^{o}$C) barrier facility provided with abundant supply of Rodent Diet CA-1 (CLEA, Japan) and water. All experiments were carried out following guidelines for animal use issued by Animal Resources Section, OIST and the Institutional Animal Care and Use Committee (IACUC) at RIKEN Center for Developmental Biology.

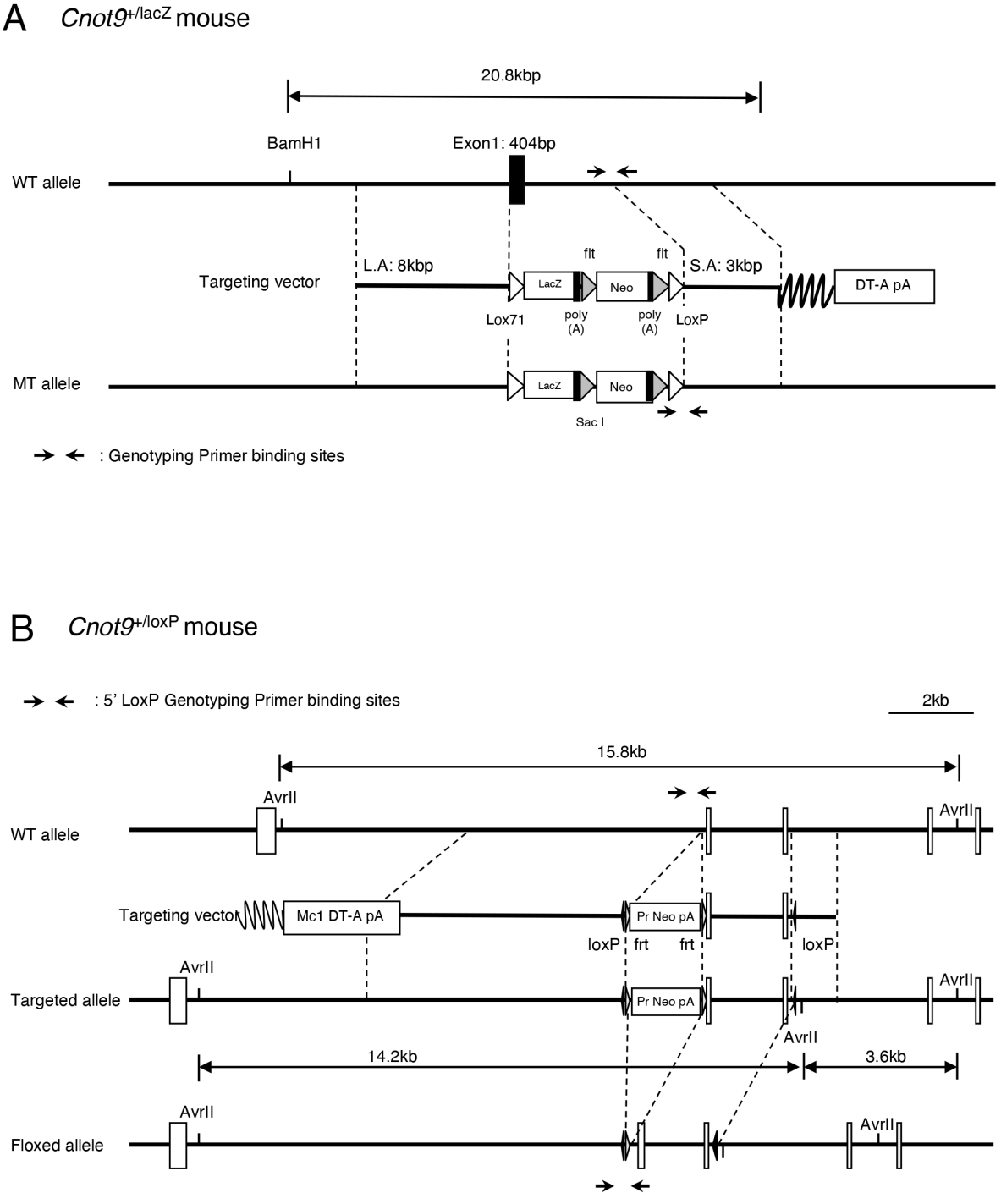


**Figure 2.1: Gene targeting strategies adopted for generation of transgenic mice** (A) LacZ knock-in mouse by targeting exon1 of *Cnot9* genomic locus (B) *Cnot9* conditional mouse by targeting exons 2 and 3 of *Cnot9* genomic locus.

| Mouse line | Primers (5' -3') | Product size |
|---|---|---|
| *Cnot9*$^{+/lacZ}$ | TTATCTGGACGCGGGTTGTGAATGCTGG<br>ACTAGTTCTAGAGCGGCCGATTTAAATACG<br>GTCCTAAGAAAGACATTCCAGGTAGAG | 416 bps (WT band), 296 bps (KO band) |
| *Cnot9*$^{+/loxP}$ | CATGGGCTCATTAGCTGTCAAACAGGTTGAG<br>CCACTGATAGATCTTCTCTCTGTCCACTTGG | 423 bps (floxed band), 212 bps (WT band) |
| Sox2-Cre | TCGATGCAACGAGTGATGAG<br>TTCGGCTATACGTAACAGGG | 482 bps |
| IL2 (Internal control) | CTAGGCCACAGAATTGAAAGATCT<br>GTAGGTGGAAATTCTAGCATCATCC | 324 bps |
| *Cnot9*$^{+/loxP}$ Sox2-Cre | GCTAGGTAGACAAAGGACTTCAGG<br>CCAACCTTGACAGCACACCAGTCTAAC<br>CCATACACTACATTGCATCTCCTTTCCCTAG | 271 bps (WT band) 546 bps (Recombined band) |

**Table 2.1: Genotyping primers used for various mouse lines alongside PCR product size**

### 2.2.2 Mice Genotyping

Tail tips from three-week-old mice within 1.5ml Eppendorf tubes were lysed in 50$\mu$l of lysis Solution I (25mM NaOH in 0.2mM EDTA) at 95$^o$C for 15 minutes. This was followed by addition of 50$\mu$l of lysis Solution II (40mM Tris-HCl, pH=7.5). Thereafter, samples were vortexed for 10 seconds, centrifuged at 120,000g for 3 min at 4$^o$C. 0.75$\mu$l of lysate supernatant was used as template for PCR based genotyping. Same protocol was used for genotyping E9.5 stage and older embryos using yolk-sac tissues. For embryos prior to E9.5 stage, Phire Tissue Direct PCR Kit (Invitrogen) was used following manufacturer's protocol with minor modifications. Briefly, 15$\mu$l of Dilution Buffer (kit) was added to tissue samples collected in 1.5 ml Eppendorf tubes, followed by addition of 1$\mu$l of DNARelease Additive (kit). Samples were mixed by vertexing 5-10 seconds followed by quick spin on a table-top centrifuge. Samples were then rested for 5 minutes at room temperature, followed by boiling at 98$^o$C for 3 minutes. Finally, after another quick spin, samples were rested on ice. Genotyping was done using 1$\mu$l of lysate. Composition of PCR mixture is tabulated below:

| Sl. No | Particulars | Volume |
|---|---|---|
| 1 | 10 X Taq Buffer (+$MgCl_2$) | 2$\mu$l |
| 2 | 2.5 mM dNTP | 2$\mu$l |
| 3 | FP | 0.4$\mu$l |
| 4 | RP1 | 0.4$\mu$l |
| 5 | RP2 (optional) | 0.4$\mu$l |
| 6 | Taq Polymerase | 0.1$\mu$l |
| 7 | dH2O | ≈13.7 $\mu$l |
| 8 | Template DNA | ≈1$\mu$l |
| Total | | 20$\mu$l |

| PCR cycles | | | |
|---|---|---|---|
| Initial Denaturation | 95$^o$C | 2 mins | |
| Denaturation | 95$^o$C | 20 sec | |
| Annealing | 60$^o$C | 30 sec | ×35 cycles |
| Extension | 72$^o$C | 30 sec | |
| Final Extension | 72$^o$C | 3 mins | |
| Resting condition | 4$^o$C | End | |

Finally, 10$\mu$l of PCR product in 1x loading dye, was resolved on 2% agarose gel.

### 2.2.3 Cell culture

HeLa cells were cultured in DMEM (low Glucose) media containing 10% fetal bovine serum (FBS). TransIT-LT1 (Mirus Bio) reagent was used for transient transfection assays based on manufacturer's protocol. For determination of reporter mRNA half-life kinetics CNOT9 KO HeLa cells were first transfected with flag-CNOT9 (wild-type) or flag-CNOT9$^{mut4}$ (mutant), for 24 hours, followed by transfection of luciferase-*Lefty2* 3'-UTR, luciferase-*Lefty1* 3'-UTR, or luciferase-*c-myb* 3'-UTR constructs for 4 hours. Cells were then treated with 2.5$\mu$g/ml ActinomycinD (Wako) for 6 hours with samples being collected at 0, 3, and 6 hours post treatment.

### 2.2.4 Western Blotting

#### Mouse Embryo

Protein lysates from individual or pooled sets of embryos were prepared by homogenization (using Fisherbrand Pellet Pestle) in TNE buffer. Buffer composition is tabulated

as follows:

| Sl. No. | Component | Volume | Final Concentration |
|---|---|---|---|
| 1 | 1M Tris-HCl (pH = 7.5) | 10 ml | 20 mM |
| 2 | 5M NaCl (autoclaved) | 15 ml | 150 mM |
| 3 | NaF | 0.21gm | 10 mM |
| 4 | Beta-glycerophosphate | 1.53 gm | 10 mM |
| 5 | EDTA | 0.29gm | 2 mM |
| 6 | NP40 (from bottle) | 5 ml | 1% |
| 7 | 200mM PMSF | 2.5ml | 1 mM |
| 8 | MQ water | | Up to 500 ml |
| After preparation, solution was filter sterilized and stored at 4$^o$C until use. | | | |

Lysates were incubated on ice for 15 minutes, with gentle pulse vertexing every 5 minutes, followed by centrifugation at 130,000g for 10 min at 4$^o$C. Supernatant was transferred into fresh Eppendorf tubes protein concentration was determined using Pierce BCA assay kit (ThermoFisher). Based on results from BCA assay, lysates concentration was adjusted to a final concentration of 1$\mu$g/$\mu$l in 1X Sample Buffer (50mM Tris-HCl pH= 6.8, 2% SDS, 0.1% Bromophenol Blue, 10% Glycerol). Lysates were boiled at 95$^o$C for 5 minutes and allowed to cool to room temperature for 10 minutes. Depending on molecular weight of the protein to be examined, 6% to 12.5% SDS-PAGE gels were prepared. Lysates were subjected to electrophoresis at 130V until desired ladder separation is achieved within resolving region of gels. Separated proteins on the gel were then electro-transferred onto 0.45um Polyvinylidene difluoride (PVDF) membranes (Millipore). Transfer was done at 12V (constant voltage) for 720 minutes using wet transfer system (Nihon-Eido). Post transfer, membrane was subjected to blocking using 5% skimmed milk in TBST (20 mM Tris, 150 mM NaCl, 0.05% Tween-20) solution for 45 to 60 minutes at room temperature (RT). Membranes were then incubated with primary antibody solution for 2 hours at RT, followed by 1hour of incubation with appropriate horse radish peroxidase (HRP) conjugated secondary antibody (1:4000 dilution). Upon completion of each antibody incubation step, membranes were washed 3 times (5 minutes each) in TBST solution with gentle shaking, to remove non-specifically bound antibodies. Finally, proteins of interest were probed by detecting chemiluminescence intensity using Image Analyzer LAS 4000 (GE Healthcare). Data was analyzed and quantified by applying area calculator tool over a rectangular selection of protein bands using ImageJ software.

**Cultured cells (in-vitro):**

As a first step towards isolation of protein lysates from cells grown in culture dishes, appropriate volume of TNE buffer was added to wells, after performing media aspi-

ration followed by two PB washes. Thereafter, with the help of a cell scraper, cells were detached from the bottom surface of wells/dishes. Using a pipette man, lysate was collected into individual Eppendorf tubes on ice. Lysates were rested on ice for 15 minutes with gentle pulse vortexing every 5 minutes. Thereafter, similar steps for protein isolation and quantification were performed as mentioned in the previous section for mouse embryos.

### 2.2.5 Antibodies

Antibodies against CNOT1 and CNOT3 were generated by Bio Matrix Research (Tokyo, Japan) and previously described previously (Chen et al., 2011). Commercially available antibodies used in this study included: anti-a-tubulin (Sigma, T9026), anti-PARP (CST, 9542S), anti-CNOT9 (Proteintech, 22503-1-AP), anti-FLAG (MBL, PM020), anti-XRN1 (Bethyl A300-443A), anti-HistoneH3 (CST, 4499S), anti-GW182 (Bethyl, A302-329A), anti-CNOT2 (CST, 34214S), anti-4EBP1 (CST, 9644S), anti-b-Actin (CST, 4970L), anti-GAPDH (CST, 2118L), anti-CNOT10 (Bethyl A304-899A), and anti-AGO2 (CST, 2897S). For western blotting, all antibodies were used at 1:1000 dilution in 5% skimmed milk solution.

### 2.2.6 Protein Immunoprecipitation

Protein lysates from E8.0 - E8.5 embryos were prepared and quantified as mentioned in section 2.2.4. 2mg of total protein was subjected to immunoprecipitation using anti-CNOT3 antibody or Control Mouse IgG (Santacruz, SC-2025) for 1 hour at 4$^o$C, followed by an additional 1-hour incubation with 50$\mu$l of Dynabeads (Invitrogen) added directly to the antibody-lysate solution. Incubation was done using a rotating mixture apparatus located in cold room area (4$^o$C). Immunoprecipitated proteins were recovered by magnetic separation of bead-antibody-protein complex. Magnetically separated complexes were washed 5 times before final elution. Elution was done in 40-50$\mu$l of 1X Sample Buffer (containing 2-ME) upon heating at 95$^o$C for 5 minutes. Thereafter, samples were centrifuged at 1500g, for 1 min at 4$^o$C. Supernatant containing immunoprecipitated proteins were transferred into fresh Eppendorf tubes and stored at -30$^o$C until further use. Loading volumes for Input and IP fractions were determined and accordingly resolved on SDS-PAGE gels. HeLa cell lysates obtained after transfecting cells with flag-CNOT9 or flag-CNOT9$^{mut4}$ or pcDNA3.0 vectors were subjected to immunoprecipitation using ANTI-FLAG M2 Affinity gel (Sigma) for 2 hours at 4$^o$C. Prior to addition of antibody conjugated beads to lysates equilibration steps was performed. Briefly, 1 ml of bead-antibody gel was aliquoted into a 1.5 ml Eppendorf tube and centrifuged at 1500g for 1 min at 4$^o$C. Post centrifugation, supernatant was discarded and 1 ml of TNE Buffer was added to resuspend antibody-bead pellet. Gentle pipetting was done to make a homogenous solution and thereafter centrifuged at 1500g for 1 min at 4$^o$C. Once again, supernatant was discarded and washing step was repeated 2 more times. Finally, at the end of final spin, 500$\mu$l of TNE buffer was added to existing beads that occupy volume equivalent of 500$\mu$l. This ensures an approximate bead concentration of 50%. In this form, antibody-conjugated beads can be stored at 4$^o$C for a maximum of 6 months. Approximately 40$\mu$l of pre-equilibrated M2 beads

per aliquot of protein lysate was used. Upon conclusion of 2-hour incubation, lysates were centrifuged at 1500g, for 1 min at 4$^o$C. Supernatant containing unbound proteins was discarded and replaced with 1ml of TNE buffer. Loosely attached pellet at the bottom of the tube was mixed by gentle pipetting, followed by centrifugation at 1500g, for 1 min at 4$^o$C. This washing step was repeated for an additional 4 times. At the end of last wash, 30$\mu$l of FLAG peptide (1$\mu$g/$\mu$l) was added to pellet and incubate at 37$^o$C for 10 minutes. Thereafter, samples were centrifuged at 2500g, for 1 min at 4$^o$C and supernatant was aliquoted into freshly labelled tubes. Finally, 15$\mu$l of 3X Sample Buffer (containing 2-ME) was added to immunoprecipitated lysates and heated at 95$^o$C for 5 minutes. Samples were allowed to cool to RT before storage at -30$^o$C until use. All lysates were subjected to BCA assay prior to IP, to ensure equal amount of starting material.

### 2.2.7 RNA Isolation and qRT-PCR analysis

All RNA extraction was done using ISOGEN II (Nippongene) reagent according to manufacturer's protocol.

**Mouse embryos:**

E7.5 to E8.5 stage embryos were individually collected in 1.5 ml Eppendorf tubes containing 300$\mu$l of Isogen II reagent. Samples were stored at -80$^o$C, until genotype of each sample was determined by PCR. Typically, 3 embryos of the same genotype were pooled into one tube. Before RNA isolation, embryo samples in Isogen solution were homogenized by passing through 26G needle. After homogenization, 100$\mu$l of additional Isogen II reagent was added to make a final volume of 1ml. Thereafter, 400$\mu$l of RNase free water was added to tissue homogenate and vortexed vigorously for 15 seconds. Samples were then allowed to rest at RT) for 8 minutes, followed by centrifugation at 13,000g for 15 minutes at 4$^o$C. 950$\mu$l of supernatant was transferred to a 2ml Eppendorf tube containing equal volume of Isopropanol, followed by addition of 1.5$\mu$l GlycoBlue (ThermoScientific). Thereafter, samples were mixed by inversion (8-10 times) and left at RT for 10 minutes. Upon conclusion of this step, samples were centrifuged at 13,000g for 10 minutes at 4$^o$C. Supernatant was discarded, and blue colored pellet was washed with 500$\mu$l of 75% Ethanol (in MQ water) followed by centrifugation at 8000g for 2 minutes at 4$^o$C. In the next step, ethanol was removed, and pellet was washed again with 500$\mu$l of 75% Ethanol. In the penultimate step, residual ethanol sticking to tube walls were removed by flash spinning tubes on a benchtop centrifuge. Lastly, total RNA was eluted from pellet, by adding 10-40$\mu$l of RNase free water. RNA concentration was measured by NanoDrop (ThermoScientific) adjusted appropriately and stored at -80$^o$C until use.

**Cultured cells (in-vitro):**

For isolating total RNA from cells growing in culture, 1ml of Isogen II was added directly to each well after aspirating out culture media and performing two PB washes. Scarping of cells was not required as pipetting the lysate 3-4 times into the well ensured

cell lysis. Lysates were collected in 1.5ml Eppendorf tubes. Thereafter, similar steps for RNA isolation and quantification were performed as mentioned in the previous section for mouse embryos.

**qRT-PCR analysis:**

For accessing mRNA expression levels via quantitative real-time PCR analysis, mRNA was first converted into complementary DNA (cDNA). SuperScript III First-strand synthesis (Invitrogen) protocol was used for this purpose. The following mix was prepared in 8-strip PCR tubes and incubated at 65$^o$C for 5 minutes, followed by incubation ice for 5 minutes.

| Sl. No | Particulars | Volume |
|---|---|---|
| 1 | Total RNA (500ng to 1$\mu$g) | $\approx$ 1-2$\mu$l |
| 2 | 2.5 mM dNTP | 1$\mu$l |
| 3 | oligo(dT) 12-18 primer | 1$\mu$l |
| 4 | MQ water | $\approx$ 6-7$\mu$l |
| Total (Mixture 1) | | 10$\mu$l |

Thereafter, the following mix (Mixture 2) was added to Mixture 1.

| Sl. No | Particulars | Volume |
|---|---|---|
| 1 | 5x First Strand Buffer | 4$\mu$l |
| 2 | RNaseOut | 0.5$\mu$l |
| 3 | SuperScript III RTase | 1$\mu$l |
| 4 | MQ water | 4.5$\mu$l |
| Total (Mixture 2) | | 10$\mu$l |

Thereafter, tubes were incubated in a thermocycler at 42$^o$C for 1 hour (reverse transcription), followed by 70$^o$C for 15 minutes (enzyme denaturation). Samples were diluted 1:10 fold in RNase free water and stored at -20$^o$C until use. For qRT-PCR reaction, the following components were added in respective amounts:

| Sl. No | Particulars | Volume |
|---|---|---|
| 1 | cDNA (1:10 dilution) | 2$\mu$l |
| 2 | SYBR Premix ExTaq (Takara) | 5$\mu$l |
| 3 | 10$\mu$M FP | 0.2$\mu$l |
| 4 | 10$\mu$M RP | 0.2$\mu$l |
| 5 | ROX reference dye II | 0.2$\mu$l |
| 6 | RNase free water | 2.4$\mu$l |
| Total | | 10$\mu$l |

Samples were run in three technical replicates using the following PCR conditions:

| **PCR cycles** | | | |
|---|---|---|---|
| Initial Denaturation | 95$^o$C | 30 sec | |
| Denaturation | 95$^o$C | 5 sec | ×40 cycles |
| Annealing and Extension | 60$^o$C | 30 sec | |
| | 95$^o$C | 15 sec | |
| Melting Curve analysis | 60$^o$C | 60 sec | |
| | 95$^o$C | 15 sec | |

Data was analyzed using Viia7 sequence detection system (Applied Biosystems) and exported in MS Excel format. In a given sample, relative mRNA expression of a target was determined by normalizing with Gapdh expression using $\Delta\Delta$Ct method (Livak and Schmittgen, 2001).

### 2.2.8 RNA Sequencing analysis

High-quality total RNA (500ng) was isolated from pooled E8.0-E8.5 stage embryos using Isogen II reagent as mentioned in Section 2.2.7 and subjected to RNA-seq library preparation using TruSeq Stranded mRNA LT Sample Prep Kit (Illumina) based on manufacturer's protocol. Paired-end RNA sequencing (109 base-pair) was done with Hiseq PE Rapid Cluster Kit v2-HS and Hiseq Rapid SBS Kit v2-HS (200 Cycle) on Hiseq2500 (Illumina) machine, following manufacturer's protocol. Assistance in library preparation and sequencing was provided by Sequencing Center, OIST. Sequencing reads were mapped to mouse reference genome provided in Ensembl database using StrandNGS software (Strand Life Sciences). Data analysis was done by mapping reads to mm10 genome sequence (Ensembl), thereby converting raw counts to corresponding FPKM scores. For downstream analysis, only protein-coding genes with FPKM scores $\geq 0.05$ were selected. Gene set enrichment analysis (GSEA) was performed using online

software that uses the Molecular Signatures Database (MSigDB) from Broad Institute, USA.

### 2.2.9 Nuclear-Cytoplasmic Fractionation

Nuclear and cytoplasmic fractions were isolated using the NE-PER kit (ThermoScientific) according to the manufacturer's protocol. Briefly, pooled embryos samples were homogenized by pipetting back and forth gently 10 times using P200 tip on ice. Cells were thoroughly washed 2 times, pelleted down at 500g for 3 minutes, and finally resuspended in 100$\mu$l of ice-cold 1X PBS. Cell counting was done using Bio-Rad automated cell counter device. Upon pooling 8-10 WT embryos, a total of 5x108 cells were recovered. Cytoplasmic lysis was done using 200$\mu$l of CER I solution followed by 11$\mu$l of CER II solution based on protocol described in kit. Nuclear protein was extracted in 100$\mu$l of NER solution. The kit manufacturer recommends the aforementioned volumes of of CER I, II and NER buffers to fractionate $2 \times 10^6$ HeLa cells. However, due to the fragile nature of embryonic cells, and estimates from standardization trials, we chose to use approximately 25 times more cells for the same about of reagents

### 2.2.10 Tissue histology and staining

E8.5 and E9.5 stage placental tissues were isolated from individual embryo horns and fixed in 4% PFA solution overnight. With the help of spatula fixed tissues were gently transferred into paraffin embedding cassettes duly label with a pencil. Tissues were washed by immersing cassettes in 1X PBS solution for a total of 30 minutes, with replacement of PBS every 10 minutes. Thereafter, tissues were dehydrated every 5 minutes in 30% EtOH, followed by 50% EtOH, 70% EtOH, 90% EtOH, and 100% EtOH. An additional 100% Ethanol dehydration step was performed to ensure minimal carryover of PBS into next set of solutions. After ethanol-based dehydration, cassettes were dipped in EtOH-Methyl benzoate solution (1:1) for 15 mins in RT, followed by incubation in 100% Methyl benzoate solution, for 3 hours at RT. Thereafter, cassettes were immersed in Xylene-Methyl benzoate solution (1:1) for 15 mins in RT, followed by Xylene solution for another 15 mins in RT. An additional Xylene incubation for 15 minutes was performed to ensure minimal carryover of Methyl benzoate solution into next set of solutions. Cassettes were then dipped in Xylene-Paraffin solution (1:1) overnight at 65$^o$C. On the following day, cassettes were sequentially transferred into 3 paraffin solutions, and incubated for 1 hour each. At the end of third paraffin step, plastic or metallic molds were placed on a 65$^o$C heat block. Molten paraffin was added to molds until half-filled. Thereafter, cassettes containing tissues were gently pushed while being immersed inside a glass Petri dish filled with molten paraffin. Using a plastic dropper tissue samples were gently picked and placed inside molds. While the paraffin remained in molten state, sample orientation was adjusted with a needle. Once adjusted, paraffin molds were placed on benchtop for 5-10 minutes allowing solidification. Molds were stored at 4$^o$C until sectioned. 8-10$\mu$m sections were generated using Microm HM325 rotary microtome. Sections were collected on MAS coated glass slides and dried at 42$^o$C for 1 hour. Thereafter, slides were stacked together

in a slide stand and placed inside a ziplock bag. In such condition slides containing paraffin sections could be stored at 4$^o$C until use.

**Dewaxing and Hematoxylin-Eosin (H-E) staining:**

Prior to paraffin dewaxing, ziplock pack sealed slides were placed at RT for 30 minutes allowing moisture to dry up. Dewaxing was done by dipping slides thrice in Xylene solution for 4 mins each in RT, followed by rehydration via serial incubations in 100% EtOH, 90% EtOH, 70% EtOH, 50% EtOH, 30% EtOH for 2 mins each in RT. Thereafter, slides were dipped twice in MQ water for 3 minutes at RT. Hydrated tissue sections were dipped in Hematoxylin 3G solution (Sakura Finetek, Japan) for 3 minutes followed by gentle rinsing in running tap water for 10 minutes. Thereafter, slides were dipped in MQ water for 30 sec followed by Eosin solution (Sakura Finetek, Japan) for 3 minutes. Post eosin stain, slides were quickly washed by immersing into MQ water for 5 seconds, followed by 70% Ethanol for 30 sec, 90% Ethanol for 1 minute, and finally in 100% Ethanol for another 1 minute. Finally, slides were dehydrated completely by dipping in 3 successive solutions of Xylene for 2 minutes each, before mounting using Entellan (Xylene Based mounting medium) or Flourinert. Slides were allowed to dry for 3-5 hours at RT. Tissue sections were imaged using Keyence BZ-X710 light microscope.

### 2.2.11 LacZ staining

Embryos were isolated from pregnant female mice and collected in individual wells of 12-well tissue culture plate filled with 1-2 ml of ice-cold PBS. During dissection, a small puncture was done with 30G tungsten needle to facilitate entry of fixative and staining solutions in subsequent steps. E7.5, E8.5 and E9.5 embryos were fixed on ice fixed using fixative solution (0.2% glutaraldehyde, 2 mM $MgCl_2$, 5 mM EGTA in PBS) for 5, 10, and 15 minutes respectively. Subsequently, excess fixative was removed by washing samples three times with 1X PBS for 10 minutes on ice. Thereafter, samples were rinsed thoroughly with ice-cold rinse buffer (0.01% DOC, 0.02% NP40, 2 mM $MgCl_2$ in PBS) for 20 min on ice. Finally samples were treated with staining solution (1mg/ml X-Gal, 0.01% DOC, 0.02% NP40, 5mM $K_4Fe(CN)_6$, 5mM $K_3Fe(CN)_6$, 2mM $MgCl_2$ in PBS) and incubated for 48-72 hours at 37$^o$C, protected from light using foil wrapping of plate. Reaction mixture should be preheated to 37$^o$C before addition of X-Gal. Post staining, whole-mount LacZ stained embryos were washed 3 times in 1X PBS at RT to remove staining solution. Whole-mount staining images were taken using Keyence BZ-X710 light microscope and thereafter samples were processed for resin embedding followed by sectioning. Processing of samples began with refixation in in 4% PFA solution overnight, followed by embedding in JB4 resin (Polysciences, Inc). Solidified resin blocks were sectioned (8-10$\mu$m) using Microtome Rotatif, HM335E. Sections were dried overnight and imaged. Counterstaining was done by dipping slides in Eosin for 1-2 seconds followed by immediate washing. Stained sections were dried at RT, mounted on coverslips using Entellan reagent (Merck Millipore), and imaged using a microscope.

### 2.2.12 Plasmids

Flag-tagged human *Cnot9* was cloned into pcDNA3. *Cnot9*$^{mut4}$ (H58A, F60A, A64Y, V71Y) and *Cnot9*$^{GW182neg}$ (P165G, Y203A, R205A, R244A) constructs were generated by point mutagenesis. Briefly, primers (tabulated at the end of this section) incorporating mutations were used to PCR amplify parent plasmid (pcDNA3-*Cnot9*) catalyzed by Phusion polymerase (Invitrogen) following manufacturer's protocol. PCR reaction mixture was digested by Dpn1 enzyme for 3 hours at 37$^o$C. Post digestion, a small fraction was run on 1% Agarose gel to confirm PCR product size and quality. Thereafter, ligation was done using Solution I from DNA ligation kit (Takara) supplemented with 0.5$\mu$l of T4 Polynucleotide Kinase (10U/$\mu$l) and 0.2$\mu$l of ATP (100mM) for 20$\mu$l reaction. Ligation was done for 1 hour at 16$^o$C followed by transformation into competent DH5a strain of *E. coli*. Transformants were selected on agar plates supplemented with antibiotics. Plasmid isolation was done using plasmid miniprep kit from Qiagen following manufacturer's instructions. Incorporated mutations were confirmed by restriction digestion and DNA sequencing. Mouse *Lefty1* 3'-UTR (425 bp), *Lefty2* 3'-UTR (1290 bp), *c-myb* 3'-UTR (1243 bp), also cloned into the pGL3 control vector (Promega) using cDNA library of E7.5 stage mouse embryos. Primers with restriction sites were designed and used for PCR based amplification. PCR products were digested using restriction enzymes, purified using Qiagen PCR purification kit, and subsequently ligated using DNA ligation Kit (Takara). Transformation, drug selection and plasmid preparation were done as mentioned above. Plasmids were confirmed by restriction digestion and DNA sequencing. *p21(cdkn1a)* 3'-UTR in pGL3.0 control vector was generated by Dr. Akinori Takahashi in the laboratory. Flag-tagged full-length silencing domain of human *Tnrc6c* (1260-1690 amino acids) was PCR amplified from RIKEN cDNA library (KIAA1582) and cloned into pcDNA3.0 vector.

| Mutant | Primers (5' - 3') | Restriction site gen. | Mutation gen. |
|---|---|---|---|
| *Cnot9*$^{mut4}$ | ATGCTGTGGGCTTCAGCTGGTACTATT | Pvu II | H58A, F60A |
| | GGGTGCAAGGTCAGGAACAGATTCT | | |
| | GGTACCATTTACGCACTTTTACAGG | Kpn I | A64Y |
| | AGCTGAAGCCCACAGCATG | | |
| | GCACTTCTGCAGGAAATTTACAATATTTATCCA | Pst I | V71Y |
| | GTAAATGGTACCAGCTGAAGCCCA | | |
| *Cnot9*$^{GW182neg}$ | ATATGTCAGACGGCTGAGGCTTTCTCC | Bgl II | Y203A, R205A |
| | ATAAGCCAAACCAGTGTCATCTAACAGGATCTTCTG | | |
| | CTTTCAGATAACCCCGCGGCACGTGAA | Sac II | R244A |
| | TCGAAGGTAACATCTCACTACATGCTTCAGCAG | | |
| | GAAATTATCGGTTTATGTCTACGAATTATG | Acc I | P165G |
| | TGTTGTTAATAAAAAGTTGATTACTTCTTGTTC | | |

### 2.2.13 Generation of CNOT9 KO HeLa cells using CRISPR/Cas9 technique

Guide RNA sequences were designed using CHOP-CHOP (https://chopchop.cbu.uib.no/), a web-based interface provided by the University of Bergen, Norway. Insert oligonucleotides targeting exon1 of human *Cnot9* were: 5'-CACCGGCACAGCCTGGCGACGGCTG-3' and 5'-AAACCAGCCGTCGCCAGGCTGTGCC-3'. These complementary oligos were annealed and cloned into pSpCas9(BB)-2A-Puro vector using the following method (Ran et al., 2013).

#### Vector [pSpCas9(BB)-2A-Puro] processing

The following reaction was prepared and incubated at 37$^o$C for 30 minutes.

| Sl. No | Particulars | Volume |
|---|---|---|
| 1 | Vector DNA (1$\mu$g/$\mu$l) | 1$\mu$l |
| 2 | Bbs1 enzyme (NEB) | 1$\mu$l |
| 3 | 10x NEB Buffer 2.1 | 2$\mu$l |
| 4 | RNase free water | 16$\mu$l |
| Total | | 20$\mu$l |

Upon conclusion, 0.5$\mu$l of Calf Intestinal Alkaline Phosphatase (CIAP) was added and incubated for 30 minutes at 50$^o$C to hydrolyze 5' phosphate group. Thereafter, solution was incubated at 70$^o$C for 10 minutes for CIAP inactivation. Vector DNA was purified using Qiagen PCR purification kit, eluted in 50$\mu$l of MQ water, and stored on ice until ligation step.

#### Phosphorylation and annealing of oligo(s)

Oligonucleotide sequences were annealed and phosphorylated in the following manner:

| Sl. No | Particulars | Volume |
|---|---|---|
| 1 | 100$\mu$M Oligo #1 | 5$\mu$l |
| 2 | 100$\mu$M Oligo #2 | 5$\mu$l |
| 3 | 10X T4 Polynucleotide Kinase Buffer | 2$\mu$l |
| 4 | 100mM ATP | 0.2$\mu$l |
| 5 | T4 Polynucleotide Kinase | 0.5$\mu$l |
| 6 | RNase free water | 7.3$\mu$l |
| Total | | 20$\mu$l |

Solution was incubated at 37$^o$C for 30 mins followed by another incubation at 95$^o$C for 5 minutes. 95$^o$C incubation was done by dropping sealed Eppendorf tube into a beaker full of boiling water. After 5 minutes, heater was turned off and water was allowed to cool to RT.

#### Ligation

Ligation was setup at 16$^o$C for 1 hour by adding reagents in the following manner:

| Sl. No | Particulars | Volume |
|---|---|---|
| 1 | Bbs1 digested plasmid vector | 50ng |
| 2 | Phosphorylated and annealed oligo | 2$\mu$l |
| 3 | Ligation Solution I | 6$\mu$l |
| 4 | RNase free water | ≈1-2 $\mu$l |
| Total | | ≈10-12$\mu$l |

5-6$\mu$l of ligation mix was used for transformation into competent DH5a strain of *E. coli*. The above method is adapted from a previously published protocol (Ran et al., 2013).

Plasmids were confirmed by DNA sequencing. HeLa cells were transfected using pSpCas9(BB)-2A-Puro vectors containing guide RNAs that target *Cnot9* genomic locus. As a guideRNA control, pSpCas9(BB)-2A-Puro vector targeting a region of EGFP gene was used. 24 hours post transfection, cells were treated with 2.5 $\mu$g/ml of puromycin for 3 days to select transfected cells. After 3 days, cells were collected, and seeded in three 10 cm culture dishes at a density of 300 cells per dish. Media was changed every 2 days. After 10-12 days of culture, small colonies were picked and seeded into individual wells of a 48 well plate and propagated further. Knockout clones were confirmed by DNA sequencing and Western blotting.

### 2.2.14 Lentiviral delivery of CNOT9 into placental lineage for rescue experiment

Mouse *Cnot9* coding sequence was amplified from E9.5 embryo cDNA library and cloned into pLV-CAG1.1 vector (kindly provided by Dr. Masahito Ikawa, Osaka University) at BamH1 and Xho1 restriction sites. Control lentivirus pLV-CAG1.1-EGFP along with packaging plasmids pMDLg/pRRE, pRSV-Rev, and pVSVG were also kindly provided by Dr. Masahito Ikawa. Virus particles were produced in culture supernatants of HEK293T cells transfected with lentiviral plasmids. Supernatant was enriched by ultracentrifugation and virus concentration was determined by ELISA for p24 protein using RETROtek Zeptometrix kit. 2$\mu$l aliquots of virus particles were prepared and stored at -80$^o$C until use.

For obtaining blastocysts, ≈28-day old females were super-ovulated by intraperitoneal injection of 7.5U pregnant mare serum gonadotropin (PMSG), followed by administration of 7.5U of human chorionic gonadotropin (HCG) after 47hours. Post HCG injection, mice were paired with stud males. Plug positive female mice were used for isolation of E2.5 stage (morula) embryos by flushing oviducts with M2 culture media supplemented with antibiotics. E2.5 embryos were cultured in-vitro in KSOM media for approximately 24 hours allowing them to form blastocysts. Prior to virus transduction, zona pellucida were removed by treatment with acidic Tyrode solution (Sigma). Equal number of zona-removed blastocysts were transduced by CNOT9 and EGFP expressing virus for 4 hours at 37$^o$C. Thereafter, embryos were transplanted into 2.5-day pseudo-pregnant ICR female mice for further development. Approximately 6-7 days later pregnant ICR females were euthanized and lentivirus transduced placenta were examined for biochemical analysis.

### 2.2.15 Statistical analysis

Unpaired, two-tailed Student's t-test was used for data analysis. Bar graphs represented Mean ± standard deviation (SD) and p-values $< 0.05$ were deemed statistically significant.

## 2.3 Results

### 2.3.1 Loss of CNOT9 causes defects in embryonic gastrulation

Generation of *Cnot9*$^{+/lacZ}$ mice has previously been described in Materials and Methods (Section 2.2.1). Loss of one *Cnot9* allele showed no detectable phenotype under normal breeding conditions compared to wild-type controls. However, upon crossing male and female *Cnot9*$^{+/lacZ}$ mice, no *Cnot9*$^{lacZ/lacZ}$ (KO) mice were born. Furthermore, no KO embryos could be genotyped at E14.5, suggesting early embryonic lethality resulting from loss of CNOT9. To identify the timing of embryonic lethality and onset of phenotypic defect in KO embryos, we investigated gastrulation stage embryos, 7 to 10 days post coitum. As seen in Fig. 2.2A and Fig. 2.2B, no obvious differences in KO embryo morphology were observed during early Bud/Headfold stages (E7.25 - E7.75) and early somite stages (E7.75 - E8.0), compared to littermate controls. Onset of phenotypic defects occurred during intermediate and late somite stages (E8.0 - E8.5) as KO embryos showed growth retardation in regions of the developing embryo-proper (Fig. 2.2C).

During E9.5 stage of development, KO embryos exhibited more severe growth defects characterized by small size, perturbed developmental pace indicated by delay in embryo curling, and lack of blood vessels within visceral yolk-sac regions (Fig. 2.2D). Contrary to previous stage of development, KO embryos exhibited higher cleaved PARP expression compared to WT littermates, suggesting cell death within these embryos (Fig. 2.2D). At E10.5 stage of embryonic development, KO embryos continued to display defects in terms of embryo size and morphology and showed sustained increase in cleaved PARP expression compared to WT littermate controls (Fig. 2.2E). Genotype

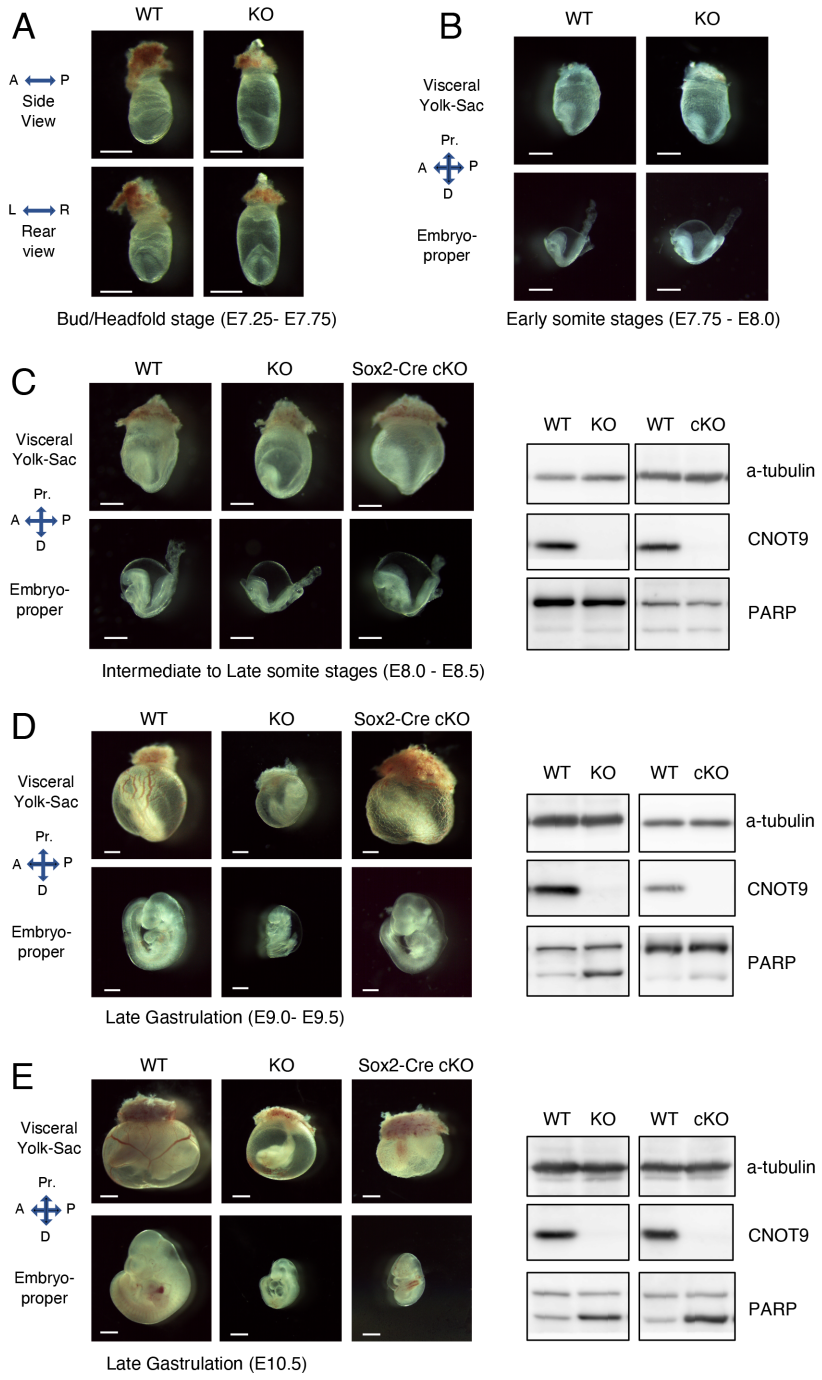


**Figure 2.2: Phenotype of CNOT9 KO and Sox2-Cre cKO embryos** Embryo morphology and size evaluation of CNOT9 KO embryos alongside WT controls during (A) Bud and Headfold stages (E7.25 – E7.75) (B) Early somite stages (E7.75 – E8.0) (C) Intermediate to Late Somite stages (E8.0 – E8.5) (D) and (E) Late gastrulation stages (E9.0 – E10.5). Western Blotting for PARP (lower band) indicates extent of tissue death in KO or cKO embryos compared to WT control. Scale: 500$\mu$m

of KO embryos were confirmed both by PCR based genotyping and western blotting.

### 2.3.2 CNOT9 KO embryo phenotype primarily contributed by epiblast lineage

Defects originating in placental lineage (trophectoderm derived cells) during stages of embryonic gastrulation and thereafter, can have a profound effect on development and viability of embryos (Perez-Garcia et al., 2018). We therefore performed histological analysis on placental regions during E8.5 and E9.5 stages and found that KO embryos possessed significantly smaller sized placenta compared to WT and HE littermate controls (Fig. 2.3A, 2.3B).

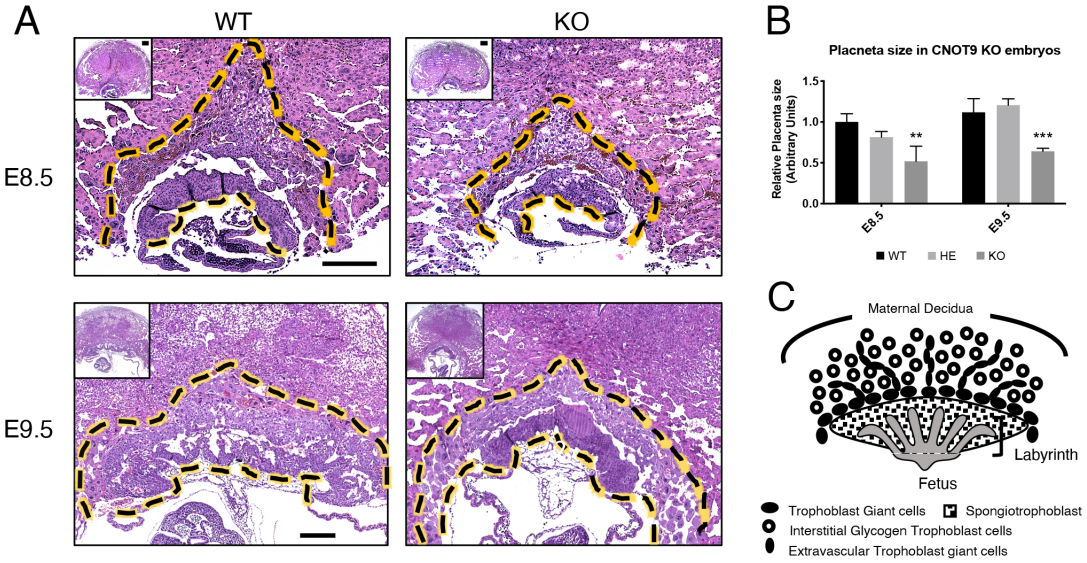


**Figure 2.3: Placenta in E8.5 and E9.5 stage CNOT9 KO embryos** (A) Placental morphology at E8.5 and E9.5 stages examined by H-E staining of paraffin embedded tissue (B) Quantification of placenta size in CNOT9 KO embryos compared to HE and WT controls (Statistical significance indicated by * $p<0.05$, ** $p<0.01$, *** $p<0.001$, values are Mean ± SD, n=3) (C) Schematic representation of placental lamination during E8.5-E9.5 stage. Scale: 250$\mu$m.

For the purpose of visual ease, the relevant region of placenta lies within yellow broken lines (Fig. 2.3A). Furthermore, a schematic representation of placental layers during this developmental stage is shown in Fig. 2.3C. A reduced or poorly developed placenta may however be caused due to an overall impairment in embryo development and differentiation. To test this observation from the standpoint of direct vs. indirect outcome of CNOT9 loss, we performed experiments using $Cnot9^{flox/flox}$ mice, as described in Materials and Methods (Section 2.2.1). $Cnot9^{flox/flox}$ mice were crossed with Sox2-Cre mice (B6.Cg-Edil3Tg(Sox2-cre)1Amc/J, Jackson Labs, USA) to generate epiblast specific knockout (cKO) mice. Similar to KO mice, no cKO mice were born suggesting embryonic lethality. A total of 32 neonate mice (across 5 batches of litters)

were sampled, yet no cKO mice could be genotyped (Table 2.2). Analysis of gastrulating cKO embryos during intermediate and late somite stages indicated no characteristic morphological differences between WT controls (Fig. 2.2C). However, during late gastrulation stages, defects in cKO embryos began to surface, initially in terms of yolk-sac vasculature, followed by growth arrest and cell death in embryo-proper (Fig. 2.2C and 2.2D).

| Genotype | Observed mice number | Expected mice number* |
|---|---|---|
| $Cnot9^{flox/+}$; +/+ (WT) | 13 | 8 |
| $Cnot9^{flox/-}$; +/+ (HE) | 6 | 8 |
| $Cnot9^{+/-}$; Cre/+ (HE) | 13 | 8 |
| $Cnot9^{-/-}$; Cre/+ (cKO) | 0 | 8 |
| Total | 32 | 32 |

**Table 2.2: Genotype assessment of CNOT9 cKO mice** Genotype frequency of 3-week-old mice across 5 independent litter sets generated from crosses between $Cnot9^{flox/flox}$ females and $Cnot9^{flox/+}$ Sox2-Cre males. *: Expected Mendelian frequency in case of complete rescue of phenotype.

### 2.3.3 Overexpression of CNOT9 in placental lineage leads to embryonic lethality

Trophoblast specific lentivirus based gene delivery has been successfully shown to complement placental defects and in some cases embryonic lethality of knockout mice (Okada et al., 2007). Prior to usage of Sox2-Cre mediated conditional depletion of CNOT9, we tested lentiviral transduction of *Cnot9* into trophectoderm lineage in an attempt to rescue KO embryo phenotype. A detailed description of plasmid construction and virus generation is discussed in Materials and Methods section. As shown in Figure 2.4A, we observed very precise expression of EGFP, exclusively within placental regions of embryos timed to E9.5 stage of embryonic development. Virus induced expression of CNOT9 and EGFP was confirmed by western blotting and qRT-PCR based analysis of placental tissue lysates as shown in Figure 2.4B and Figure 2.4C, respectively. For the purpose of surrogacy, 4 ICR dams were transplanted with 28 blastocysts each (14 blastocysts transduced by pLV-EGFP and other 14 transduced by pLV-CNOT9). Based on experiment summary indicated in Table 2.3, more than 90% (10/11] of pLV-mCNOT9 transduced blastocysts did not have any adjoining embryo-proper tissue. This suggests that overexpression of CNOT9 within trophoblast lineage is likely to affect differentiation of embryo proper. This result was also supported by biochemical evidence of elevated p53 protein levels in CNOT9 transduced placenta compared to EGFP transduced controls (Figure 2.4D). Further investigation needs to be done to confirm this observation.

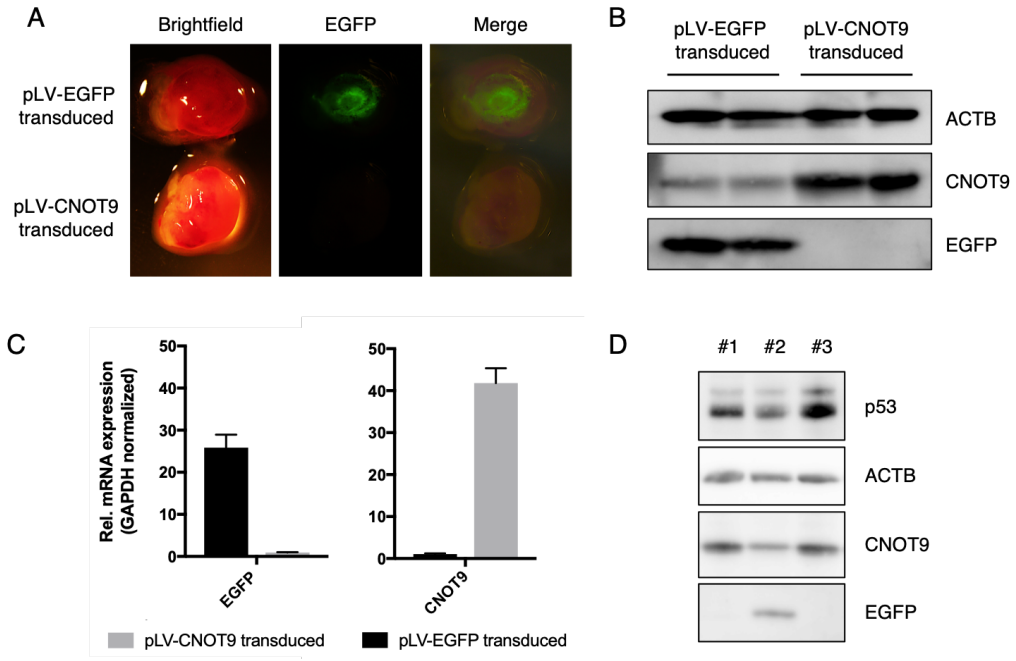


**Figure 2.4: Gene targeting strategies adopted for generation of transgenic mice** (A) LacZ knock-in mouse by targeting exon1 of *Cnot9* genomic locus (B) CNOT9 conditional mouse by targeting exons 2 and 3 of *Cnot9* genomic locus.

| Dam no. | Embryos Implanted | E9.5 embryo condition | E9.5 placenta condition | Remarks |
|---|---|---|---|---|
| 1 | - | - | - | Dead on following day |
| 2 | 0 | - | - | No embryos implanted |
| 3 | 2 | Normal | EGFP +ve | pLV-EGFP transduced |
| 4 | 12 | Nonexistent | EGFP -ve | pLV-CNOT9 transduced |
| | | Nonexistent | EGFP -ve | pLV-CNOT9 transduced |
| | | Very small | EGFP -ve | pLV-CNOT9 transduced |
| | | Nonexistent | EGFP -ve | pLV-CNOT9 transduced |
| | | Normal | EGFP -ve | pLV-CNOT9 transduced |
| | | Nonexistent | EGFP -ve | pLV-CNOT9 transduced |
| | | Nonexistent | EGFP -ve | pLV-CNOT9 transduced |
| | | Very small | EGFP -ve | pLV-CNOT9 transduced |
| | | Normal | EGFP +ve | pLV-EGFP transduced |
| | | 1 embryo only | EGFP+ve, EGFP-ve | Two fused placentae |
| | | Very small | EGFP -ve | pLV-CNOT9 transduced |
| | | Normal | EGFP +ve | pLV-EGFP transduced |
| | | Nonexistent | EGFP -ve | Two fused placentae |

**Table 2.3: Placental CNOT9 overexpression leads to loss of embryo proper.** Summary of phenotypes observed in E8.5–E9.5 stage embryos developed from blastocysts transduced by pLV-EGFP and pLV-CNOT9 viruses

### 2.3.4 *Cnot9* expression pattern during embryonic gastrulation

*Cnot9*$^{+/lacZ}$ embryos between E7.5 to E9.5 stages were used to perform $\beta$-galactosidase ($\beta$-gal) staining indicative of spatiotemporal expression pattern of *Cnot9* (Figure 2.5).

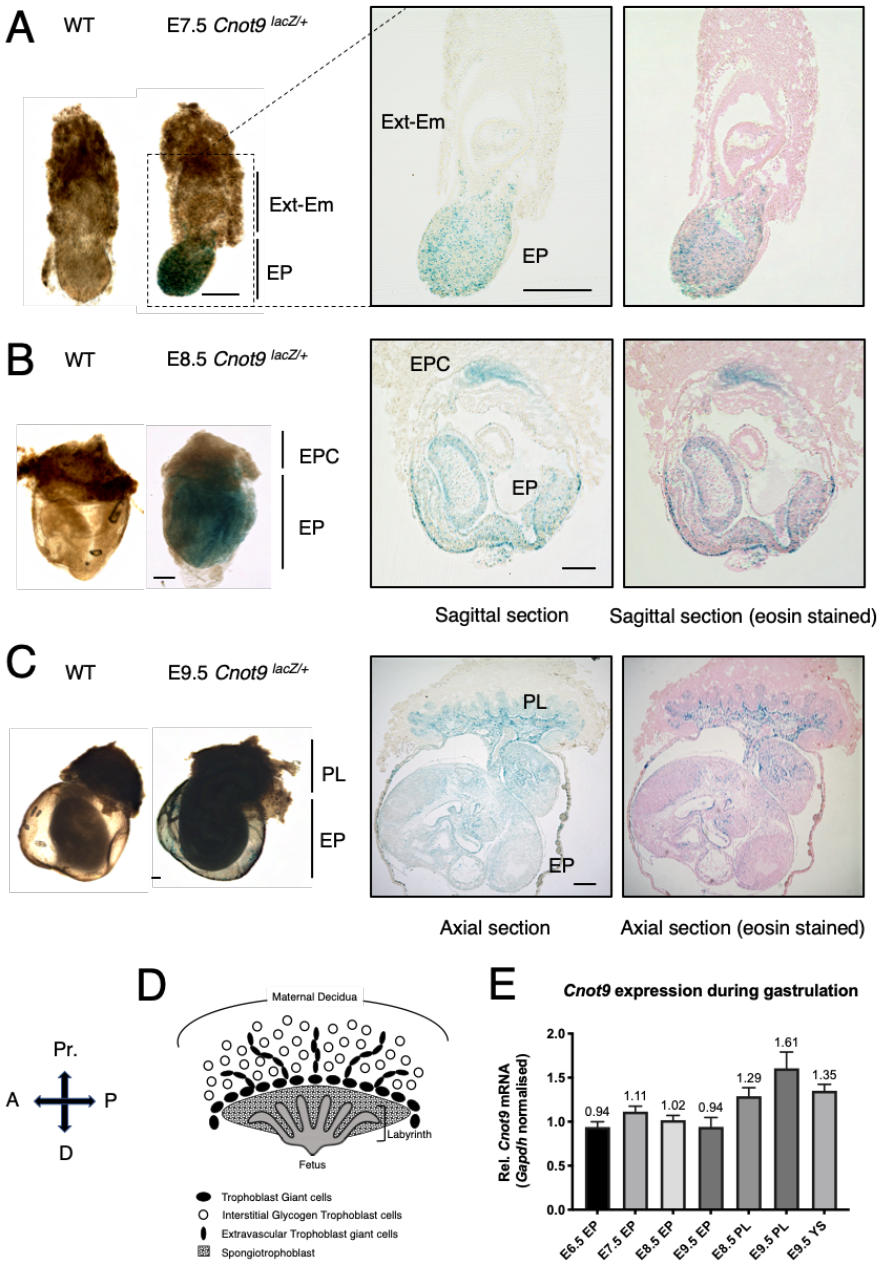


**Figure 2.5: spatiotemporal expression pattern of *Cnot9* during gastrulation** LacZ staining of *Cnot9*$^{+/lacZ}$ embryos at (A) E7.5 (B) E8.5 (C) E9.5 stages of gastrulation. (D) Schematic representation of various cell types in E8.5- E9.5 placenta. (E) Mean *Cnot9* mRNA expression levels, relative to *Gapdh*, in various embryo regions. Scale: 250$\mu$m, Ext-Em: extra embryonic, EPC: Ectoplacental cone, EP: Embryo-proper, PL: Placenta, YS: Yolk-sac, A: Anterior end, P: Posterior end, Pr.: Proximal end, D: Distal end.

At E7.5 stage, $\beta$-gal staining was predominantly seen within the epiblast region that would eventually contribute to form the embryo-proper (Figure 2.5A). At 8.5 stage, $\beta$-gal staining was seen in various parts of the embryo-proper that included neuroepithelium, the trunk region, and the caudal region of embryo. More importantly, $\beta$-gal staining was also seen in extra-embryonic yolk-sac and within the ectoplacental cone (EPC) region of the embryo (Figure 2.5B). A day later, E9.5 stage embryos showed strong $\beta$-gal staining within labyrinthine and spongiotrophoblast regions of the placenta relative to weak and punctuated signal from regions of the embryo-proper (Figure 2.5C). A schematic representation of placental layers during E9.5 stage is depicted for visualization of lacZ expression within the placenta (Figure 2.5D). In addition to lacZ staining, *Cnot9* mRNA expression (relative to Gapdh) at various regions of gastrulating WT embryos, was determined by qRT-PCR analysis (Figure 2.5E). In agreement with $\beta$-gal staining pattern, *Cnot9* expression was found to be approximately $> 1.5$ higher in E9.5 placenta compared to embryo-proper. Besides E9.5 stage, other stages of gastrulation, showed nearly uniform expression levels of *Cnot9* mRNA.

### 2.3.5 Gene expression in gastrulating embryos regulated by CNOT9

Phenotype observed upon in KO gastrulating embryos served as a framework for investigating gene expression control mediated by CNOT9. In an attempt to investigate molecular function of CNOT9, we performed RNA-Sequencing analysis of three independent E8.0-E8.5 stage WT and KO samples. From a total of 15534 candidates, only 384 protein coding genes were upregulated >2-fold, while another 338 were downregulated >2-fold in KO embryos.

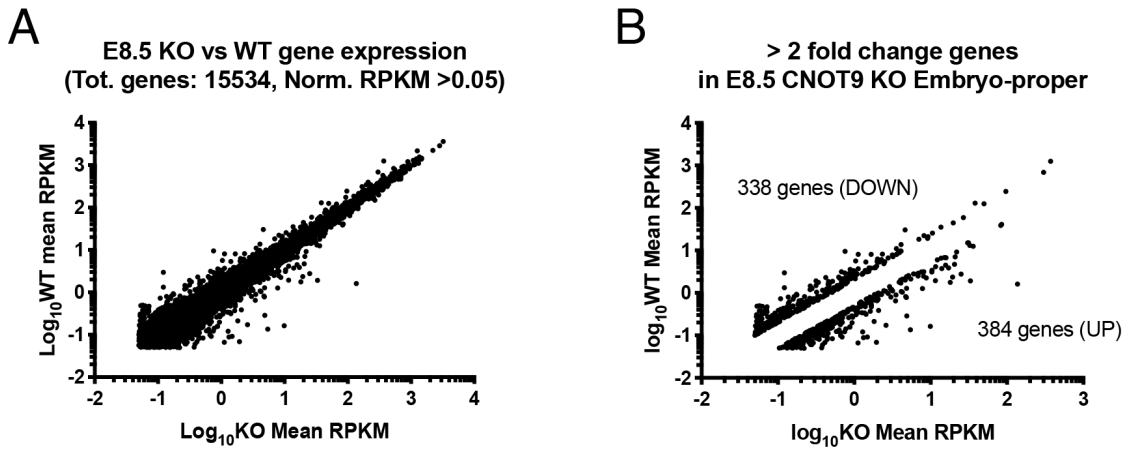


**Figure 2.6: Number of upregulated and downregulated targets in KO embryos** identified by RNA-Seq Dot-plots representing (A) overall gene expression pattern in WT and KO embryos. (B) more than 2-fold upregulated and downregulated targets.

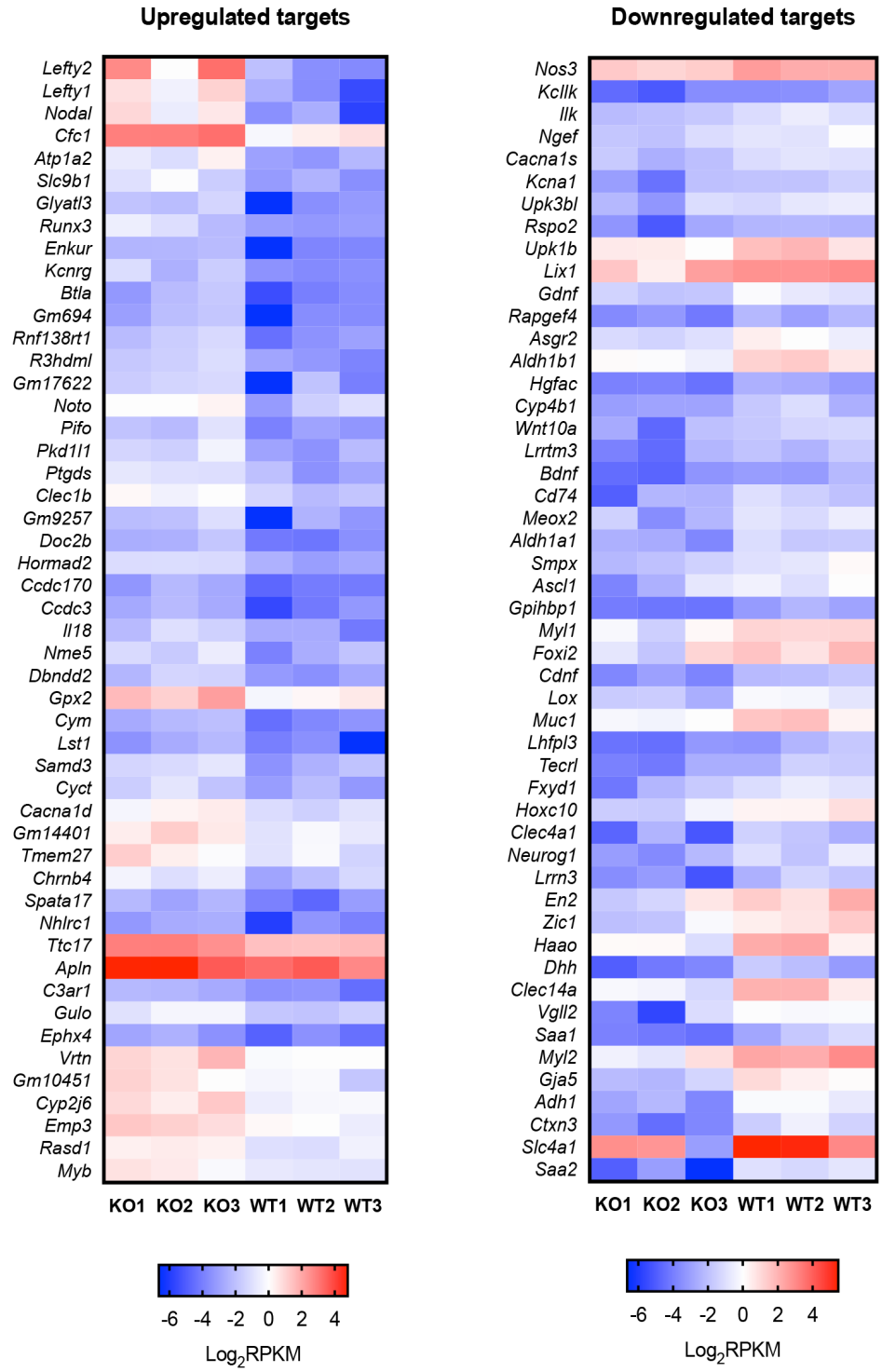


**Figure 2.7: Top 50 upregulated and downregulated targets of CNOT9 in embryos** Heat-map indicating top 50 upregulated (left) and downregulated (right) targets in three independent sets of WT and KO embryos. Values are $Log_2$RPKM ± SD [n=3]

This statistic is based on normalized RPKM scores (Figure 2.6A and 2.6B). Top few upregulated targets include: Lefty2, *Lefty1*, *Nodal*, *Crypto-1*, and *Noto* that have previously been known to play profound roles in embryonic gastrulation (Meno et al., 1996, Meno et al., 1998, Saijoh et al., 1999, Lowe et al., 2001). Top 50 of these targets have been represented in the form of a heatmap in Figure 2.7. In-silico results were further validated by qRT-PCR based analysis using cDNA samples obtained from E8.5 stage WT and KO embryos (Figure 2.8A). With the exception of *Noto*, other targets that showed upregulation at E8.5 stage, also showed either a trend or a significant increase during E7.5 stage. This suggests that despite the lack of phenotypic defects during E7.5 stage, molecular events leading to abnormal embryo phenotype has already perpetuated within KO embryos. In addition to validation of individual targets, we also performed pathway analysis using gene-set enrichment analysis (GSEA) algorithm made available by the Broad Institute, USA. GSEA clearly identified Nodal and TGF-$\beta$ signaling pathways to be affected in KO embryos, thereby summarizing the nature of gastrulation defects (Figure 2.8B). In addition to upregulated targets involved in gastrulation, E8.5 stage KO embryos also showed higher expression for *Oct4* and *c-myb* mRNAs (Figure 2.8A).

A

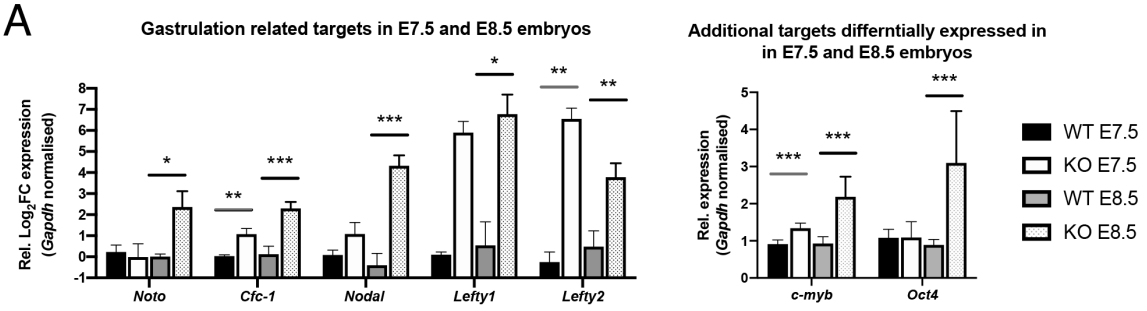


B

| Gene Set Name/Description | # Genes in Gene Set (K) | # Genes in Overlap (k) | k/K | p-value | FDR q-value |
|---|---|---|---|---|---|
| Regulation of signaling by NODAL | 11 | 3 | 0.2727 | 7.41E-07 | 2.50E-03 |
| Signaling by NODAL | 20 | 3 | 0.15 | 5.07E-06 | 8.56E-03 |
| TGF-beta signaling pathway | 85 | 4 | 0.0471 | 1.33E-05 | 1.50E-02 |
| Genes defining inflammatory response | 200 | 5 | 0.025 | 2.26E-05 | 1.91E-02 |

**Figure 2.8: Validation of upregulated targets and pathway identification** (A) Relative mRNA expression levels of upregulated targets in E7.5 and E8.5 stage KO embryos for (left) gastrulation targets (right) additional targets involved in embryo development. Values are Mean $\pm$ SD [n=5, $p < 0.05$ (*), $p < 0.01$ (**), $p < 0{,}001$ (***)] Grey and black bars indicate comparison between WT and KO embryos at stages E7.5 and E8.5, respectively. (B) List of top upregulated pathways in CNOT9 KO embryos mainly involved in TGF-$\beta$ signaling pathways influenced by Nodal and other competing ligands.

Downregulated targets mainly suggested retarded embryo growth and differentiation characterized by significantly reduced expression levels of *Myl2*, *Epo*, *Fgf8*, *Sox10* and Pax family members - *Pax1*, *Pax5* and *Pax7* (Figure 2.9). Top 50 downregulated targets have been represented as a heatmap in Fig. 2.7. Upon performing GSEA, downregulated targets did not clearly correspond to any specific signaling pathway (data not shown). A list of different primers used for qRT-PCR analysis has been listed in Table 2.4.

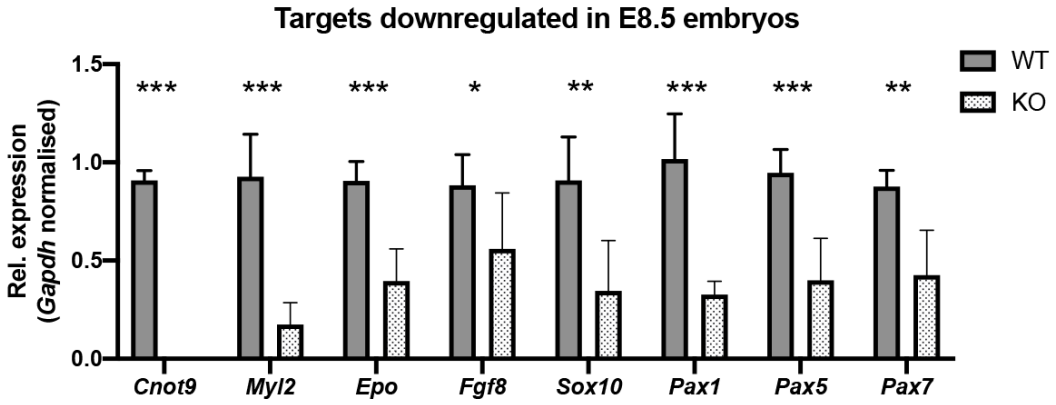


**Figure 2.9: Validation of downregulated targets in KO embryos** Relative mRNA expression levels of downregulated targets in E8.5 KO embryos. Values are Mean ± SD [n=5, $p < 0.05$ (*), $p < 0.01$ (**), $p < 0{,}001$ (***)]

| Sl. No | Target | Forward Primer (5'-3') | Reverse Primer (5'-3') |
|---|---|---|---|
| 1 | *Lefty1* | actcagtatgtggccctgcta | aacctgcctgccacctct |
| 2 | *Lefty2* | gccctcatcgactctaggc | agctgctgccagaagttcac |
| 3 | *Noto* | tgtttgcaaagcagcacaa | ttggaaccagatcctcacct |
| 4 | *Cfc1* | tgtgttctgggcagtttctg | cctagggcaccacagtct |
| 5 | *Nodal* | tggtagggaagacccacaac | tgccaagcatacatctcagg |
| 6 | *c-myb* | cctcaaagcctttaccgtacc | ctgtcttcccacaggatgc |
| 7 | *Oct4* | aagttggcgtggagactttg | tctgagttgctttccactcg |

**Table 2.4:** List of primers used for qRT-PCR based analysis

### 2.3.6 CNOT9 is core component of CCR4-NOT complex in gastrulating embryos

Before accessing the role of CNOT9 in mediating target mRNA decay, we wished to confirm its presence within the CCR4-NOT complex in gastrulating embryos. As shown in Figure 2.10, CNOT9 was immunoprecipitated (IP'd) by anti-CNOT3 antibody alongside other CCR4-NOT subunits such as CNOT1 and CNOT2, compared to Control IgG. Furthermore, GW182, a component of the miRNA-RISC complex was also IPed, implying interactions between the CCR4-NOT complex and the RISC complex in inducing miRNA mediated decay of target mRNA. 4EBP1 and a-tubulin served as controls for this assay.

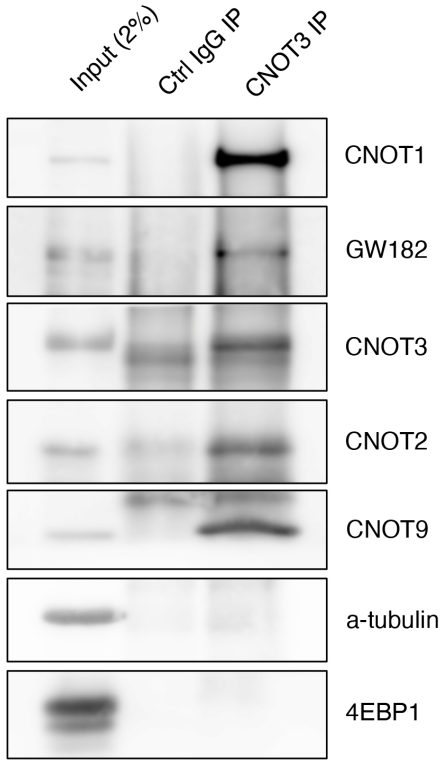


**Figure 2.10: CNOT9 is part of the CCR4-NOT complex during gastrulation.** Co-IP assay with anti-CNOT3 antibody on mouse embryo lysates IP'd CNOT9 and GW182.

### 2.3.7 Subcellular localization of CNOT9 in gastrulating embryos:

To examine subcellular localization of CNOT9 during gastrulation, we performed nuclear-cytoplasmic fractionation using E8.0 to E8.5 embryo lysates. As shown in Figure 2.11, majority of CNOT9 protein is localized within cytoplasmic fraction, likely to be bound to the CCR4-NOT complex. XRN1 protein is a well-known shuttling molecule and is therefore seen in both nuclear and cytoplasmic fractions with appreciable degree of

abundance. Histone H3 was used as control for nuclear fraction while Tubulin was used as cytosolic fraction control.

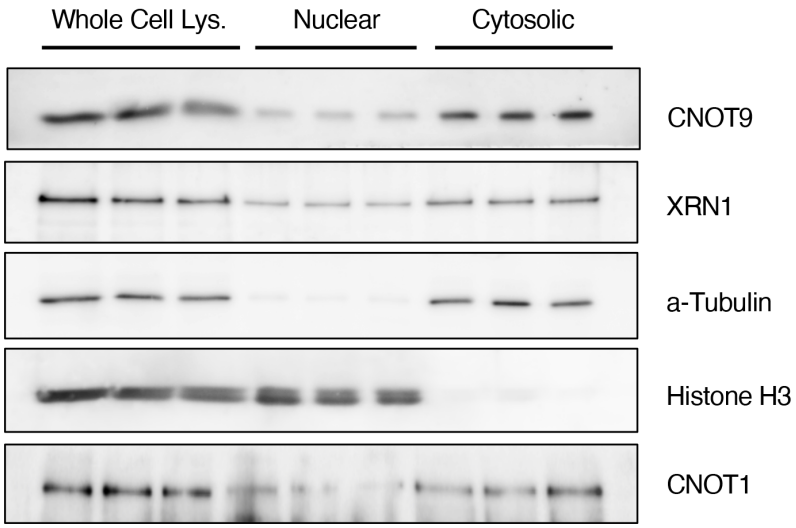


**Figure 2.11: Nuclear-Cytoplasmic fractionation of E8.0-E8.5 stage embryos**

### 2.3.8 CNOT9 contributes to *Lefty1/2* mRNA decay, in-vitro:

With the understanding of CNOT9 being a part of the cytoplasmic mRNA decay complex we hypothesized its function in facilitating decay of its targets. To investigate the role of CNOT9 in the context of mRNA decay, we pursued two candidate targets - *Lefty1* and *Lefty2*, as identified and validated in Section 2.3.5. One of the main reasons for picking these targets among others, is the presence of miRNA binding sites within respective 3'UTR elements that may facilitate mRNA decay, in-cis. Based on information available from TargetScan mouse database, a schematic representation of microRNA binding loci within 3'UTR of *Lefty1*, *Lefty2*,and *c-myb* mRNA is shown in Figure 2.12. We found that addition of these 3'UTR elements downstream of luciferase coding element, led to a significant reduction in luciferase activity relative to vector-only (pGL3.0) control (Figure 2.13). Furthermore, with the exception of *Lefty1* 3'UTR, *luciferase* transcripts conjugated with 3'UTR elements also saw a significant reduction in mRNA expression levels relative to vector-only controls (Figure 2.13).

In the next step, we investigated the role of CNOT9 in facilitating mRNA decay of luciferase reporters conjugated with individual 3'UTR elements. As seen from Fig. 2.14A, mRNA decay kinetics determined by ActinomycinD chase assay showed a clear stabilization of *Lefty2* 3'UTR conjugated reporter mRNA, whereas in the case of *Lefty1* 3'UTR, the stabilization was minimal. As expected, *c-myb* 3'UTR known to possess multiple microRNA binding sites, showed clear impairment in reporter mRNA decay in absence of CNOT9 (Figure 2.14A). *p21(cdkn1a)* 3'UTR conjugated reporter, used as a negative control, did not show any significant difference in decay kinetics (Figure 2.14A).

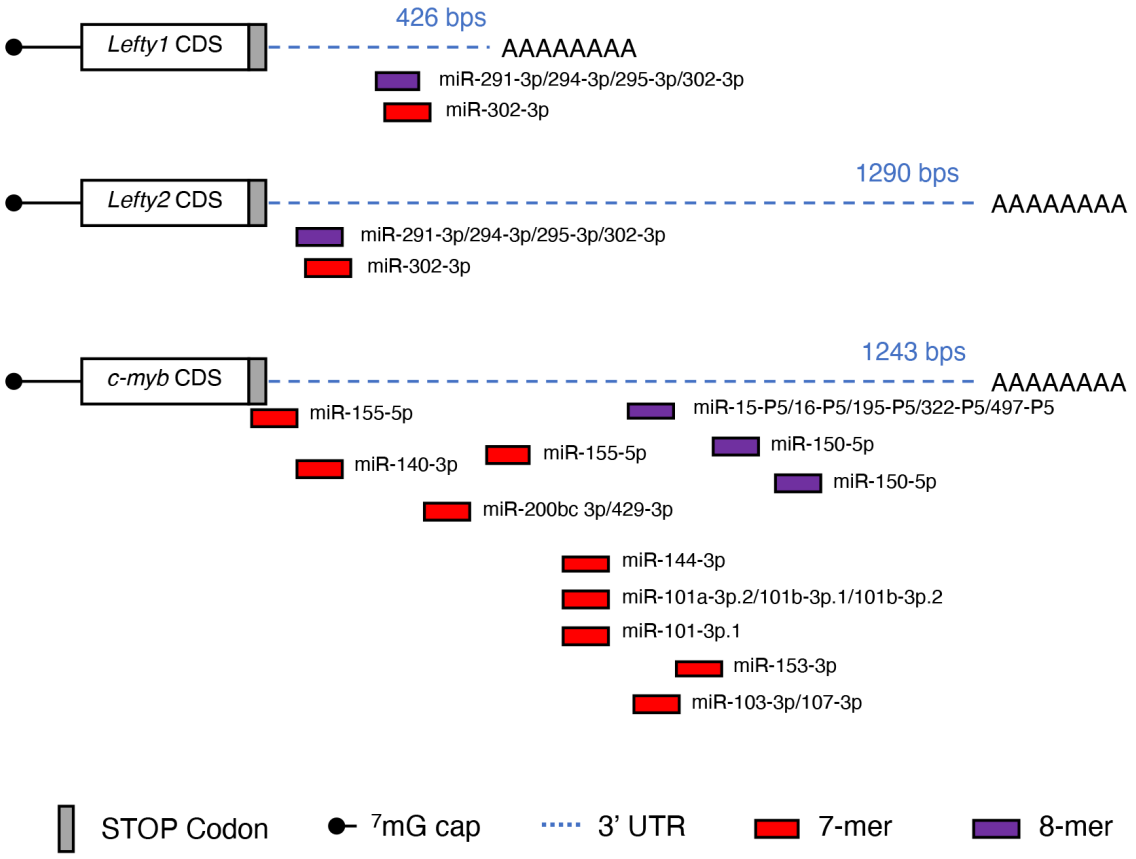


**Figure 2.12: microRNA binding sites within 3'UTR elements of *Lefty1/2* and *c-myb*** Schematic representation of 3'UTR elements for *Lefty1*, *Lefty2* and *c-myb* mRNA with positions of microRNA binding sites

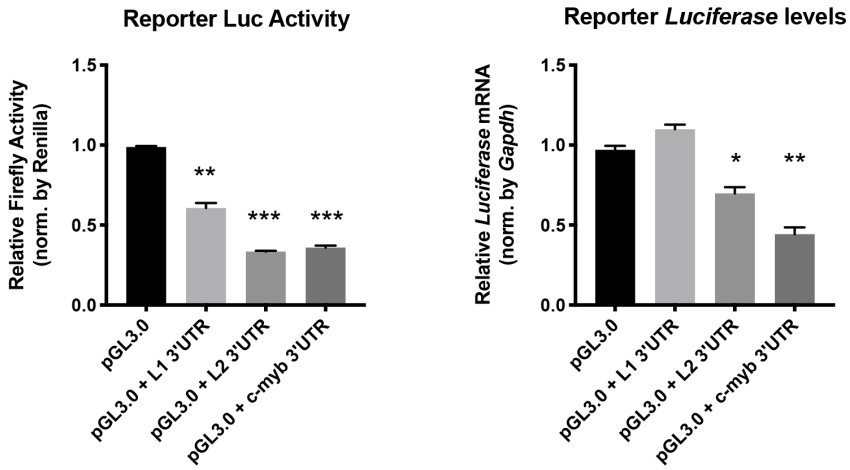


**Figure 2.13: Reporter luciferase assay to study contribution of cloned 3'UTR element** Luciferase activity (left) and mRNA expression (right) in cells transfected with *Lefty1* (L1), *Lefty2* (L2), or *c-myb* 3'UTR elements relative to control. Values are Mean ± SD [n=3, $p < 0.05$ (*), $p < 0.01$ (**), $p < 0{,}001$ (***)]

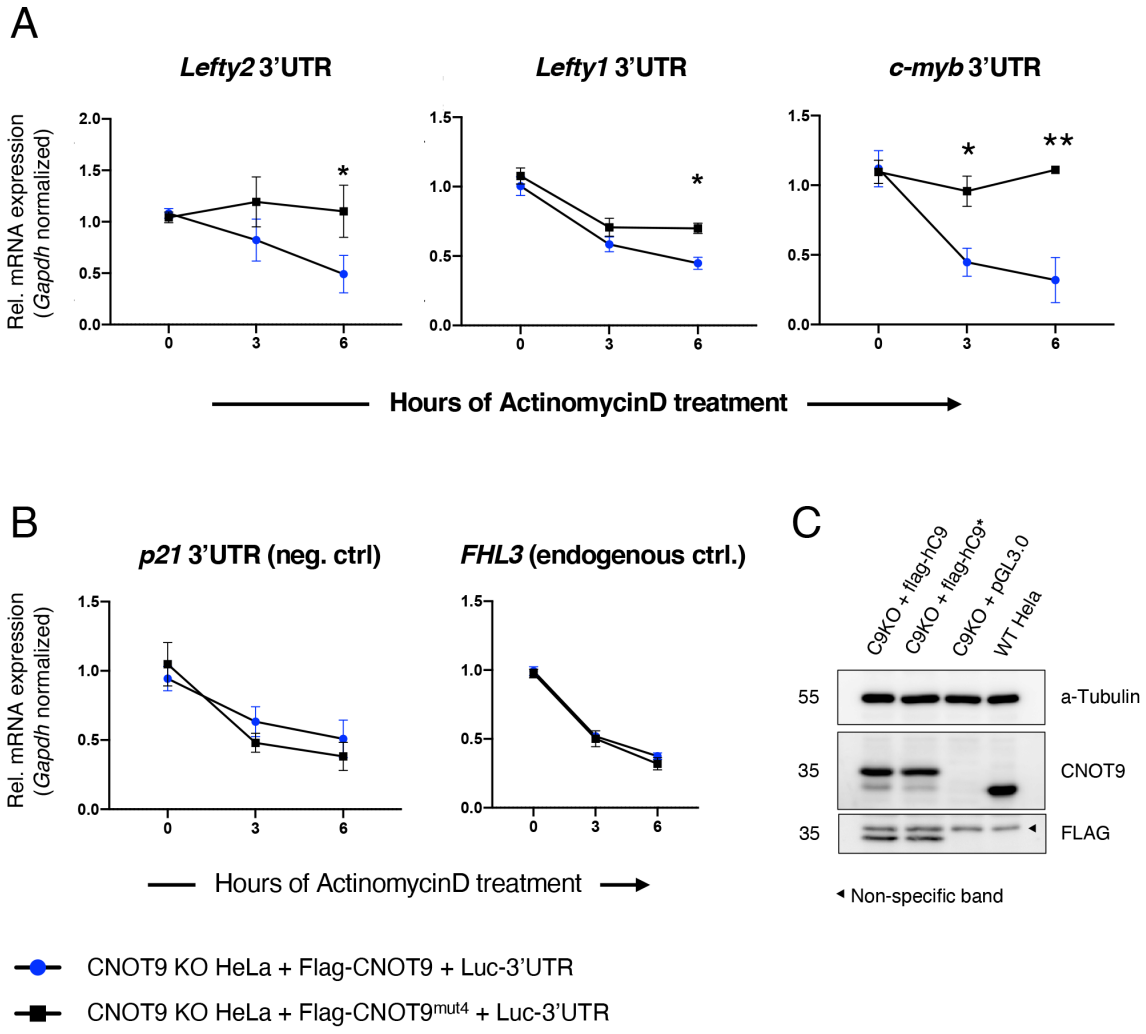


**Figure 2.14: Decay kinetics of Luciferase reporter conjugated with 3'UTR elements** (A) of *Lefty1*, *Lefty2*, and *c-myb* (B) of *p21* 3'UTR as non-target control and *Fhl3* as endogenous control. Blue dots represent relative expression of reporter mRNA in CNOT9 KO cells reconstituted with human CNOT9, whereas black dots represent expression in CNOT9 KO cells reconstituted with mutant CNOT9 (CNOT9$^{mut4}$) that cannot interact with CNOT1. (C) Western Blotting suing anti-CNOT9 and anti-FLAG antibodies to ensure equal expression of CNOT9 and CNOT9$^{mut4}$ proteins. Values are Mean ± SD [n=3, $p < 0.05$ (*), $p < 0.01$ (**)]

Similar decay kinetics for *Fhl3* mRNA (endogenous control) under different treatment conditions, implied uniform dose-response to ActinomycinD treatment (Figure 2.14B). Western blotting using anti-CNOT9 and anti-FLAG antibodies, confirmed equal extent of expression for wildtype and mutant forms of CNOT9 across different treatments (Figure 2.14C).

## 2.4 Discussion

The mammalian CCR4-NOT complex is profoundly involved in regulation of gene expression during early embryonic development. In this study we highlighted the physiological role of subunit CNOT9 in during embryonic gastrulation. CNOT9 knockout mice exhibited developmental abnormalities during mid-gastrulation stages (E8.0 to E8.5) leading to embryonic lethality at E9.5 stage. KO embryos showed a spectrum of defects that included reduced size, arrested growth, and pale colorization of embryo-proper, impaired yolk-sac vasculature, and significantly reduced placenta. Chorioallantoic fusion defects were not observed in E8.5 KO embryos (data not shown). To determine the weightage contribution of epiblast vs. trophoblast derived cells, we examined phenotype of embryos that underwent epiblast specific depletion of CNOT9. A marginal delay in onset of phenotype and timing of embryo lethality was observed in Sox2-Cre conditional knockout mice, suggesting that phenotypic defects in KO embryos were mainly contributed by cells originating from the epiblast lineage. In other words, wildtype trophoblast lineage cells could not adequately rescue the phenotype observed in whole body knockouts. As a first step towards examining function, we investigated embryo-wide expression pattern of *Cnot9* using whole-mount LacZ staining and qRT-PCR based analysis. During onset of gastrulation (≈E7.5), *Cnot9* was almost exclusively expressed throughout the epiblast. However, late in gastrulation, (E8.5 to E9.5) expression was also seen within extra-embryonic regions including regions of the developing placenta. It is worth noting that both E8.5 and E9.5 placental regions showed higher expression of *Cnot9* compared to relative levels within adjoining embryo proper. Unfortunately, due to timing and nature of defects, both KO and conditional knockout mice models limit our understanding of CNOT9 within a functional placenta. It would be worth investigating CNOT9 function within placental lineage via in-vitro trophoblast stem cell-based differentiation assays, or in-vivo models that can induce placenta specific depletion.

Prior to assessment of lineage contribution (trophoblast vs. epiblast) using Sox2-Cre mice model, we had attempted an alternate rescue approach involving lentivirus-based complementation (Okada et al., 2007). During standardization of this method, we made a serendipitous observation. CNOT9 overexpression specifically in trophoblast derived cells strongly correlated to non-viable development of adjoining embryo-proper, compared to EGFP overexpression controls. This suggests that, overexpression of CNOT9 also has phenotypic consequences on embryo development possibly due to aberrant activity of the CCR4-NOT complex. Further investigation in this direction shall offer a definitive molecular understanding on CNOT9 overexpression.

Phenotypic defects in KO embryos served as a template for investigating molecular function of CNOT9. E8.0 to E8.5 staged WT and KO embryos were pooled and subjected to bulk RNA Sequencing analysis. With biochemical validation, we observed significant upregulation in mRNA levels of *Lefty1/2*, *Nodal*, *Cfc-1*, among others that have previously been shown to have profound roles in embryonic development (Conlon et al., 1994, Meno et al., 1998, Meno et al., 1999, Yan et al., 1999).For instance, overexpression of *Lefty2* in zebrafish embryos blocks head and trunk mesoderm forma-

tion (Meno et al., 1999). *Cfc-1* overexpression in mice caused downregulation of genes involved in cardiac differentiation starting mid gastrulation stages whereas in chick, its gain-of-function led to suppression of posterior mesodermal fates while promoting anterior mesoderm development (Chu et al., 2005, Lin et al., 2016). *Nodal* overexpression has been shown to promote differentiation of mouse ES cells into endoderm and mesoderm lineages at the expense of neuroectoderm formation (Pfendler et al., 2005). Despite these findings, very little is known from the standpoint of post-transcriptional regulation of such transcripts and their consequences on embryo development. Having said that, one report showed *Lefty2* regulation via microRNA-127 in mouse ES cells (Ma et al., 2016). We therefore present a model where upregulation of gastrulation related transcripts can be studied with physiological relevance.

We focused on *Lefty1* and *Lefty2* transcripts mainly because of the extent of upregulation and presence of canonical microRNA binding sites in their 3'UTR elements. With the help of TargetScan database, we found that both mRNAs contain an AAGCACU element that serves as binding sites for miR-291-3p, miR-294-3p, miR-295-3p, miR-302-3p microRNA. We therefore cloned 3'UTR elements in pGL3.0 luciferase expression vectors. In WT HeLa cells, relative to vector only control, luciferase reporter expression and activity was significantly reduced when conjugated with *Lefty1* and *Lefty2* 3'UTRs. We further clarified that, in presence of human CNOT9 that cannot interact with the CCR4-NOT complex ($Cnot9^{mut4}$), mRNA decay of reporters containing *Lefty1* or *Lefty2* 3'UTRs was significantly compromised. Due to very high sequence conservation of human vs. mouse CNOT9 proteins (99.7%), and microRNA binding sites within UTR elements of mouse and human *Lefty* transcripts, we believe that a similar mechanism is likely to be present in humans.

Pale color of E8.5 - E9.5 stage KO embryos can be explained in terms of dysfunctional waves of primitive and definitive waves of erythropoiesis depending on *c-myb* expression. Downregulation of *c-myb* transcription has previously been reported to be imperative for erythropoietin (epo) induced differentiation (Todokoro et al., 1988). Furthermore, retinoic acid has been shown to suppress *c-myb* expression (Mandelbaum et al., 2018). CNOT9 is believed to be a retinoic acid inducible and therefore, in agreement with these ideas, our data suggests a strong correlation in terms of loss of CNOT9, elevation of *c-myb* expression, and reduced Epo expression (Hiroi et al., 2002).The difference however lies in the manner in which *c-myb* mRNA expression is elevated. The previous two evidences showed transcriptional control in *c-myb* expression, while our data suggests post-transcriptional control (via mRNA stabilization) in the backdrop of CNOT9 loss. Although defects in blood formation may be triggered by improper germ layer differentiation at earlier stages of gastrulation, we believe that elevation of *c-myb* mRNA can inhibit EPO induced erythroid differentiation in CNOT9 KO or conditional knockout mice. Further analysis using mice models for erythroid specific deletion can help elucidate this aspect of CNOT9 function.

CNOT9 KO embryos also show increased expression of *Oct4* mRNA. To understand such increase from the standpoint of mRNA decay, we cloned its 3'UTR element from E6.5 cDNA library. However, no effect of 3'UTR element was seen on reporter mRNA

expression levels in WT HeLa cells. Although we cannot provide an exact mechanism in support of its increase, we speculate that may be indirectly contributed by higher abundance of cells in undifferentiated state within KO embryos, compared to controls.

CNOT9 has regulatory roles within the complex that assist mRNA decay processes by interacting with CNOT1 and stimulating catalysis via CNOT6/6L and CNOT7/8 (Pavanello et al., 2018). This idea was further perpetuated by an in-vitro study of the human CCR4-NOT complex, that suggested stimulus dependent CNOT9 interaction with RBPs resulting in targeted mRNA decay (Raisch et al., 2019). In congruity with this idea we observed a similar trend in our RNA-Seq data. Only 722 (less than 5%) out of 15534 total detected protein coding genes underwent more than 2-fold significant change suggesting that developmental stimulus controls expression of very specific targets via CNOT9, leaving a fraction of them unaffected.

# Chapter 3

# Molecular interactions of mammalian CNOT9 protein

## 3.1 Motivation

This chapter revisits the current molecular model that supports CNOT9 as a catalyst in mediating interactions between CNOT1 and TNRC6 (GW182) family of proteins, thereby promoting microRNA mediated translation suppression and mRNA decay (Fabian et al., 2011, Huntzinger et al., 2013, Chen et al., 2014, Mathys et al., 2014). Key highlights of these studies relevant for our research have been tabulated in Table 3.1

Although the above concepts are well supported by crystal structure analysis and biochemical evidence, a few questions pertaining to protein-protein interactions remain unaddressed. The following two observations from previous studies prompted us to readdress this topic:

1 Mutant CNOT1 $^{K1426S,\ G1451Y,\ R1458A,\ Q1549A}$ and
CNOT1 $^{K1426S,\ G1451Y,\ R1458A,Q1549A,\ I1423D}$ that cannot bind CNOT9, interacted with SD of TNRC6 proteins with comparable affinity relative to wild-type CNOT1 protein (Chen et al., 2014). This contradicts the idea that interaction of TNRC6s with CNOT1 predominantly occurs at the DUF3819 domain that is bound to CNOT9 (Huntzinger et al., 2013, Chen et al., 2014).

2 CNOT9 was shown to interact with SD of TNRC6 proteins only when bound to CNOT1 (Chen et al., 2014). This was supported by lack of interactions between CNOT9 $^{H58A,\ F60A,\ A64Y,\ V71Y}$ (CNOT1 binding mutant) and SD of TNRC6, in HEK293T cells (Chen et al., 2014). However, another study performed in the same cell line, claimed possibility of direct interactions between CNOT9 and a fragment of TNRC6 SD, dependent on hydrophobic interactions between tryptophan binding pockets on CNOT9 and tryptophan(W) residues on TNRC6 protein (Mathys et al., 2014). Neither studies clearly account for contribution from endogenously expressed proteins (CNOT1 and CNOT9) that can potentially influence their claims.

| Sl. No. | Observation/Result/Claim | Reference | Method/Data |
|---|---|---|---|
| 1 | TNRC6 proteins interact with CNOT1 at more than one locus, DUF3819 domain being the major site | (Huntzinger et al., 2013) | Co-IP assay [Fig 9A] |
| 2 | DUF3819 domain of CNOT1 also interacts with CNOT9 | (Chen et al., 2014) | [Fig 1B, 1C] |
| 3 | DUF3819-CNOT9 binary complex is the major interaction site for the TNRC6 silencing domain (SD) | (Chen et al., 2014) | Co-IP assay, [Fig 1E] |
| 4 | CNOT9 homodimerization and interaction with CNOT1 (via DUF3819) in mutually exclusive | (Chen et al., 2014) | CNOT1-CNOT9 is stable helix-helix hydrophobic interaction |
| 5 | CNOT9 (H58A, F60A, A64Y, V71Y) mutant cannot interact with CNOT1 and TNRC6s | (Chen et al., 2014) | Co-IP assay [Fig 2E, 4C, 4F] |
| 6 | CNOT9 (P165G, Y203A, R205A, R244A) mutant cannot interact with TNRC6s but interacts with CNOT1 | (Chen et al., 2014) | Co-IP assay, [Fig 4C, 4D] |
| 7 | DUF3819 domain of CNOT1 is not sufficient for recruitment of TNRC6s (requires WT CNOT9) | (Chen et al., 2014) | Co-IP assay, [Fig 4C, S5J] |
| 8 | DUF3819 (CNOT9 binding domain) interaction with TNRC6 SD is strengthened in presence of CNOT9 | (Mathys et al., 2014) | Co-IP assay, [Fig 1E] |
| 9 | CNOT9 can directly interact with SD in a W motif-dependent manner | (Mathys et al., 2014) | Co-IP assay, [Fig 1E] |

**Table 3.1: Literature summary on protein-protein interactions involving CNOT9**

Based on these the above findings CNOT1$\Delta C^{1-1585}$ (truncated CNOT1 lacking C-terminal domain) should not interact with silencing domain of TNR6C in presence of mutant CNOT9 that either compromises CNOT9-CNOT1 interaction or CNOT9-SD interaction. This was not attempted by previous studies and remains to be tested. In addition to this, we wanted to see the efficacy of CNOT1 and TNRC6 interactions

in absence of any endogenous CNOT9. To do this, we decided to generate CNOT9 KO cell lines and test various aspects of the current model of CNOT9 dependent vs. independent CNOT1-TNRC6 interaction. We further used KO cells to investigate the contribution of CNOT9 in translation repression and decay of reporter mRNA.

## 3.2 Materials and Methods

### 3.2.1 Plasmids

Generation of *Cnot9*$^{mut4}$ (H58A, F60A, A64Y, V71Y) and *Cnot9*$^{GW182neg}$ (P165G, Y203A, R205A, R244A) constructs have been mentioned in Section 2.2.11 (Materials and Methods, Chapter 2). These were used to generate EGFP-tagged *Cnot9*$^{mut4}$ and *Cnot9*$^{GW182neg}$ constructs in pEGFP-C1 vector by PCR based amplification. Plasmid expressing wild-type CNOT9, CNOT1, and truncated CNOT1(CNOT1$\Delta$C$^{1-1585}$) conjugated with EGFP was previously generated in the lab. FLAG-tagged human TNRC6C silencing domain (amino acids: 1260-1690) was cloned into pcDNA3.0 vector between BamH1 and Xho1 sites. To investigate the role of CNOT9 in translation repression and mRNA decay, Renilla luciferase containing let-7 miRNA interaction element followed by polyadenylation signal-sequence was subcloned from pAWH-Rluc-let-7-Poly(A) vector (Tomari Lab) to pcDNA3.0 vector at BamH1 and EcoR1 sites, to ensure promoter compatibility for mammalian expression.

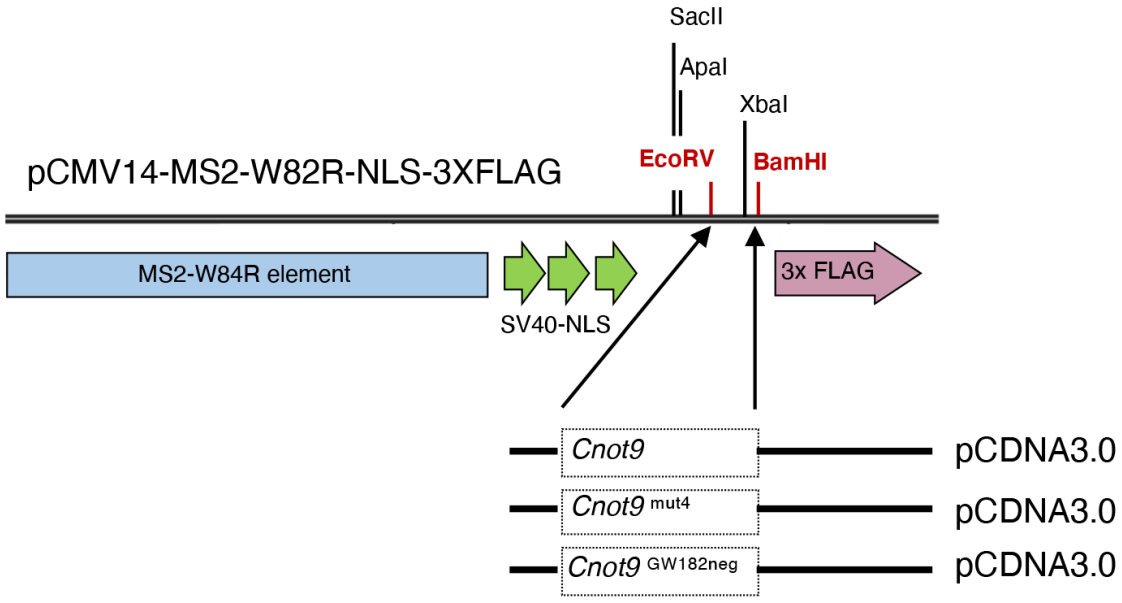


**Figure 3.1: Strategy to generate MS2-tagged CNOT9 and mutants for tethering assay** Schematic representation of sites used for cloning Cnot9, Cnot9 mut4, and Cnot9 GW182neg into pCMV14-MS2-W82R-NLS-3XFLAG vector

Likewise, Renilla luciferase containing let-7 miRNA interaction element followed by $A_{114}$-$N_{40}$ (114 adenosines internalized by a 40 nt unrelated sequence) and a hammerhead ribozyme sequence (HhR) was subcloned from pAWH-Rluc-let-7-$A_{114}$-$N_{40}$-HhR vector

to pcDNA3.0 vector at BamH1 and EcoR1 sites. pcDNA3.0 vectors to pCMV14-MS2-W82R-NLS-3XFLAG vector within EcoRV and BamH1 sites, in frame of upstream MS2 element and downstream 3XFLAG tag. A schematic of this is shown in Figure 3.13.1. Bait construct for tethering assay containing Firefly luciferase followed by nine MS2 stem loop elements was previously constructed in pCI-neo vector. Cloned constructs were confirmed by DNA sequencing and expression in HEK293T cells.

### 3.2.2 Cell lines

Human cell lines HEK293T and HeLa were used for ectopic expression experiments. CNOT9 KO cells were generated as mentioned in Section 2.2.12 (Materials and Methods, Chapter 2).

### 3.2.3 Reporter Tethering assay

CNOT9 KO HeLa cells were seeded in 12-well plates at a density of $10^5$ cells/well. At ≈80% confluency, transfection was done in using TransIT-LT1 (Mirus Bio) reagent as listed below:

| Sl. No | Particulars | Volume/well |
|---|---|---|
| 1 | Opti-MEM media | 100$\mu$l |
| 2 | Plasmid DNA* (each stocked at 1$\mu$g/$\mu$l) *[pCMV14-MS2-CNOT9/CNOT9$^{GW182neg}$/CNOT9$^{mut4}$ pCINeo-Firefly-Luc-9XMS2BS and pRenilla-Luc-TK]* | 1$\mu$g |
| 3 | TransIT-LT1 reagent | 3$\mu$l |
| Total | | 103$\mu$l |

* To ensure a total of 1$\mu$g DNA, 333$\mu$g of each plasmid was transfected

Components for transfection were added in the order indicated. Transfection mix was incubated at RT for 20 mins before adding dropwise to cells. Luciferase assay was done 24 hours post transfection using DLR Assay Kit (Promega) following manufacturer's protocol. Data was recorded using Centro LB 960 luminometer (Berthold).

### 3.2.4 Reporter Assay for miRNA mediated translation suppression and mRNA decay

WT HeLa cells were maintained in 10-cm dishes prior to commencement of experiment. Transfection of Control and CNOT9 siRNA was done following reverse transfection method, using Lipofectamine RNAi Max Kit (ThermoFisher) as mentioned below:

250$\mu$l of Transfection mix was added per well, followed by gentle swirling to ensure even coating of bottom surface. Coated tissue culture plate was incubated for 5 minutes

| Sl. No | | Ingredients | Volume/well |
|---|---|---|---|
| 1 | | Opti-MEM media | 250$\mu$l |
| 2 | Transfection Mix | Control or CNOT9 siRNA* (50$\mu$M stock) | 0.5$\mu$l |
| 3 | | Lipofectamine RNAi Max | 5$\mu$l |
| 4 | Cell suspension | | 750$\mu$l |
| **Total Volume (approximately) | | | 1000$\mu$l |

at RT inside laminar flow. Thereafter HeLa cells harvested from culture dishes were seeded into wells coated with siRNA at a density of $5 \times 10^4$ cells per well and incubated at 37$^o$C for 36 hours. After 36 hours, media change was performed prior to Reporter luciferase transfection. Recipe for transfection solution is tabulated below:

| Sl. No | Ingredients | Volume/well |
|---|---|---|
| 1 | Opti-MEM media | 100$\mu$l |
| 2 | pGL3.0 vector* (Stock Conc. = 1$\mu$g/$\mu$l) | 0.9$\mu$l |
| 3 | RLuc-Let7-SynPolyA or RLuc-Let7-$A_{114}$-HhR (Stock Conc. = 1$\mu$g/$\mu$l) | 0.1$\mu$l |
| 4 | Trans-IT reagent | 2.0$\mu$l |
| **Total Volume (approximately) | | 103$\mu$l |

Transfection mix was incubated at RT for 20 mins before adding dropwise to cells. After 24 hours, cells were harvested, and luciferase assay was performed using DLR Assay Kit (Promega) following manufacturer's protocol. Data was recorded using Centro LB 960 luminometer (Berthold).

### 3.2.5 RNA and Protein Isolation

Total RNA was isolated from cells using Isogen II protocol as described previously in Section 2.2.11 (Materials and Methods, Chapter 2). Protein isolation was done using TNE buffer, composition and procedure of which has been described in Section 2.2.4 (Materials and Methods, Chapter 2). Methods used for protein co-immunoprecipitation has been previously mentioned in Section 2.2.6 (Materials and Methods, Chapter 2).

### 3.2.6 Mass Spectrometry

Approximately 3mg of total protein was used for IP assays. Immunoprecipitated proteins bound to antibody conjugated beads were solubilized in 1 ml of 50mM Ammonium Bicarbonate (Ambic) solution (pH= 8.0) and centrifuged at 500g for 2 minutes at 4$^o$C. Supernatant was discarded, and washing was repeated. Thereafter, 100$\mu$l of 0.5M $NH_4OH$ (pH = 11-12) solution was added to pellet, mixed gently and incubated at RT for 5 minutes. This was followed by centrifugation at 500g for 2 minutes at 4$^o$C.

Supernatant was transferred into fresh Eppendorf tubes and procedure was repeated to increase yield of immunoprecipitated proteins. Solvent removal was performed for 200$\mu$l of supernatant (that contained eluted proteins) using a SpeedVac or Rotavapor, followed by resuspension of pellet (sticking to walls of tube, not visible) in 10$\mu$l of 4X LDS buffer (ThermoFisher). Maximum resuspension was ensured by gently vortexing tube on a shaking stand for 10 mins at RT. Thereafter, 5$\mu$l of 100mM Dithiothreitol (DTT) was added to solution, followed by addition of MQ water to make a final volume of 40$\mu$l. Samples along with protein Ladder were heat denatured at 75$^o$C for 10 mins before loading on pre-cast 4-12% gradient SDS-PAGE gels. Electrophoretic separation of proteins in 1XMOPS buffer (ThermoFisher) was done at 200V for 50 mins to achieve maximum separation. Post electrophoresis, gel was fixed using fixative solution (50% MeOH in 10% Acetic acid solution) for 30 minutes under gentle shake. Thereafter gels were stained with CBB Staining Solutions A and B (Nacalai) for 4 hours, followed by destaining in MQ water to remove excess stain. Gels were imaged before excising out protein bands across different lanes. Finally, trypsin digestion was performed overnight at 37$^o$C and post elution, digested peptides were injected into LC-ESIMS machine for characterization.

### 3.2.7 Antibodies

Antibodies against CNOT1, CNOT3, CNOT6, CNOT6L and CNOT7 were generated by Bio Matrix Research (Tokyo, Japan) as previously described (Chen et al., 2011). Commercially available antibodies used for immunoblotting included: anti-a-tubulin (Sigma, T9026), anti-CNOT9 (Proteintech, 22503-1-AP), anti-FLAG (MBL, PM020), anti-EGFP (MBL, 598), anti-RNF219 (Bethyl A302-540A), anti-GW182 (Bethyl, A302-329A), anti-CNOT2 (CST, 34214S), anti-4EBP1 (CST, 9644S), anti-b-Actin (CST, 4970L), anti-GAPDH (CST, 2118L), anti-CNOT10 (Bethyl A304-899A), and anti-AGO2 (CST, 2897S). For western blotting, all antibodies were used at 1:1000 dilution in 5% skimmed milk solution. For IP assay Anti-FLAG M2 Affinity gel (Sigma Aldrich, A2220) was equilibrated in TNE buffer (10 mM NaF, 20 mM Tris-HCl, 150 mM NaCl, 2 mM EDTA, 1% NP-40, 1 mM PMSF, 10 mM $\beta$-glycerophosphate) prior to use.

### 3.2.8 siRNA

Double strand RNA oligonucleotides targeting the following cDNA sequences were synthesized by Sigma Aldrich:

| Sl. No | Sequence | Purpose |
|---|---|---|
| 1 | 5'-UUCUCCGAACGUGUCACGU-3' | Control siRNA |
| 2 | 5'-CAUGCUGUGGCAUUCAUUUGG-3' | CNOT9 siRNA #1 |
| 3 | 5'-GCUCUGGCAUUACUGCAAUGU-3' | CNOT9 siRNA #2 |
| 4 | 5'-GGAAUCUGGAAGUGAACUUUC-3' | CNOT9 siRNA #3 |
| 5 | 5'-CCUUCGACUCUCAGAUAAU-3' | CNOT9 siRNA #4 |

# 3.3 Results

## 3.3.1 Investigating CNOT9 interacting proteins

Using FLAG-CNOT9, FLAG-CNOT9$^{mut4}$ and FLAG-CNOT9$^{GW182neg}$ proteins as bait, we immunoprecipitated interacting proteins of CNOT9 and identified them by Western Blotting and as shown in Figure 3.2. Identified proteins bound to FLAG-CNOT9 include, and not being limited to, CNOT1, CNOT2, CNOT6, CNOT6L, CNOT7 and GW182 (TNRC6). CNOT9 mutant (CNOT9$^{GW182neg}$), despite being incompetent for direct interactions with GW182, co-immunoprecipitated the latter, possibly via indirect associations with CNOT1. In other words C-terminal domain of CNOT1 may have facilitated interactions with GW182, when interactions via DUF3189 domain was likely to be compromised by bound CNOT9$^{GW182neg}$ mutant. Furthermore, in agreement with expectation, CNOT9$^{mut4}$ due to lack of CNOT1 interaction failed to associate with other components of the CCR4-NOT complex as well as GW182 protein (Figure 3.2).

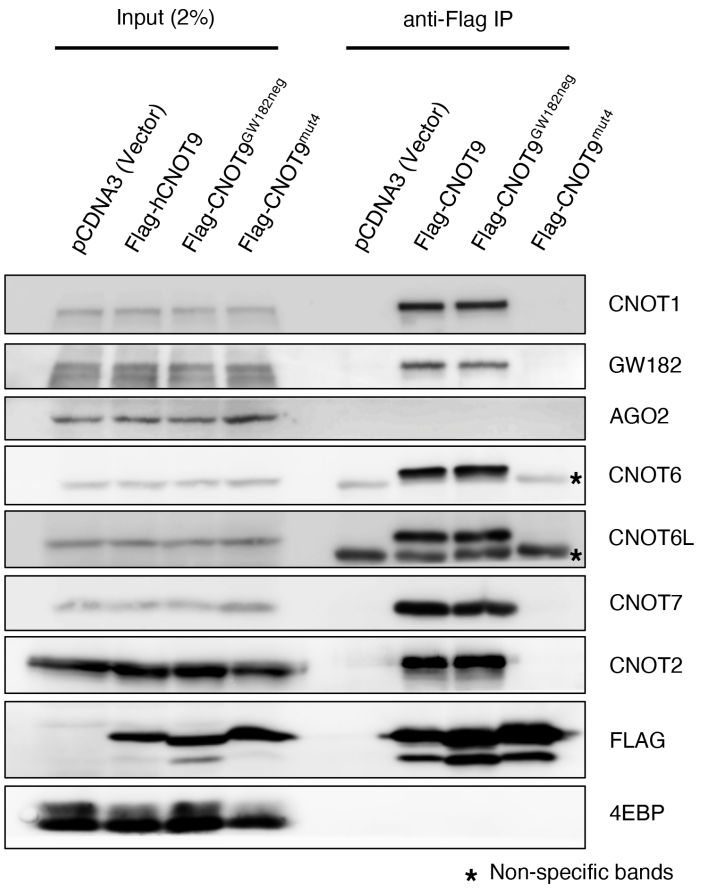


**Figure 3.2: CNOT9 interacting proteins in HeLa cells** Western Blotting based detection of proteins co-immunoprecipitated with FLAG tagged CNOT9, CNOT9$^{GW182neg}$, and CNOT9$^{mut4}$, in wild-type HeLa cells.

To validate the above result and have a comprehensive understanding of CNOT9 interacting proteins, we performed mass spectroscopic analysis of immunoprecipitated fractions. Prior to mass spectrometric analysis, immunoprecipitated proteins in respective fractions were resolved on 4-12% gradient gel was shown below (Figure 3.3). IP using Rabbit anti-CNOT9 antibody in WT HeLa cells (lane 3, Figure 3.3) was also tested alongside FLAG IPs.

A list of unique peptides corresponding to various proteins co-immunoprecipitated by CNOT9 and its mutant isoforms were identified by LC-MS (Table 3.2). Besides CCR4-NOT subunits, proteins TAB182(TNKS1BP1), RNF219, RAVER1, PRPSAP1, NPM1, MTMR4, CAPZA, and CAPZB were found to interact with CNOT9 in a CNOT1 dependent manner. Unfortunately, mass spectrometry could not detect unique peptides corresponding to either GW182 or AGO2 proteins in any fraction.

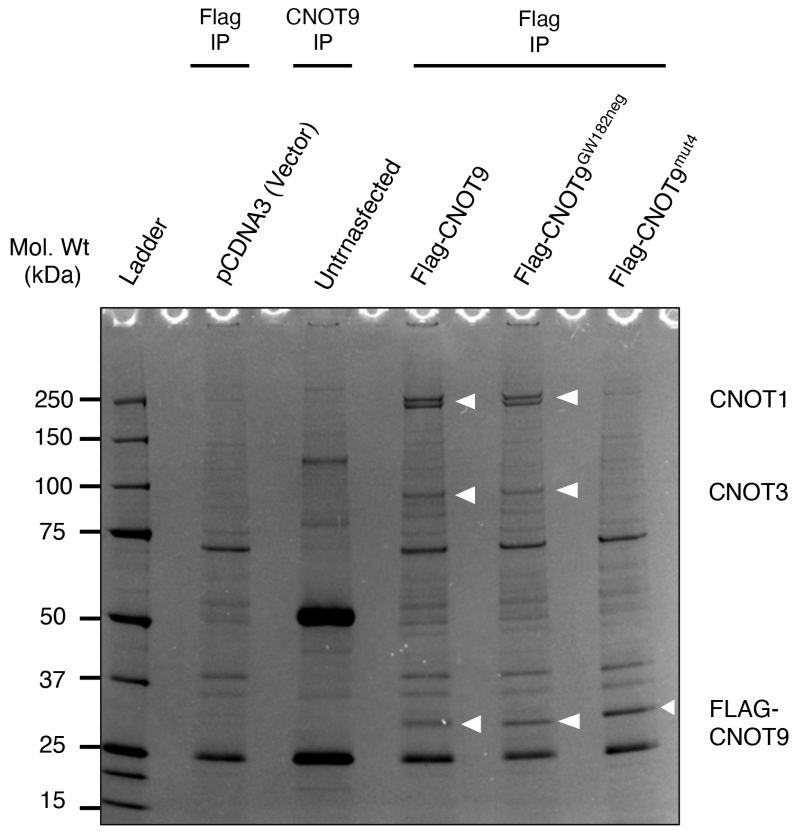


**Figure 3.3: In-gel separation of CNOT9 co-immunoprecipitated proteins.** Western Blotting based detection of proteins co-immunoprecipitated with FLAG tagged CNOT9, CNOT9$^{GW182neg}$, and CNOT9$^{mut4}$, in wild-type HeLa cells.

| Accession | Description | Mol. Weight(kDa) | Unique peptides in cells transfected with | | | |
|---|---|---|---|---|---|---|
| | | | pcDNA3 | FLAG-CNOT9 | FLAG-CNOT9$^{GW182neg}$ | FLAG-CNOT9$^{mut4}$ |
| A5YKK6 | CNOT1 | 266.8 | 0 | 73 | 53 | 0 |
| B7Z1E5 | CNOT9 | 36.8 | 0 | 24 | 24 | 25 |
| Q9C0C2 | TNKS1BP1 | 181.7 | 0 | 22 | 11 | 0 |
| Q9UIV1 | CNOT7 | 32.7 | 0 | 8 | 11 | 0 |
| O75175 | CNOT3 | 81.8 | 0 | 13 | 9 | 0 |
| Q9H9A5 | CNOT10 | 82.3 | 0 | 11 | 7 | 0 |
| Q9NZN8 | CNOT2 | 59.7 | 0 | 9 | 7 | 0 |
| Q5W0B1 | RNF219 | 81.1 | 0 | 13 | 6 | 0 |
| B4DP31 | PRPSAP1 | 31.2 | 0 | 6 | 5 | 0 |
| Q9UFF9 | CNOT8 | 33.5 | 0 | 5 | 4 | 0 |
| Q9UKZ1 | CNOT11 | 55.2 | 0 | 2 | 3 | 0 |
| E9PAU2 | RAVER1 | 79.5 | 0 | 1 | 2 | 0 |
| B1AK88 | CAPZB | 33.8 | 0 | 2 | 1 | 0 |
| Q9NYA4 | MTMR4 | 133.3 | 0 | 1 | 1 | 0 |
| H0Y9Z5 | CNOT6L | 63.7 | 0 | 1 | 1 | 0 |
| Q96LI5 | CNOT6 | 63.0 | 0 | 1 | 1 | 0 |
| P52907 | CAPZA | 32.9 | 0 | 1 | 1 | 0 |
| E5RI98 | NPM1 | 11.9 | 0 | 1 | 1 | 0 |

**Table 3.2: List of co-immunoprecipitated proteins detected by mass spectrometry** Number of unique peptides corresponding to immunoprecipitated proteins across various IP fractions, determined by mass spectroscopy

### 3.3.2 Contribution of CNOT9 in CNOT1-TNRC6 interaction

Based on preliminary evidence of CNOT9 interacting proteins, we investigated the importance of CNOT9 in mediating interactions between CNOT1 and GW182 proteins specially when C-terminal domain-based interaction is compromised. To test this, we used a construct expressing truncated from of CNOT1(1-1585) lacking C-terminal domain and fused with N-terminal EGFP (indicated as EGFP-CNOT1ΔC). FLAG tagged silencing domain of TNRC6C (GW182) protein was used as bait for IP assay (indicated as FLAG-GW182-FL-SD). Based on results shown in Figure 3.4, it was found that truncated CNOT1 protein interacted with silencing domain of TNRC6C only when co-expressed with wild-type form of CNOT9. This clearly suggests the importance of CNOT9 at its binding locus (DUF3819 domain), in facilitating efficient interactions between CNOT1 and TNRC6C proteins.

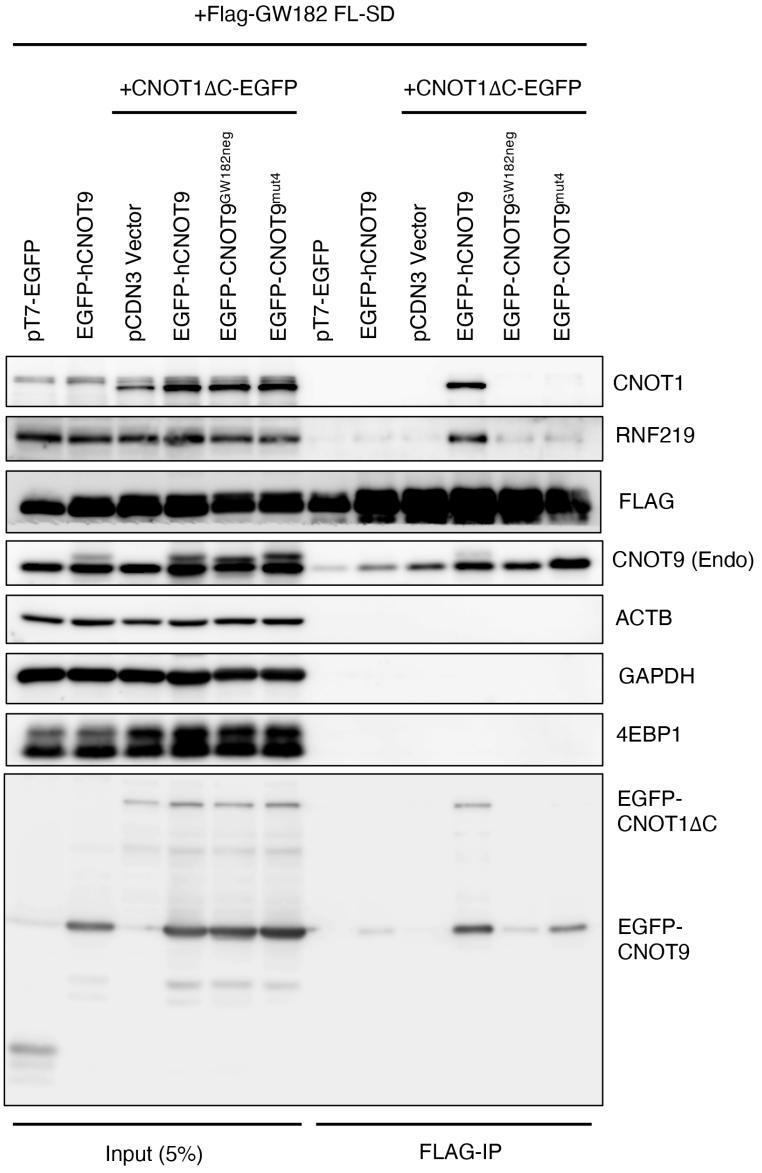


**Figure 3.4: DUF3819 domain occupancy for CNOT1-GW182 interactions** CNOT1ΔC protein Co-IP by FLAG-GW182 FL-SD in presence of CNOT9 and mutants (CNOT9$^{GW182neg}$ and CNOT9$^{mut4}$) in wild-type HeLa cells

### 3.3.3 CNOT1-TNRC6 interaction in CNOT9 KO HeLa cells

Despite the previous result, there exists a possibility of CNOT9 being structurally and functionally dispensable for overall interactions between TNRC6C and CNOT1 proteins.

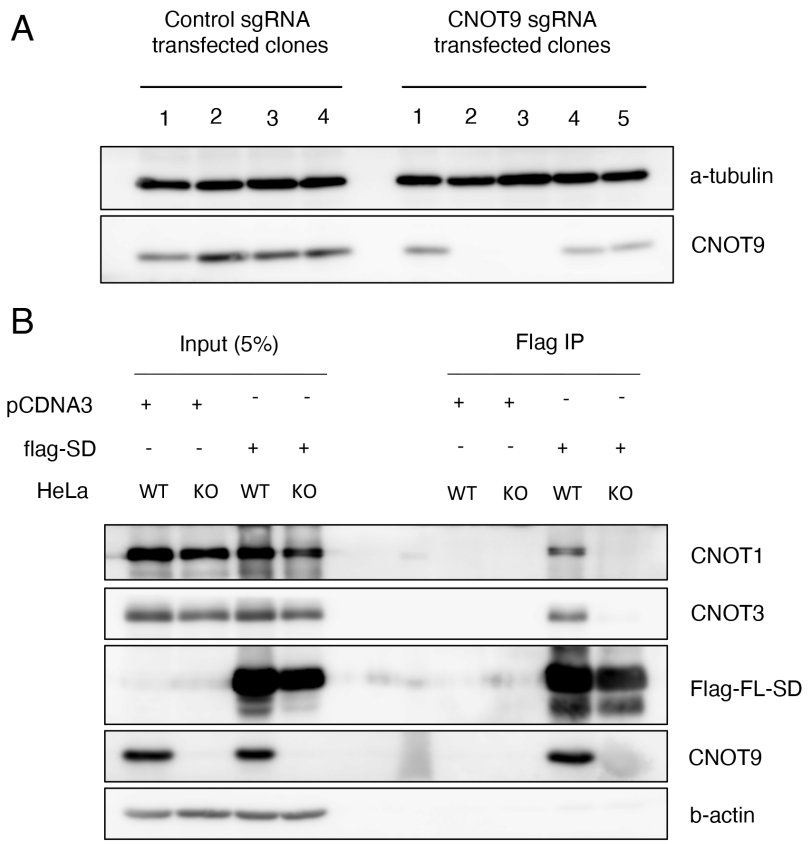


**Figure 3.5: CNOT1-GW182 interactions in CNOT9 knockout condition** CNOT1-GW182 interactions in CNOT9 knockout condition

Hence, we re-investigated interactions between TNRC6C(GW182) and CNOT1 proteins in a system completely devoid of CNOT9. Hence, we generated CNOT9 KO HeLa cells using CRISPR-Cas9 technique and validated by western blotting (Figure 3.5A).

For interaction study, FLAG tagged silencing domain of TNRC6C (GW182) protein was exogenously expressed in WT and CNOT9 KO HeLa cells and interacting proteins were immunoprecipitated using anti-FLAG antibodies. Based on results shown in Figure 3.5B, FLAG-tagged silencing domain could not immunoprecipitate CNOT1 and CNOT3 proteins in absence of CNOT9. B-actin immunoblot served as a negative control for IP assay and as a loading control for input fraction.

### 3.3.4 Contribution of CNOT9 in translation suppression and mRNA decay

Role of CNOT9 in translation repression and mRNA decay was assessed in-vitro, using reporter tethering assay, as illustrated in Figure 3.6A. MS2-fusion proteins with CNOT9 and mutant CNOT9 were validated by western blotting in WT HeLa cells as shown in Figure 3.6B. Thereafter, contribution of wild-type CNOT9 and its mutant isoforms were compared by measuring reporter luciferase activity and expression levels in

CNOT9 KO HeLa cells. As shown in Figure 3.6C, reporter activity was approximately 2-fold lower when tethered by MS2-tagged CNOT9 or MS2-tagged CNOT9$^{GW182neg}$ mutant, compared to control. Additionally, MS2-tagged CNOT9$^{mut4}$ mutant showed no differences in tethering efficiency compared to MS2-only control suggesting that CNOT9 interaction with CNOT1 is required for mediating translation suppression. Furthermore, no differences in reporter mRNA levels of were observed across all four experimental conditions, suggesting no significant contribution of CNOT9 in mRNA decay (Figure 3.6C).

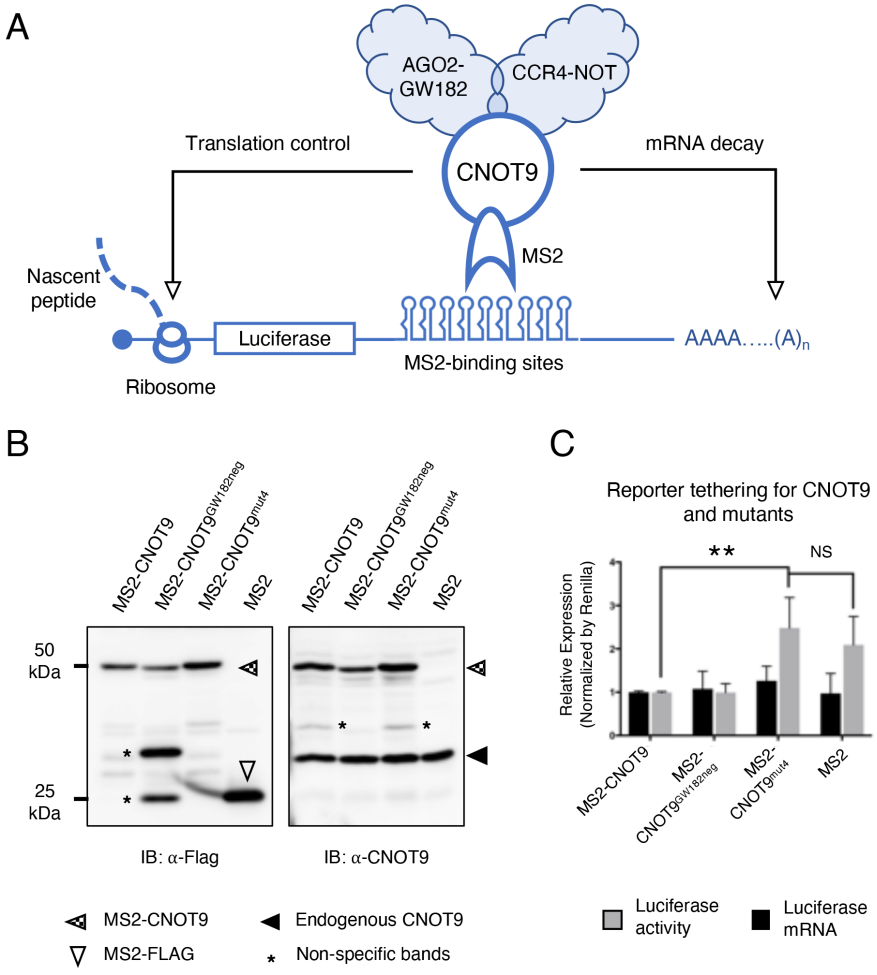


**Figure 3.6: CNOT1-GW182 interactions in CNOT9 knockout condition**(A) Schematic representation of tethering MS2 tagged CNOT9 to reporter luciferase reporter containing MS2-binding sites (B) Validation of MS2 fusion protein expression in WT HeLa cells by western blotting. Arrowheads represent bands corresponding to various proteins (CNOT9, CNOT9-MS2, and MS2-FLAG), whereas non-specific bands are indicated by * (C) Relative expression levels for Firefly LUCIFERASE reporter activity and Firefly *Luciferase* reporter mRNA in CNOT9 KO cells transfected by MS2 fused CNOT9 or MS2 fused mutant CNOT9. Values are Mean ± SD [n=5, $p < 0.01$ (**)

Next we analyzed the role of CNOT9 specifically in the context of microRNA mediated translation suppression. Luciferase-based reporter assay used to test this idea has been illustrated in Figure 3.7A. In cells expressing CNOT9, luciferase reporter conjugated with Let7 miRNA sites followed by a synthetic polyadenylation element, is likely to undergo both translational repression and mRNA decay under steady state conditions. On the other hand, luciferase reporter conjugated with Let7 miRNA sites followed by a stretch of 114 adenosine residues attached to a deadenylation resistant Hammerhead ribozyme motif element, should largely be susceptible only to translational suppression. Thus, by comparing differences in activities of both reporters, the extent of translation repression can be assessed. Based on results shown in Figure 3.7C, depletion of CNOT9 by siRNA treatment, led to a significant ≈3-fold increase in reporter luciferase activity for both reporters in a manner largely driven by translation suppression. Cell lysates subjected to luminometric analysis were also used for western blotting to confirm CNOT9 depletion as shown in Figure 3.7B.

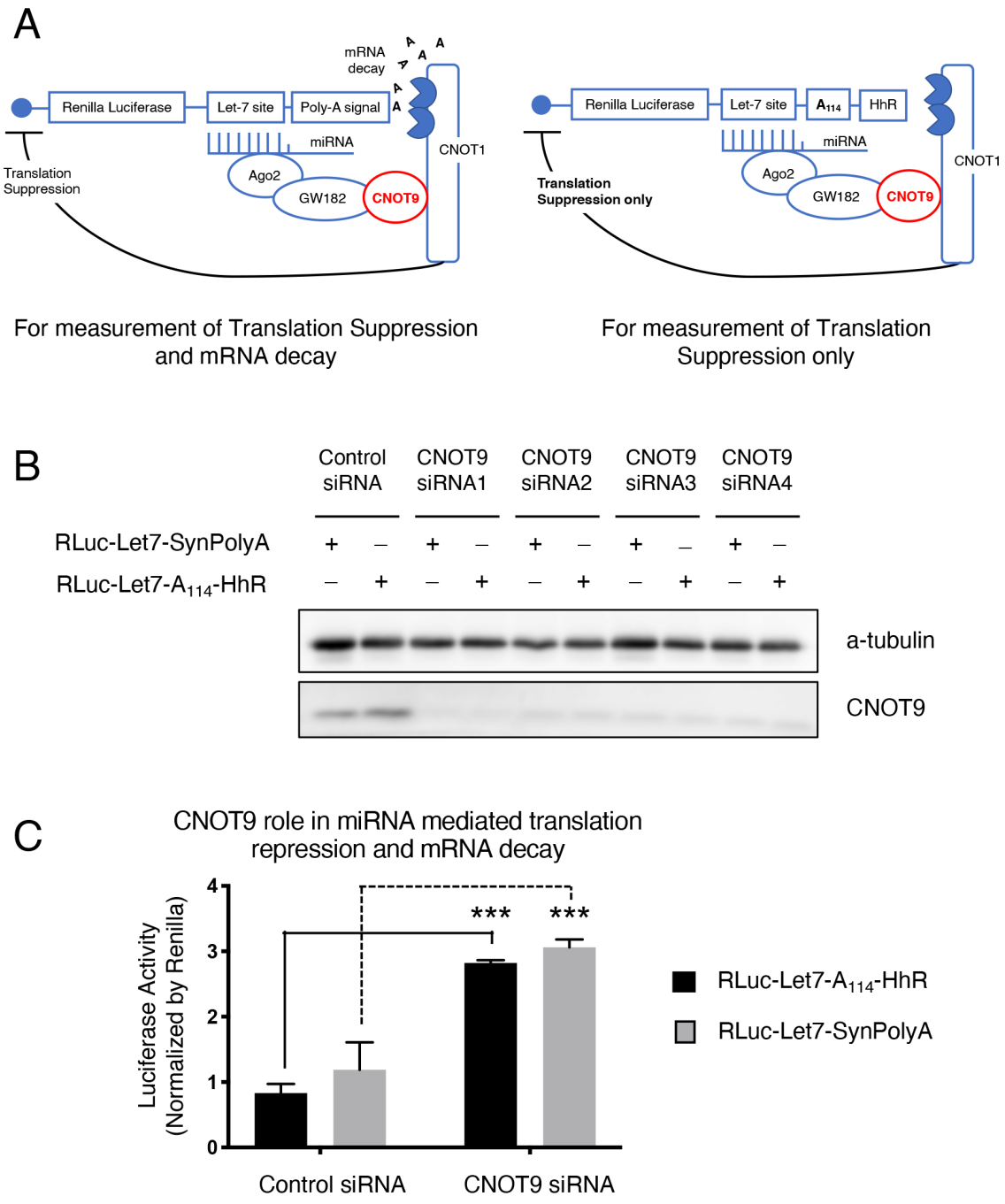


**Figure 3.7: Reporter assay for miRNA induced translational suppression and decay** (A) Schematic representation of possible mechanisms of miRNA mediated translational repression and mRNA decay using reporter constructs (B) Validation of CNOT9 knockdown using 4 different siRNAs against CNOT9 alongside control. (C) CNOT9 contribution in miRNA mediated translational repression and mRNA decay. Values are Mean ± SD [n=4, $p < 0.001$ (***)]

## 3.4 Discussion

In this section, we attempted to readdress the importance of CNOT9 in the context of CNOT1-GW182 (TNRC6) interactions mainly to clarify certain contradictory observations made by previous studies. We also sought to investigate the role of CNOT9 in mechanisms involving translation repression and mRNA decay, under in-vitro conditions.

As a starting point, CNOT9 interacting proteins were identified by western blotting and mass-spectroscopic analysis in HeLa cells. Majority of interacting proteins were either core components of the multi-subunit CCR4-NOT complex, or non-core proteins such as RAVER1 and RNF219, that have been known to associate with the complex (Miyasaka et al., 2008, Youn et al., 2018). Western Blotting identified GW182 (TNRC6), a component of the miRNA-RISC complex, as an interaction partner of CNOT9, although mass spectrometry analysis could not confirm unique peptides corresponding to the same. Further, AGO2 protein could not be detected in the pool of CNOT9 interacting proteins either via western blotting or mass spectroscopy, possibly due to poor sensitivity of the IP assay in identifying indirect interactions. It many also be attributed to low-interaction/weak affinity of AGO2 towards the CCR4-NOT complex under steady-state conditions. Such interactions may however be detected by crosslinking protein lysates prior to antibody based immunoprecipitation steps. Another interesting observation was made with regard to CNOT4 protein. Our study could not detect CNOT4 protein in IP fractions, although a recent study had reported weak yet direct interactions between CNOT9 and CNOT4 proteins in human cells lines (Keskeny et al., 2019).

Next, we investigated interaction between CNOT1 and FLAG-tagged silencing domain of TNRC6C protein. We found that CNOT1 could not interact with silencing domain of TNRC6C protein in absence of CNOT9. This came as a surprise because, a certain degree of interaction between CNOT1 and silencing domain of TNRC6C was expected to occur via C-terminal domain of CNOT1 (Huntzinger et al., 2013). A possible explanation for this result can be perceived as follows: CNOT9 binding to CNOT1 allows the latter to adopt a stable conformation that favors interaction with TNRC6C proteins. Further assessment and validation of interactions between CNOT1 and TNRC6 family of proteins needs to be done to address this hypothesis.

Using lysates from KO cell lines, we tested if CNOT9 contributed to structural integrity of the CCR4-NOT complex. In previous studies, depletion of individual CCR4-NOT subunits has been shown to compromise overall structural integrity of the complex (Ito et al., 2011a, Ito et al., 2011b, Suzuki et al., 2015). In the same vein, we tested if absence of CNOT9 also showed similar effects. WT and CNOT9 KO cell lysates immunoprecipitated using anti-CNOT2 and anti-CNOT3 antibodies did not show significant differences in IP efficiency of other subunits of the CCR4-NOT complex (data not shown).

Lastly, we chose to investigate the role of CNOT9 in translation repression and

mRNA decay with the help of two different luciferase-reporter based assays. It was understood that CNOT9 operates mainly in the context of translation repression, in-vitro. These observations need further testing and validation in different in-vitro and in-vivo systems, primarily using untransformed cell-types or cell-lines that more closely resemble physiological conditions. To conclude, CNOT9 is an important node between two key cellular machineries – the CCR4-NOT deadenylase complex and the miRNA-RISC complex, that is likely to support translation repression in higher eukaryotes.

# Chapter 4

# Molecular targets of CNOT9 in mouse ES cells

## 4.1 Motivation

Phenotype exhibited by complete knockout and Sox2-Cre conditional knockout embryos highlighted the importance of CNOT9 during gastrulation, more importantly in differentiation of the epiblast lineage. However, at the point of phenotype emergence, the epiblast lineage comprises of multiple heterogenous populations of lineage committed cell-types expressing divergent gene expression profiles (Peng et al., 2016). An example of tissue heterogeneity can be reflected from differential expression levels of FLK1 and PDGFRA that directs progenitor mesoderm cells towards extraembryonic and lateral plate mesoderm (Flk1+/Pdgfra-), Cardiac mesoderm (Flk1+/Pdgfra+), and Paraxial mesoderm (Flk1-/Pdgfra+) lineages (Kouskoff et al., 2005, Irion et al., 2010). In another example, presence of retinoic acid gradient has been found to induce heterogeneity in *Fgf8* expression along anterior-posterior axis of embryos (Kumar and Duester, 2014). Therefore, in the context of such non-uniformity, phenotype-based bulk analysis is likely to yield a low-throughput landscape of gene expression. In other words, a pan-embryo average measure of gene expression will not adequately reflect differences that are region-specific or lineage-specific. One way to address this issue involves analysis of gene expression profiles at single cell resolution (Cheng et al., 2019, Pijuan-Sala et al., 2019). An alternate and more conventional approach involves in-vitro stem-cell based derivation of specific cell-types and lineages.

Mouse embryonic stem cells (mESCs) have served as an excellent model to understand gene expression and phenotype associated with early embryonic differentiation (Evans and Kaufman, 1981, Martin, 1981, Prelle et al., 2002). They can be stably propagated in culture conditions in presence of leukemia inhibitory factor (LIF) and chemical inhibitors to Wnt and ERK signaling pathways (Smith et al., 1988, Williams et al., 1988, Ying et al., 2008). ES cells have similar characteristics as that of pre-implantation epiblast cells (Nichols et al., 2009). In addition, these cells are capable of producing various cell types upon treatment with reagents that induce lineage specific differentiation. For instance, FGF signaling and retinoic acid treatment on mouse

ES cells drives neuroectoderm differentiation whereas Wnt3a and activin treatment induces differentiation in the direction of mesendoderm lineage (Yamaguchi et al., 1999, Nishikawa et al., 2007, Niwa, 2007, Greber et al., 2010, Niwa, 2010). Likewise allowing ES Cells to grow as aggregated embryoid bodies (EBs), have shown their ability to differentiate into adult lineages such as hematopoietic, vascular, pancreatic, hepatic and neuronal lineages (Murry and Keller, 2008).

We therefore chose to generate CNOT9 KO mESCs and use them to investigate various phenotypic and molecular alterations under conditions of self-renewal and differentiation. Using this simplified model, we aim to readdress KO embryo phenotype and potentially use it to perform rescue experiments.

## 4.2 Materials and Methods

### 4.2.1 Derivation of CNOT9 KO mESCs

Our method for isolation and culture of mESCs has been adapted from Protocol #8 of Chapter 4, and Protocols #6 and #7 of Chapter 8, of the textbook titled "Manipulating the Mouse Embryo" (Behringer, 2014). Key procedures have been summarized as follows:

**Derivation of E3.5 blastocysts:**

Ovulation was hormonally induced in four-week-old *Cnot9* heterozygous *Cnot9*$^{+/lacZ}$ female mice by 7.5U of Pregnant Mare Serum Gonadotropin (PMSG) administered intraperitonially. This was followed by intraperitoneal administration of 7.5U of Human Chorionic Gonadotropin (HCG), 47 hours post PMSG injection. Immediately thereafter, female mice were crossed overnight with *Cnot9* heterozygous (*Cnot9*$^{+/lacZ}$) stud males. On the following day, vaginal plug positive females were identified. Two days after plug sight, female mice were dissected and E2.5 morula stage embryos were harvested by flushing oviducts with M2 media. Harvested embryos were transferred into 1×KSOM media supplemented with GSK3$\beta$ inhibitor (CHIR99021) and ERK inhibitor (PD0325901) and incubated overnight at 37$^o$C, 5% $CO_2$. On the following day, embryos progressed to form E3.5 blastocysts.

**Culturing blastocyst outgrowths over fibroblast feeder layers:**

Twenty-four hours prior to blastocyst development, gamma irradiated mitotically arrested mouse embryonic fibroblasts (MEFs) were seeded on gelatin coated 48-well plates at a density of $2.5\times10^4$cells/cm$^2$. Composition of media used to seed MEFs is mentioned below:

| Sl. No. | Reagent | Stock Conc. | Add vol. (ml) | Final Conc. |
|---|---|---|---|---|
| 1 | DMEM High Glucose | - | 500 | |
| 2 | Inactivated FBS | 100% | 50 | 10% |
| 3 | 2-ME (Stock of 55mM in PBS) | 1000x | 0.5 | 0.1 mM |
| 4 | Penicillin/Streptomycin | 100x | 5 | 1x |
| 5 | Non-essential amino acids | 100x | 5 | 0.1 mM |
| 6 | HEPES, pH=7.5 | 1000 mM | 0.5 | $\approx$ 1 mM |

On the following day, culture media for MEF feeders was replaced by complete mES media (mES media supplemented with LIF and 2i), composition of which is tabulated below:

**mES media (Shelf life: 1month)**

| Sl. No. | Reagent | Stock Conc. | Add vol. (ml) | Final Conc. |
|---|---|---|---|---|
| 1 | KO-DMEM High Glucose | - | 500 | |
| 2 | KSR | 100% | 67 | 20% |
| 3 | FBS | 100% | 33 | |
| 4 | $\beta$-ME (Stock of 55mM in PBS) | 1000x | 0.6 | 0.1 mM |
| 5 | Penicillin/Streptomycin | 100x | 6 | 1x |
| 6 | Non-essential amino acids | 100x | 6 | 0.1 mM |
| 7 | L-glutamine | 200mM | 6 | 2 mM |

**Complete mES media (Shelf life: 1week)**

| Sl. No. | Reagent | Stock Conc. | Add vol. (ml) | Final Conc. |
|---|---|---|---|---|
| 1 | mES cell media | - | 50 ml | |
| 2 | LIF (ESG1106, Millipore) | $10^6$ U/ml | 75$\mu$l | 1500 U/ml |
| 3 | 2i* (CHIR99021) | 30mM | 5$\mu$l | 3 $\mu$M |
| 4 | 2i*(PD0325901) | 10mM | 5$\mu$l | 1 $\mu$M |

Two to three hours post media change, healthy blastocysts in KSOM+2i media were seeded into individual wells of 48 well plate. Prior to seeding, blastocysts were rinsed thrice in 100$\mu$l droplets of complete mES media, to ensure minimal media crossover. Blastocyst quality was determined based on appearance of blastomeric cavity and polarization of inner cell mass (ICM cells). Blastocysts were cultured for 3-5 days until outgrowths were seen.

**Derivation of ES cell colonies from blastocyst outgrowths:**

Once outgrowths were observed, media change was carefully performed without displacing colonies from underlying feeders. After 48 hours of culture, outgrowths were dissociated by trypsinization followed by repeated rounds of pipetting to produce smaller cell clumps consisting of 5-10 cells. Cell clumps were transferred into freshly seeded MEF feeders on 48-well plates and cultured for 2-3 days until colonies emerged. As colony size increased, ES cells were subsequently trypsinised and transferred into 24-well plates, followed by 6-well plates and finally into 10-cm dishes. At every step, a passage density of ≈1:6 was maintained.

**Genotyping ES cell clones:**

During passage of ES cells 6-well plates to 10-cm dishes, a fraction of them were seeded on 35mm dishes for genotyping. These cells were plated on gelatin coated dishes lacking feeder cells. Within 45-60 minutes of seeding, loosely attached and floating ES cells were transferred into another gelatin coated 35mm dish, leaving behind a majority of strongly adherent MEF feeders. This method was repeated once more to obtain >90% enrichment in ES cells population. Enriched pools of ES cells were cultured for an additional 24-36 hours to have sufficient lysates for PCR based genotyping and western blotting.

**Preparing frozen ES cell stocks:**

Approximately 60-70% confluent ES cell colonies grown on 10cm culture dishes were considered for cryo-preservation. ES cells were fed with fresh media 2-4 hours prior to cell banking. Trypsinised ES cells along with feeder fibroblasts were resuspended in cryopreservative solution composed of 10% DMSO and 90% complete mES media at a density of $\approx 3.5 \times 10^6$ cells/ml. Cells were frozen overnight at -80$^o$C, flowed by transfer into liquid nitrogen tanks for long-term storage.

### 4.2.2 Retinoic acid (RA) induced differentiation of mES cells

ES cells were grown under feeder free conditions prior to RA induced differentiation. Fibroblast depleted ES cells were seeded into 6-well tissue culture plates at a density of $10^5$ cells per well. After attaining 50% confluency, cells were cultured for 48 hours in ES media lacking LIF and inhibitors. This refractory period allowed quenching of LIF induced self-renewal and primed cells to undergo differentiation in subsequent steps. After 48 hours, cells were treated with ES media (-LIF -2i) supplemented with 1$\mu$M retinoic acid. Cells were harvested at periodic intervals for study marker gene expression upon RA treatment. A schematic of the aforementioned method is shown in Figure 4.1.

### 4.2.3 Genotype confirmation by PCR and Western Blotting

Harvested ES cells were pelleted down by centrifugation at 300g for 4 minutes. Media supernatant was removed, and pellet was subsequently resuspended in 1 ml of PBS.

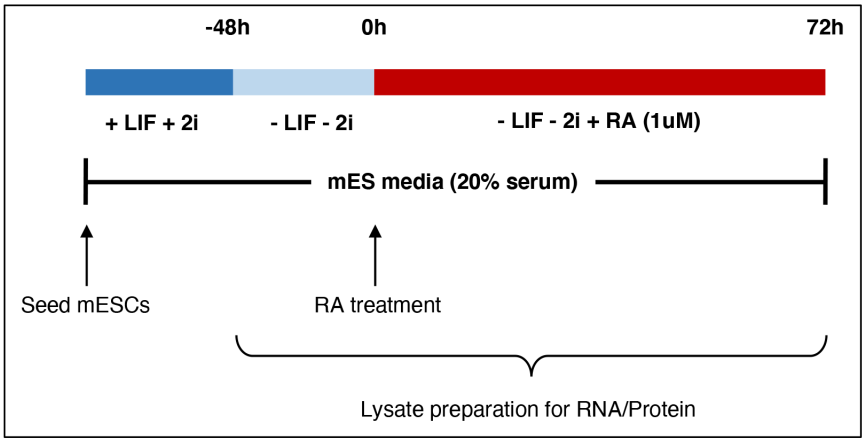


**Figure 4.1: Protocol design for RA induced differentiation of mESCs**

Resultant cell suspension was split into two tubes at 1:9 ratio. The smaller fraction was lysed for DNA isolation while the other was considered for isolation of proteins as detailed below:

**DNA isolation:**

100$\mu$l of cell suspension was pelted by centrifugation at 300g for 4 minutes and supernatant was carefully discarded. Pellet was resuspended in 20$\mu$l of dilution buffer followed by addition of 1$\mu$l DNA release solution provided in Phire Tissue Direct PCR Kit (Thermo Scientific). Cell suspension was vortexed at maximum intensity for 10 seconds and incubated at room temperature for 5 minutes. Thereafter tubes were incubated at 98$^o$C for 3 minutes, followed by cooling on ice for 10-15 minutes. Resulting lysate was used for PCR based genotyping at 1:10, 1:100, and 1:1000 dilutions.

**Protein isolation:**

900$\mu$l of cell suspension was pelleted by centrifugation at 300g for 4 minutes. After carefully removing supernatant, cell pellet was resuspended in 100$\mu$l TNE buffer (10mM NaF, 20mM Tris-HCl, 150mM NaCl, 2mM EDTA, 1% NP-40, 1mM PMSF, 10mM $\beta$-glycerophsosphate). Cells were incubated for 15 minutes on ice with pulse vortexing (2-3 seconds) every 5 minutes. Subsequently, lysates were contrifuged at 13000g for 10 minutes at 4$^o$C and supernatant containing proteins were trnasferred into fresh tubes. Total protein concentration was measured using BCA assay (ThermoScientific) and adjusted to 1$\mu$g/$\mu$l using 3$\times$Sample buffer.

### 4.2.4 Cell Growth Assay

Feeder subtracted mESCs were seeded on gelatin coated 6-well plates (TPP, Switzerland) at a density of $10^5$ cells/well. Cell growth was monitored using IncuCyte S3 Live-Cell Analysis System (Essen Bioscience) while being incubated at 37$^o$C, 5% $CO_2$.

### 4.2.5 Imaging ES cells colony

Blastocyst outgrowths and ES cell colonies were imaged using Leica TCS SP8 inverted microscope.

### 4.2.6 qRT-PCR based gene expression analysis

RNA isolation and cDNA synthesis were done as described previously in Section 2.2.7 (Materials and Methods, Chapter 2). Primers used for real-time PCR are listed in Table 4.1.

| Sl. No | Target | Forward Primer (5'-3') | Reverse Primer (5'-3') |
|---|---|---|---|
| 1 | *Lefty1* | actcagtatgtggccctgcta | aacctgcctgccacctct |
| 2 | *Lefty2* | gccctcatcgactctaggc | agctgctgccagaagttcac |
| 3 | *Cyp26b1* | ccaggactgtatgcccatga | ccactcaccaacaaaaagacaag |
| 4 | *Rarb* | cagaagtgctttgaagtgggc | cgtctagctccgctgtcatc |
| 5 | *Nodal* | tggtagggaagacccacaac | tgccaagcatacatctcagg |
| 6 | *Nestin* | tctgactctgtagaccctgcttc | tctgactctgtagaccctgcttc |
| 7 | *Oct4* | aagttggcgtggagactttg | tctgagttgctttccactcg |
| 8 | *Pax6* | cccggcagaagatcgtag | tcacacaaccgttggatacc |
| 9 | *Gapdh* | ctgcaccaccaactgcttag | gtcttctgggtggcagtgat |
| 10 | *Essrb* | atcaactgggccaagcac | gaatctccatccaggcactc |
| 11 | *Sox2* | ggcagagaagagagtgtttgc | tcttctttctcccagcccta |
| 12 | *c-myc* | gtgctgcatgaggagacacc | gcctcttctccacagacacc |
| 13 | *Shh* | ttctgtgaaagcagagaactcc | gacgtaagtccttcaccagctt |
| 14 | *T* | atcaccagccactgctttcc | cccggttcctccattacatc |
| 15 | *Afp* | caaagccctacagaccatgaa | ccgagaaatctgcagtgaca |
| 16 | *Gata4* | tcaaaccagaaaacggaagc | cagacagcactggatggatg |
| 17 | *Gata6* | tggcacaggacagtccaag | ggtctctacagcaagatgaatgg |
| 18 | *Cnot9* | gtctgcgcatcatggagtc | aaccagtgtcatccaagagga |
| 19 | *Pax3* | agtatggacaaagtgcctttca | tagtctgtggaggccggaaa |
| 20 | *c-fos* | gttcctggcaatagtgtgttcca | tgacaatgaacatggacgctga |
| 21 | *Cebpa* | aaacaacgcaacgtggaga | gcggtcattgtcactggtc |
| 22 | *Wnt3a* | cttagtgctctgcagcctga | gagtgctcagagaggagtactgg |
| 23 | *Gsc* | gagacgaagtacccagacgtg | gcggttcttaaaccagacctc |
| 24 | *Sox7* | cacgctgcctgagaaaaac | gggagtactcacccctgtcc |
| 25 | *Klf4* | gctcctctacagccgagaatc | atgtccgccaggttgaag |
| 26 | *Nanog* | ttcttgcttacaagggtctgc | cagggctgccttgaagag |
| 27 | *Fgf8* | caggtcctggccaacaag | gtatcggtctccacaatgagc |
| 28 | *c-jun* | agtagcccccaacctctttg | gggacacagctttcacccta |

**Table 4.1: Primers used for qRT-PCR based gene expression in mESCs**

### 4.2.7 Antibodies

Commercially available antibodies used for immunoblotting included: anti-a-tubulin (Sigma, T9026), anti-CNOT9 (Proteintech, 22503-1-AP), anti-GAPDH (CST, 2118L), anti-LEFTY1/2 (SantaCruz, sc-365845), anti-LEFTY1 (CST, 12647), and anti-PARP (CST, 9542S). For western blotting, all antibodies were used at 1:1000 dilution in 5% skimmed milk solution.

## 4.3 Results

### 4.3.1 Characterization of CNOT9 KO mESCs:

ES cells grown under in-vitro culture conditions were routinely monitored and passaged to maintain stemness. Expansion of ES cell clones from blastocysts outgrowth stage to colony formation was recorded as shown in Figure 4.2A. Genotype of ES clones were determined by analyzing PCR products on agarose gels as shown in Figure 4.2B. In addition to that, genotype was also confirmed by western blotting using anti-CNOT9 and anti-$\beta$-galactosidase antibodies as shown in Figure 4.2C. A total of 18 different ES clones were isolated and genotyped as indicated below in Table 4.2.

| Sl. No. | mES clone ID | Genotype |
|---|---|---|
| 1 | H8 | WT |
| 2 | H22 | WT |
| 3 | H23 | WT |
| 4 | H2 | HE |
| 5 | H3 | HE |
| 6 | H9 | HE |
| 7 | H10 | HE |
| 8 | H18 | HE |
| 9 | H24* | HE |
| 10 | H1 | KO |
| 11 | H6 | KO |
| 12 | H7 | KO |
| 13 | H11 | KO |
| 14 | H15 | KO |
| 15 | H17 | KO |
| 16 | H20 | KO |
| 17 | H25 | KO |
| 18 | H28 | KO |

**Table 4.2: Genotypes corresponding to various mES cell clones**
H24 clone (*) was slow growing and didn't have sharp colony boundaries.
Passage number for all clones at the time of freeze-stocking ranged from 6-8.

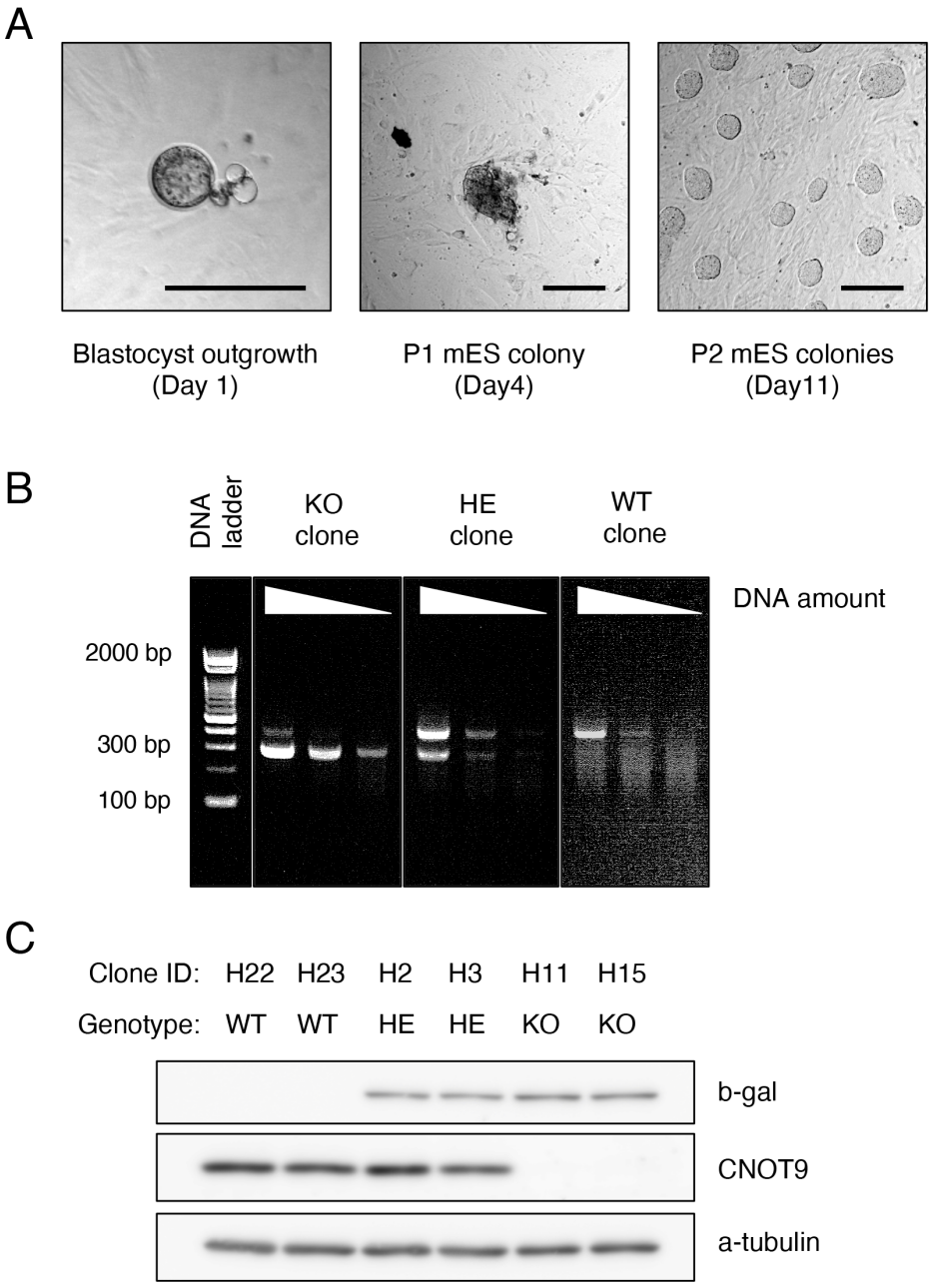


**Figure 4.2: Generation of ES cell colonies from blastocyst outgrowths and genotyping** (A) Brightfield images of ES cell colonies generated from blastocyst outgrowth after two passages. Scale: 0.2 mm (B) PCR based genotyping of CNOT9 KO, HE and WT mES clones. Upper band corresponds to WT allele (416 bp) while lower band corresponds to KO allele (296 bp). Upper band seen for KO clone at high density is likely to be contributed by residual feeder cells. (C) WT (H22, H23), HE (H2, H3), and KO (H11, H15) clones confirmed by western blotting using anti-CNOT9 and anti-$\beta$-galactosidase antibodies.

### 4.3.2 Growth rates analysis of CNOT9 KO mESCs

ES cell growth was monitored while being cultured on gelatin coated TPP plates using automated cell growth analysis setup (IncuCyte). Percentage confluence was used as a measure of cell growth. As seen from Figure 4.3, preliminary results suggest similar growth trends for WT, HE and KO mES cells.

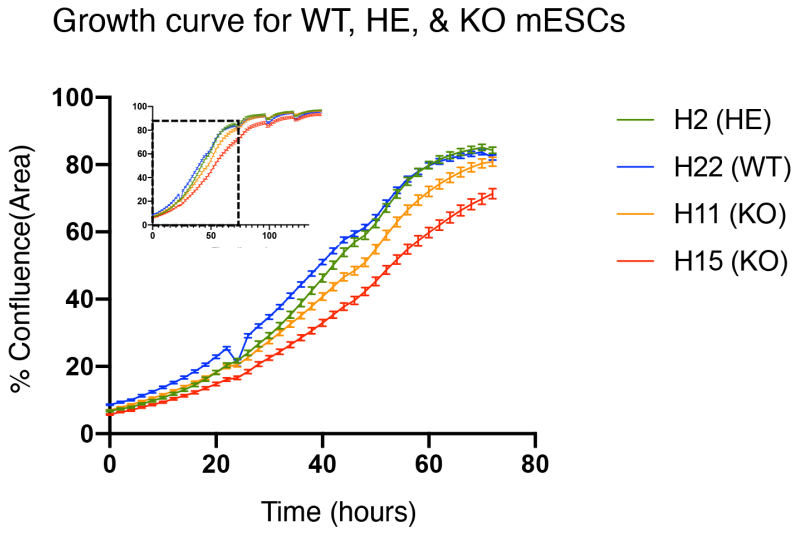


**Figure 4.3: Growth rate comparison between WT and CNOT9 KO mESCs** Cell growth kinetics for WT (clone H22), HE (clone H2) and KO (clones H11 and H15) mES cells determined by measurement of % confluence over time. Values are Mean ± SD. Inset plot indicates cell growth monitored over a total of 150 hours.

### 4.3.3 Gene expression in CNOT9 KO mESCs

Preliminary gene expression analysis was conducted for three different ES cell clones of each genotype. qRT-PCR analysis and western blotting was done to investigate gene expression at mRNA and protein level, respectively. At the outset, we investigated mRNA levels of previously identified targets that were found to be upregulated in CNOT9 KO embryos. ES cells cultured in-vitro have been known to express a subset of gastrulation related targets such as *Lefty1/2*, *Nodal* among others (Besser, 2004, Kim et al., 2014). As seen from Figure 4.4A, both *Lefty1* and *Lefty2* mRNA were significantly upregulated in CNOT9 KO mES cells. Upregulation of *lefty* transcripts was also reflected in protein levels as shown in Figure 4.4B and Figure 4.4C. No change in *Nodal* mRNA expression was observed across genotypes (Figure 4.4A). Furthermore, based on expression of cleaved PARP protein, KO ES cells did not show differences in extent of cell death compared to controls (Figure 4.4B and Figure 4.4C).

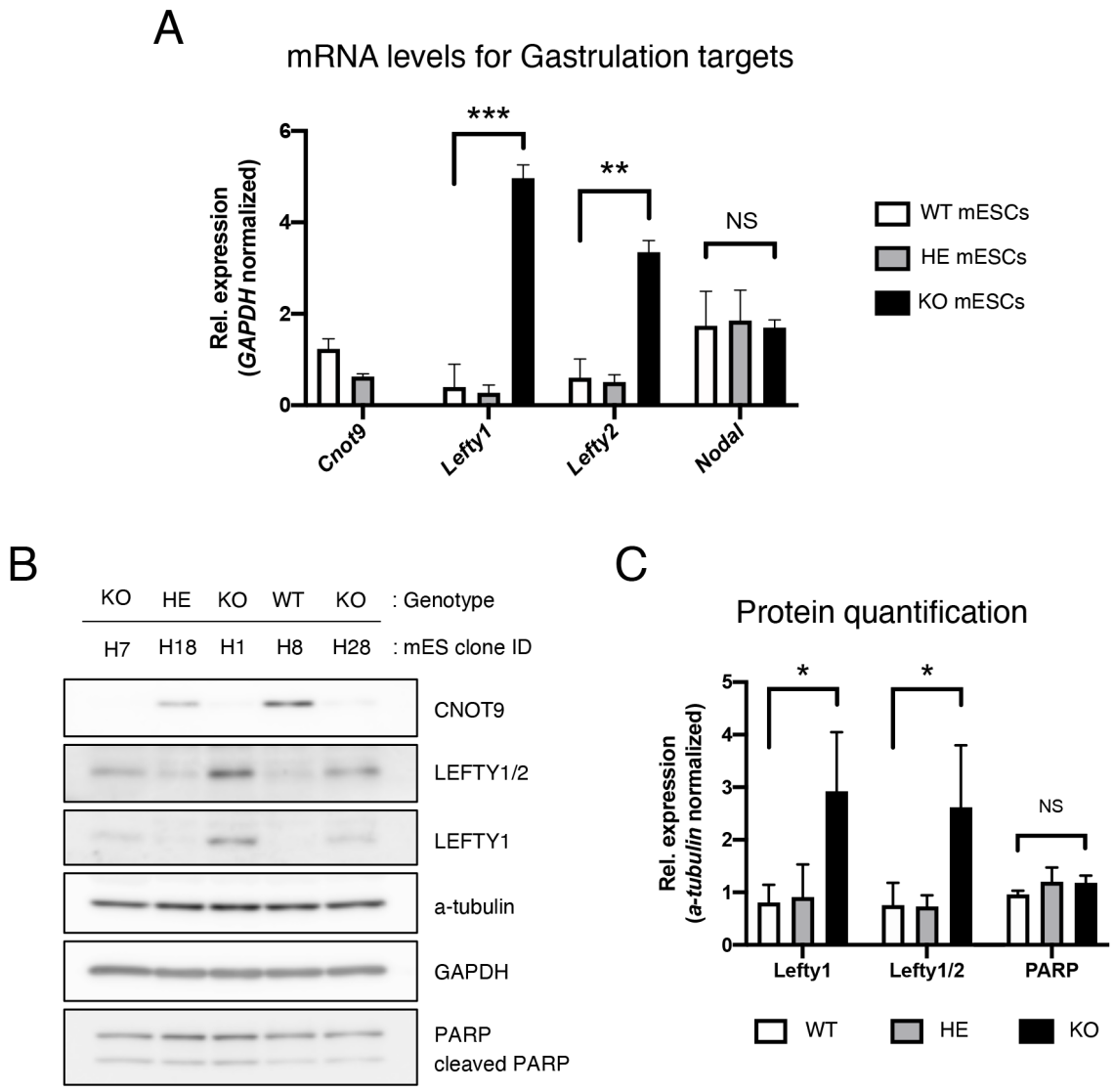


**Figure 4.4: Relative expression of gastrulation related markers in CNOT9 KO mESCs** (A) Relative expression levels for *Lefty1*, *Lefty2*, *Nodal*, and *Cnot9* mRNA in WT, HE and CNOT9 KO mESCs. (B) Protein expression levels for CNOT9, LEFTY1/2 and PARP in WT, HE and KO mESCs. a-tubulin and GAPDH were used as housekeeping controls. (C) Quantification of protein levels for LEFTY and PARP proteins across genotypes. Values are Mean ± SD [n=3, $p < 0.05$ (*), $p < 0.01$ (**), $p < 0.001$ (***), NS (not significant)]

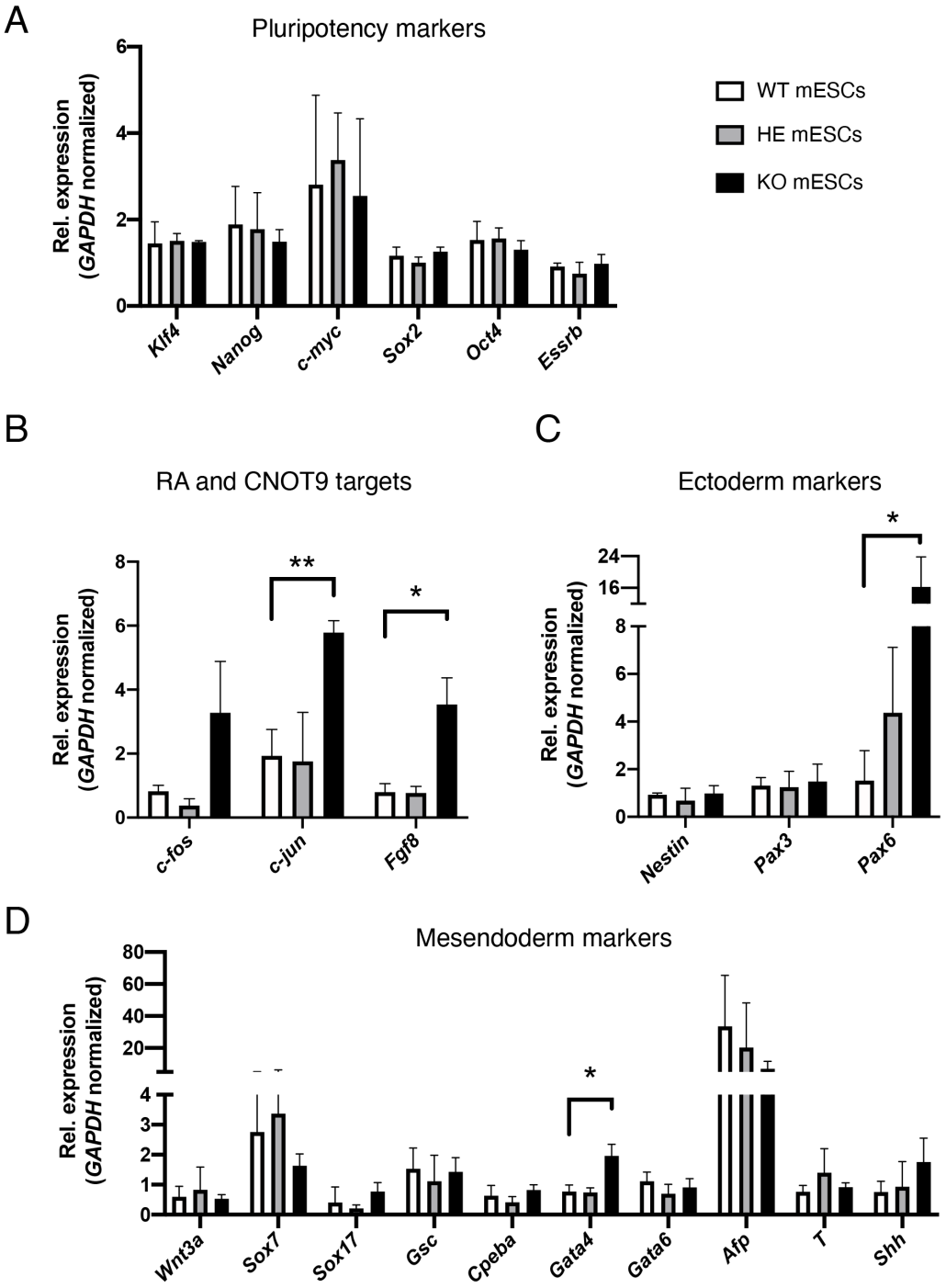


**Figure 4.5: Relative expression of other possible targets of CNOT9 in mESCs** qRT-PCR based relative expression levels for (A) pluripotency markers WT, HE and CNOT9 KO mESCs. (B) Previously characterized RA and CNOT9 targets (C) markers of ectoderm differentiation (D) markers of mesendoderm differentiation. Values are Mean ± SD [n=3, $p < 0.05$ (*), $p < 0.01$ (**)]

Self-renewal and stemness of CNOT9 KO ES cells were analyzed based on expression levels of *Klf4, Nanog, c-myc, Sox2, Oct4,* and *Essrb* mRNA. As seen from Figure 4.5A, no differences in transcript levels of stemness markers were observed in CNOT9 KO mESCs compared to WT and HE controls.

Based on the idea that CNOT9 acts a molecular intermediary in RA induced gene expression, we performed preliminary expression analysis on a few previously identified targets (Hiroi et al., 2002). As seen in Figure 4.5B expression levels of RA regulated targets such as *c-jun* and *Fgf8* were significantly altered in CNOT9 KO mESCs thereby suggesting CNOT9 contribution in mediating effects of RA in mES cells.

Furthermore, basal expression levels for various Ectoderm markers and Mesendoderm markers were also compared between WT and CNOT9 KO mESCs, at non-differentiating (stem) conditions. At the transcript level, no major change in expression of such markers were observed, with the exception of ectoderm marker *Pax6* and mesendoderm marker *Gata4* (Figure 4.5C and Figure 4.5D).

### 4.3.4 RA induced differentiation of mESCs

Addition of RA to cultured ES cells has been known to induce neuroectoderm differentiation, characterized by increase in receptors and enzymes required for RA intake and activity alongside concomitant loss of pluripotency (Stavridis et al., 2010, Zhang et al., 2015). In our attempt to investigate RA induced differentiation of CNOT9 KO mESCs, we first standardized a protocol for monitoring gene expression dynamics upon RA treatment using WT mESCs, details of which are indicated in Section 4.2.2 (Materials and Methods, Chapter 4). Based on data shown in Figure 4.6, our protocol could efficiently capture ES cell responsiveness to RA.

Loss of pluripotency was confirmed by reduced expression of *Klf4* and *Nanog* mRNA levels while neuroectodermal fate was reflected by increased expression of *Nestin* and reciprocally reduced expression of mesoderm markers – *Lefty1*, *Lefty2* and *Nodal*. *Rarb* and *Cyp26b1* expression served as positive controls for RA treatment. *Cnot9* expression was reduced during initial phase of RA treatment although levels recovered during later stages of differentiation.

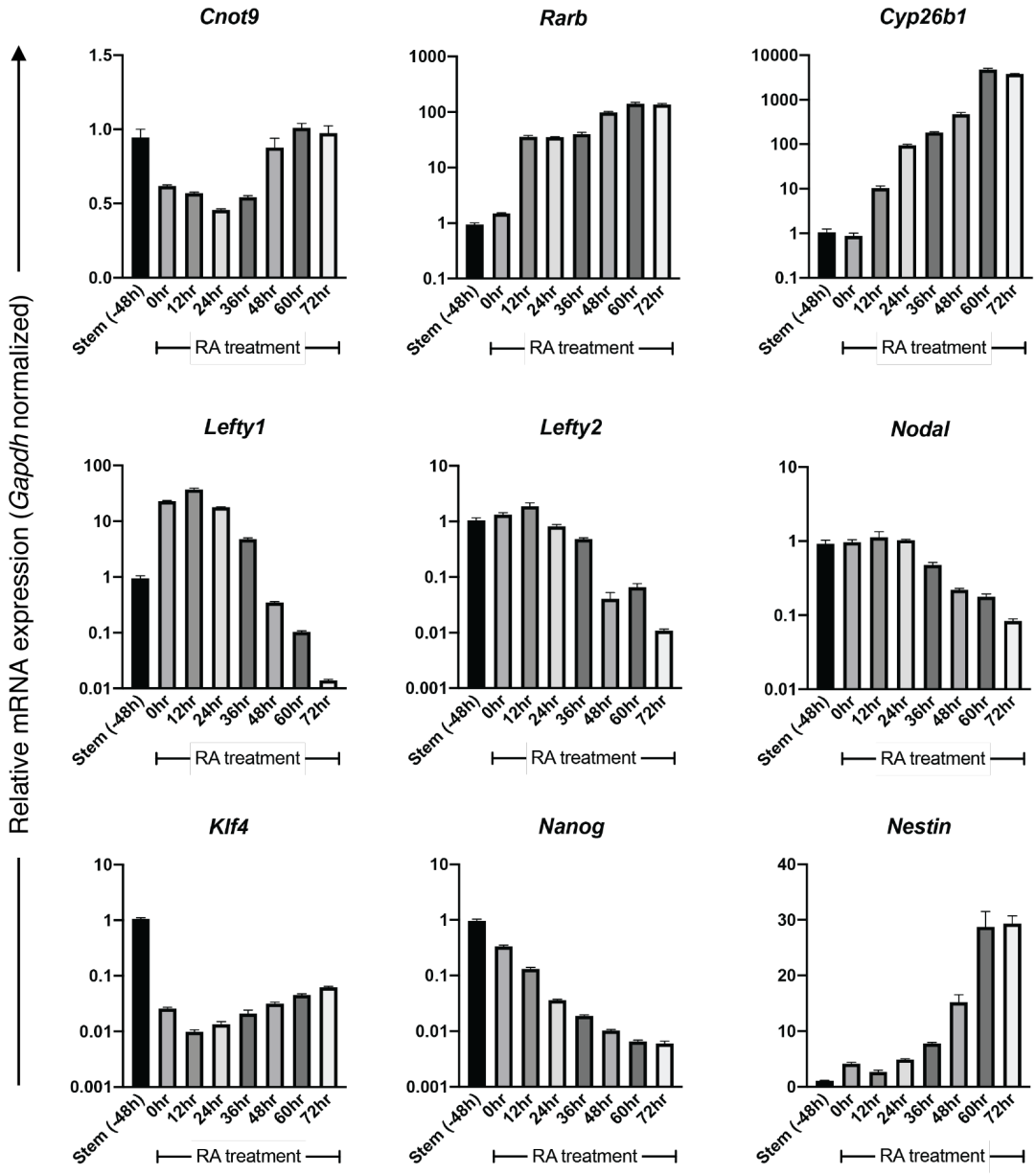


**Figure 4.6: Dynamics of gene expression in mESCs upon RA treatment** Relative expression levels of CNOT9 and other targets during time course of 1$\mu$M RA induced differentiation of WT mESCs. Values are Mean ± SD [n=3]

## 4.4 Discussion

Mouse ES cell based in-vitro model was successfully generated to investigate molecular function of CNOT9 keeping in consideration KO embryo phenotypes during gastrulation. ES cells were morphologically characterized by rounded colonies grown on feeder

fibroblasts and subsequently confirmed for high expression levels of stemness markers relative to fibroblasts and other cell-types. CNOT9 KO mES cells were viable and showed growth rates comparable to WT and HE controls. State of pluripotency (determined by stemness marker expression levels) of KO cells was also comparable to WT and HE clones. In other words, CNOT9 is dispensable at the level of ES cells although its requirement along various courses of differentiation remains to be seen.

Based on preliminary molecular characterization, CNOT9 KO ES cells showed elevated expression levels for *Lefty1* and *Lefty2* transcripts compared to WT and HE controls. This was in agreement with in-vivo results obtained from KO embryos. In addition, loss of CNOT9 resulted in upregulation of downstream effectors of retinoic acid such as *c-jun* and *Fgf8*. The motivation behind investigation of such targets came from a previous study that deemed CNOT9 as a RA-inducible gene (Hiroi et al., 2002). Interestingly, increase in *c-jun* expression in KO mESCs was contrary to expectation as previous report suggested CNOT9 as a positive modulator of *c-jun* transcription in F9 cells (Hiroi et al., 2002). On the other hand, *Fgf8* expression levels in absence of CNOT9, fits the narrative of being an reciprocally induced by retinoic acid (Kumar and Duester, 2014). In summary, such preliminary findings need further investigation to identify mechanisms of CNOT9 action on its targets.

After successfully isolating and propagating ES cells in-vitro, a protocol for inducing stem cell differentiation was standardized. Our method involved a refractory period of 48 hours to allow cells to transition from a state of self-renewal to lineage-specific differentiation. During this period, intracellular effects of LIF, GSK3b inhibitor and ERK inhibitor were quenched and cells were primed to undergo differentiation in presence of appropriate ligands.

In future, we plan to perform comprehensive gene expression analysis to identify CNOT9 targets under various condition of ES cell differentiation. It would be worth investigating phenotypic and molecular overlap between differentiating CNOT9 KO ES cells (in-vitro) vs. gastrulation stage KO embryos (in-vivo). In other words, CNOT9 KO and control ES cells shall be compared in terms of their ability to undergo lineage differentiation under in-vitro conditions. We expect to observe induction of cell death in CNOT9 KO ES cells when subjected to one or more forms of lineage commitment in agreement with KO embryo phenotype, in-vivo.

# Chapter 5

# Conclusions and Future Work

> "It's not birth, marriage, or death, but gastrulation which is truly the most important event in your life."
>
> Prof. Lewis Wolpert
> (founding father of modern developmental biology)

The above quote emphasizes the importance of gastrulation, a process that occurs during very early stages of embryonic development in humans. During this process, few hundreds of cells within an embryo attain distinct fates that eventually specialize to form the brain, heart, stomach, limbs, and all other aspects that make us a biological entity. In other words, this is what separates us from being a ball of cells to one of the most complex life forms on earth. At the molecular level, gastrulation is a well-controlled scheme of events where gene expression in one set of cells determines the fate of others, and vice-versa. However, our current understanding on specifics of such gene expression dynamics is very limited and largely scattered. A majority of existing studies till date have identified transcription regulation as a key determinant of that drives modulates gene expression during gastrulation. In our attempt, we focused on the aspect of post-transcriptional regulation of gene expression primarily contributed by the decay of messenger RNA, during the course of embryonic gastrulation. These mechanisms are regulated by the activity of a cellular complex known as the "CCR4-NOT complex". With remarkably high structural similarity and functional conservation of this complex, laboratory mice serve as an excellent model to understand similar phenomena that occur in humans. In our research we investigated the physiological role of CNOT9, a subunit of the CCR4-NOT complex. Its significance was reflected from the observation that mice lacking CNOT9 expression undergo developmental arrest during gastrulation leading to embryonic lethality prior to mid-gestation.

We showed that phenotype of CNOT9 KO embryos was primarily contributed by defects in the epiblast lineage. This was also in agreement with b-galactosidase staining data that showed major expression in epiblast derived regions of the embryo between embryonic days 7.5 to 8.5. At the molecular level, CNOT9 KO embryos showed significantly high expression of *Lefty1, Lefty2,* and *c-myb* mRNA, among others. Using an in-vitro model we showed that this increase is contributed by impairment in mRNA

decay. In future, it would be worth the while to generate an in-vivo model, to support the current hypothesis. Generation of mice expressing mutant CNOT9 ($Cnot9^{mut4}$), that cannot interact with CNOT1, would be an ideal step in this direction. Depending on phenotype exhibited by these mice, the role of CNOT9 as part of the mRNA decay complex would be precisely established.

In an attempt to rescue knockout embryo phenotype, we had also generated a lentivirus-based complementation system that induced CNOT9 expression specifically within trophoblast derived placental tissue. To our surprise, we found that CNOT9 overexpression within the placental lineage highly correlated with developmental retardation/defects in the adjoining epiblast-derived embryo proper. It is likely that CNOT9 overexpression at low expressing/ectopic sites leads to dominant-negative effects that gets manifested at the physiological level. Use of a relatively mild or controlled over-expression system is likely to can potentially serve as an effective tool to examine rescue effects. Currently, lack of a pan-placenta specific promoter driven Cre recombinase model, limits our understanding of placental genetics and its contribution to embryo development. This issue can be addressed by in-silico promoter/enhancer capture using CAGE (Cap Analysis of Gene Expression) technology on bulk or single-cell cDNA libraries generated from cells or placental lineage. Identified promoters and enhancers may thereafter be used to generate Cre knock-in mice that can support placenta specific depletion of a target genomic region of interest.

Alternatively, the Sox2-Cre system can also be utilized to generate placenta specific depletion of a given gene of interest. This involves generation of a transgenic mouse line that contains a stop codon flanked by loxP elements inserted within a given exon. Cre expressing embryos will recombine loxP sites and therefore remove the stop codon and help generate a functional form of the gene throughout the epiblast. Due to absence of Sox2 dependent Cre activity within the placental lineage, these tissues will not express the exon of interest and a placenta-specific loss-of-function effects can be investigated.

To have a comprehensive understanding of CNOT9 function along various forms of embryonic lineage commitment and differentiation, we generated knockout ES cells as an in-vitro model. As a preliminary observation, loss of CNOT9 did not show any distinct phenotype in terms of cell growth and viability under growth conditions that support stemness and self-renewal. We expect to observe an indispensable requirement of CNOT9 in one or more forms of ES cell differentiation, that can explain in-vivo phenotype of KO embryos that undergo developmental defects followed by cell death during gastrulation.

We also evaluated existing models and theories relating to the molecular function of CNOT9, in ways that have not been tested before. In our experimental conditions we observed that, in absence of CNOT9, flag-tagged silencing domain of GW812 could not associate with CCR4-NOT subunit CNOT1. This observation was made in a transformed cell line (HeLa) that has been in culture for many years and is therefore less likely to be a representative physiological model. Hence, additional experiments using in-vitro systems such as KO ES cells, shall help in developing a more concrete under-

standing on this aspect of CNOT9 function.

In summary, our study presents novel insights on the role of CCR4-NOT complex in regulating gene expression control during gastrulation via subunit CNOT9.

# References

AJIRO, M., KATAGIRI, T., UEDA, K., NAKAGAWA, H., FUKUKAWA, C., LIN, M. L., PARK, J. H., NISHIDATE, T., DAIGO, Y. & NAKAMURA, Y. 2009. Involvement of RQCD1 overexpression, a novel cancer-testis antigen, in the Akt pathway in breast cancer cells. Int J Oncol, 35, 673-81.

AJIRO, M., NISHIDATE, T., KATAGIRI, T. & NAKAMURA, Y. 2010. Critical involvement of RQCD1 in the EGFR-Akt pathway in mammary carcinogenesis. Int J Oncol, 37, 1085-93.

BASQUIN, J., ROUDKO, V. V., RODE, M., BASQUIN, C., SERAPHIN, B. & CONTI, E. 2012. Architecture of the nuclease module of the yeast Ccr4-not complex: the Not1-Caf1-Ccr4 interaction. Mol Cell, 48, 207-18.

BAWANKAR, P., LOH, B., WOHLBOLD, L., SCHMIDT, S. & IZAURRALDE, E. 2013. NOT10 and C2orf29/NOT11 form a conserved module of the CCR4-NOT complex that docks onto the NOT1 N-terminal domain. RNA Biol, 10, 228-44.

BEHM-ANSMANT, I., REHWINKEL, J., DOERKS, T., STARK, A., BORK, P. & IZAURRALDE, E. 2006. mRNA degradation by miRNAs and GW182 requires both CCR4:NOT deadenylase and DCP1:DCP2 decapping complexes. Genes Dev, 20, 1885-98.

BEHRINGER, R. 2014. Manipulating the mouse embryo : a laboratory manual, Cold Spring Harbor, New York, Cold Spring Harbor Laboratory Press.

BESSER, D. 2004. Expression of nodal, lefty-a, and lefty-B in undifferentiated human embryonic stem cells requires activation of Smad2/3. J Biol Chem, 279, 45076-84.

BHASKAR, V., ROUDKO, V., BASQUIN, J., SHARMA, K., URLAUB, H., SERAPHIN, B. & CONTI, E. 2013. Structure and RNA-binding properties of the Not1-Not2-Not5 module of the yeast Ccr4-Not complex. Nat Struct Mol Biol, 20, 1281-8.

BLASCO-MORENO, B., DE CAMPOS-MATA, L., BOTTCHER, R., GARCIA-MARTINEZ, J., JUNGFLEISCH, J., NEDIALKOVA, D. D., CHATTOPADHYAY, S., GAS, M. E., OLIVA, B., PEREZ-ORTIN, J. E., LEIDEL, S. A., CHODER, M. & DIEZ, J. 2019. The exonuclease Xrn1 activates transcription and translation of mRNAs encoding mem-

brane proteins. Nat Commun, 10, 1298.

BOLAND, A., CHEN, Y., RAISCH, T., JONAS, S., KUZUOGLU-OZTURK, D., WOHLBOLD, L., WEICHENRIEDER, O. & IZAURRALDE, E. 2013. Structure and assembly of the NOT module of the human CCR4-NOT complex. Nat Struct Mol Biol, 20, 1289-97.

BRAUN, K. A. & YOUNG, E. T. 2014. Coupling mRNA synthesis and decay. Mol Cell Biol, 34, 4078-87.

BULBROOK, D., BRAZIER, H., MAHAJAN, P., KLISZCZAK, M., FEDOROV, O., MARCHESE, F. P., AUBAREDA, A., CHALK, R., PICAUD, S., STRAIN-DAMERELL, C., FILIPPAKOPOULOS, P., GILEADI, O., CLARK, A. R., YUE, W. W., BURGESS-BROWN, N. A. & DEAN, J. L. E. 2018. Tryptophan-Mediated Interactions between Tristetraprolin and the CNOT9 Subunit Are Required for CCR4-NOT Deadenylase Complex Recruitment. J Mol Biol, 430, 722-736.

CHAPAT, C. & CORBO, L. 2014. Novel roles of the CCR4-NOT complex. Wiley Interdiscip Rev RNA, 5, 883-901.

CHEN, C., ITO, K., TAKAHASHI, A., WANG, G., SUZUKI, T., NAKAZAWA, T., YAMAMOTO, T. & YOKOYAMA, K. 2011. Distinct expression patterns of the subunits of the CCR4-NOT deadenylase complex during neural development. Biochem Biophys Res Commun, 411, 360-4.

CHEN, C. Y., ZHENG, D., XIA, Z. & SHYU, A. B. 2009. Ago-TNRC6 triggers microRNA-mediated decay by promoting two deadenylation steps. Nat Struct Mol Biol, 16, 1160-6.

CHEN, J., RAPPSILBER, J., CHIANG, Y. C., RUSSELL, P., MANN, M. & DENIS, C. L. 2001. Purification and characterization of the 1.0 MDa CCR4-NOT complex identifies two novel components of the complex. J Mol Biol, 314, 683-94.

CHEN, Y., BOLAND, A., KUZUOGLU-OZTURK, D., BAWANKAR, P., LOH, B., CHANG, C. T., WEICHENRIEDER, O. & IZAURRALDE, E. 2014. A DDX6-CNOT1 complex and W-binding pockets in CNOT9 reveal direct links between miRNA target recognition and silencing. Mol Cell, 54, 737-50.

CHENG, S., PEI, Y., HE, L., PENG, G., REINIUS, B., TAM, P. P. L., JING, N. & DENG, Q. 2019. Single-Cell RNA-Seq Reveals Cellular Heterogeneity of Pluripotency Transition and X Chromosome Dynamics during Early Mouse Development. Cell Rep, 26, 2593-2607 e3.

CHU, J., DING, J., JEAYS-WARD, K., PRICE, S. M., PLACZEK, M. & SHEN, M. M. 2005. Non-cell-autonomous role for Cripto in axial midline formation during vertebrate embryogenesis. Development, 132, 5539-51.

COLLART, M. A. 2016. The Ccr4-Not complex is a key regulator of eukaryotic gene expression. Wiley Interdiscip Rev RNA, 7, 438-54.

COLLART, M. A. & STRUHL, K. 1993. CDC39, an essential nuclear protein that negatively regulates transcription and differentially affects the constitutive and inducible HIS3 promoters. EMBO J, 12, 177-86.

COLLART, M. A. & STRUHL, K. 1994. NOT1(CDC39), NOT2(CDC36), NOT3, and NOT4 encode a global-negative regulator of transcription that differentially affects TATA-element utilization. Genes Dev, 8, 525-37.

CONLON, F. L., LYONS, K. M., TAKAESU, N., BARTH, K. S., KISPERT, A., HERRMANN, B. & ROBERTSON, E. J. 1994. A primary requirement for nodal in the formation and maintenance of the primitive streak in the mouse. Development, 120, 1919-28.

COOKE, A., PRIGGE, A. & WICKENS, M. 2010. Translational repression by deadenylases. J Biol Chem, 285, 28506-13.

DOMINICK, G., BOWMAN, J., LI, X., MILLER, R. A. & GARCIA, G. G. 2017. mTOR regulates the expression of DNA damage response enzymes in long-lived Snell dwarf, GHRKO, and PAPPA-KO mice. Aging Cell, 16, 52-60.

DRAPER, M. P., LIU, H. Y., NELSBACH, A. H., MOSLEY, S. P. & DENIS, C. L. 1994. CCR4 is a glucose-regulated transcription factor whose leucine-rich repeat binds several proteins important for placing CCR4 in its proper promoter context. Mol Cell Biol, 14, 4522-31.

DRIEVER, W., SIEGEL, V. & NUSSLEIN-VOLHARD, C. 1990. Autonomous determination of anterior structures in the early Drosophila embryo by the bicoid morphogen. Development, 109, 811-20.

DUBRULLE, J. & POURQUIE, O. 2004. fgf8 mRNA decay establishes a gradient that couples axial elongation to patterning in the vertebrate embryo. Nature, 427, 419-22.

DUPRESSOIR, A., MOREL, A. P., BARBOT, W., LOIREAU, M. P., CORBO, L. & HEIDMANN, T. 2001. Identification of four families of yCCR4- and Mg2+-dependent endonuclease-related proteins in higher eukaryotes, and characterization of orthologs of yCCR4 with a conserved leucine-rich repeat essential for hCAF1/hPOP2 binding. BMC Genomics, 2, 9.

EVANS, M. J. & KAUFMAN, M. H. 1981. Establishment in culture of pluripotential cells from mouse embryos. Nature, 292, 154-6.

EZZEDDINE, N., CHANG, T. C., ZHU, W., YAMASHITA, A., CHEN, C. Y., ZHONG, Z., YAMASHITA, Y., ZHENG, D. & SHYU, A. B. 2007. Human TOB, an antiproliferative transcription factor, is a poly(A)-binding protein-dependent positive regulator of cytoplasmic mRNA deadenylation. Mol Cell Biol, 27, 7791-801.

FABIAN, M. R., CIEPLAK, M. K., FRANK, F., MORITA, M., GREEN, J., SRIKUMAR, T., NAGAR, B., YAMAMOTO, T., RAUGHT, B., DUCHAINE, T. F. & SONENBERG, N. 2011. miRNA-mediated deadenylation is orchestrated by GW182 through two conserved motifs that interact with CCR4-NOT. Nat Struct Mol Biol, 18, 1211-7.

FABIAN, M. R., FRANK, F., ROUYA, C., SIDDIQUI, N., LAI, W. S., KARETNIKOV, A., BLACKSHEAR, P. J., NAGAR, B. & SONENBERG, N. 2013. Structural basis for the recruitment of the human CCR4-NOT deadenylase complex by tristetraprolin. Nat Struct Mol Biol, 20, 735-9.

FERRANDON, D., KOCH, I., WESTHOF, E. & NUSSLEIN-VOLHARD, C. 1997. RNA-RNA interaction is required for the formation of specific bicoid mRNA 3' UTR-STAUFEN ribonucleoprotein particles. EMBO J, 16, 1751-8.

FUJINO, Y., YAMADA, K., SUGAYA, C., OOKA, Y., OVARA, H., BAN, H., AKAMA, K., OTOSAKA, S., KINOSHITA, H., YAMASU, K., MISHIMA, Y. & KAWAMURA, A. 2018. Deadenylation by the CCR4-NOT complex contributes to the turnover of hairy-related mRNAs in the zebrafish segmentation clock. FEBS Lett, 592, 3388-3398.

FUNAKOSHI, Y., DOI, Y., HOSODA, N., UCHIDA, N., OSAWA, M., SHIMADA, I., TSUJIMOTO, M., SUZUKI, T., KATADA, T. & HOSHINO, S. 2007. Mechanism of mRNA deadenylation: evidence for a molecular interplay between translation termination factor eRF3 and mRNA deadenylases. Genes Dev, 21, 3135-48.

GARAPATY, S., MAHAJAN, M. A. & SAMUELS, H. H. 2008. Components of the CCR4-NOT complex function as nuclear hormone receptor coactivators via association with the NRC-interacting Factor NIF-1. J Biol Chem, 283, 6806-16.

GARCES, R. G., GILLON, W. & PAI, E. F. 2007. Atomic model of human Rcd-1 reveals an armadillo-like-repeat protein with in vitro nucleic acid binding properties. Protein Sci, 16, 176-88.

GIRALDEZ, A. J., MISHIMA, Y., RIHEL, J., GROCOCK, R. J., VAN DONGEN, S., INOUE, K., ENRIGHT, A. J. & SCHIER, A. F. 2006. Zebrafish MiR-430 promotes deadenylation and clearance of maternal mRNAs. Science, 312, 75-9.

GREBER, B., WU, G., BERNEMANN, C., JOO, J. Y., HAN, D. W., KO, K., TAPIA, N., SABOUR, D., STERNECKERT, J., TESAR, P. & SCHOLER, H. R. 2010. Conserved and divergent roles of FGF signaling in mouse epiblast stem cells and human embryonic stem cells. Cell Stem Cell, 6, 215-26.

HAAS, M., SIEGERT, M., SCHURMANN, A., SODEIK, B. & WOLFES, H. 2004. c-Myb protein interacts with Rcd-1, a component of the CCR4 transcription mediator complex. Biochemistry, 43, 8152-9.

HARIGAYA, Y., TANAKA, H., YAMANAKA, S., TANAKA, K., WATANABE, Y., TSUTSUMI, C., CHIKASHIGE, Y., HIRAOKA, Y., YAMASHITA, A. & YAMAMOTO, M. 2006. Selective elimination of messenger RNA prevents an incidence of untimely meiosis. Nature, 442, 45-50.

HIROI, N., ITO, T., YAMAMOTO, H., OCHIYA, T., JINNO, S. & OKAYAMA, H. 2002. Mammalian Rcd1 is a novel transcriptional cofactor that mediates retinoic acid-induced cell differentiation. EMBO J, 21, 5235-44.

HU, G., KIM, J., XU, Q., LENG, Y., ORKIN, S. H. & ELLEDGE, S. J. 2009. A genome-wide RNAi screen identifies a new transcriptional module required for self-renewal. Genes Dev, 23, 837-48.

HUNTZINGER, E., KUZUOGLU-OZTURK, D., BRAUN, J. E., EULALIO, A., WOHLBOLD, L. & IZAURRALDE, E. 2013. The interactions of GW182 proteins with PABP and deadenylases are required for both translational repression and degradation of miRNA targets. Nucleic Acids Res, 41, 978-94.

INOUE, T., MORITA, M., HIJIKATA, A., FUKUDA-YUZAWA, Y., ADACHI, S., ISONO, K., IKAWA, T., KAWAMOTO, H., KOSEKI, H., NATSUME, T., FUKAO, T., OHARA, O., YAMAMOTO, T. & KUROSAKI, T. 2015. CNOT3 contributes to early B cell development by controlling Igh rearrangement and p53 mRNA stability. J Exp Med, 212, 1465-79.

IRION, S., CLARKE, R. L., LUCHE, H., KIM, I., MORRISON, S. J., FEHLING, H. J. & KELLER, G. M. 2010. Temporal specification of blood progenitors from mouse embryonic stem cells and induced pluripotent stem cells. Development, 137, 2829-39.

ITO, K., INOUE, T., YOKOYAMA, K., MORITA, M., SUZUKI, T. & YAMAMOTO, T. 2011a. CNOT2 depletion disrupts and inhibits the CCR4-NOT deadenylase complex and induces apoptotic cell death. Genes Cells, 16, 368-79.

ITO, K., TAKAHASHI, A., MORITA, M., SUZUKI, T. & YAMAMOTO, T. 2011b. The role of the CNOT1 subunit of the CCR4-NOT complex in mRNA deadenylation and cell viability. Protein Cell, 2, 755-63.

JOLY, W., CHARTIER, A., ROJAS-RIOS, P., BUSSEAU, I. & SIMONELIG, M. 2013. The CCR4 deadenylase acts with Nanos and Pumilio in the fine-tuning of Mei-P26 expression to promote germline stem cell self-renewal. Stem Cell Reports, 1, 411-24.

KELLY, M., BURKE, J., SMITH, M., KLAR, A. & BEACH, D. 1988. Four mating-

type genes control sexual differentiation in the fission yeast. EMBO J, 7, 1537-47.

KESKENY, C., RAISCH, T., SGROMO, A., IGREJA, C., BHANDARI, D., WEICHENRIEDER, O. & IZAURRALDE, E. 2019. A conserved CAF40-binding motif in metazoan NOT4 mediates association with the CCR4-NOT complex. Genes Dev, 33, 236-252.

KIM, D. K., CHA, Y., AHN, H. J., KIM, G. & PARK, K. S. 2014. Lefty1 and lefty2 control the balance between self-renewal and pluripotent differentiation of mouse embryonic stem cells. Stem Cells Dev, 23, 457-66.

KOCH, P., LOHR, H. B. & DRIEVER, W. 2014. A mutation in cnot8, component of the Ccr4-not complex regulating transcript stability, affects expression levels of developmental regulators and reveals a role of Fgf3 in development of caudal hypothalamic dopaminergic neurons. PLoS One, 9, e113829.

KOUSKOFF, V., LACAUD, G., SCHWANTZ, S., FEHLING, H. J. & KELLER, G. 2005. Sequential development of hematopoietic and cardiac mesoderm during embryonic stem cell differentiation. Proc Natl Acad Sci U S A, 102, 13170-5.

KUMAR, S. & DUESTER, G. 2014. Retinoic acid controls body axis extension by directly repressing Fgf8 transcription. Development, 141, 2972-7.

LAU, N. C., KOLKMAN, A., VAN SCHAIK, F. M., MULDER, K. W., PIJNAPPEL, W. W., HECK, A. J. & TIMMERS, H. T. 2009. Human Ccr4-Not complexes contain variable deadenylase subunits. Biochem J, 422, 443-53.

LIN, X., ZHAO, W., JIA, J., LIN, T., XIAO, G., WANG, S., LIN, X., LIU, Y., CHEN, L., QIN, Y., LI, J., ZHANG, T., HAO, W., CHEN, B., XIE, R., CHENG, Y., XU, K., YAO, K., HUANG, W., XIAO, D. & SUN, Y. 2016. Ectopic expression of Cripto-1 in transgenic mouse embryos causes hemorrhages, fatal cardiac defects and embryonic lethality. Sci Rep, 6, 34501.

LIVAK, K. J. & SCHMITTGEN, T. D. 2001. Analysis of relative gene expression data using real-time quantitative PCR and the 2(-Delta Delta C(T)) Method. Methods, 25, 402-8.

LOH, B., JONAS, S. & IZAURRALDE, E. 2013. The SMG5-SMG7 heterodimer directly recruits the CCR4-NOT deadenylase complex to mRNAs containing nonsense codons via interaction with POP2. Genes Dev, 27, 2125-38.

LOWE, L. A., YAMADA, S. & KUEHN, M. R. 2001. Genetic dissection of nodal function in patterning the mouse embryo. Development, 128, 1831-43.

MA, H., LIN, Y., ZHAO, Z. A., LU, X., YU, Y., ZHANG, X., WANG, Q. & LI, L. 2016. MicroRNA-127 Promotes Mesendoderm Differentiation of Mouse Embryonic

Stem Cells by Targeting Left-Right Determination Factor 2. J Biol Chem, 291, 12126-35.

MACDONALD, P. M. & KERR, K. 1998. Mutational analysis of an RNA recognition element that mediates localization of bicoid mRNA. Mol Cell Biol, 18, 3788-95.

MAITY, A., MCKENNA, W. G. & MUSCHEL, R. J. 1995. Evidence for post-transcriptional regulation of cyclin B1 mRNA in the cell cycle and following irradiation in HeLa cells. EMBO J, 14, 603-9.

MANDELBAUM, J., SHESTOPALOV, I. A., HENDERSON, R. E., CHAU, N. G., KNOECHEL, B., WICK, M. J. & ZON, L. I. 2018. Zebrafish blastomere screen identifies retinoic acid suppression of MYB in adenoid cystic carcinoma. J Exp Med, 215, 2673-2685.

MARTIN, G. R. 1981. Isolation of a pluripotent cell line from early mouse embryos cultured in medium conditioned by teratocarcinoma stem cells. Proc Natl Acad Sci U S A, 78, 7634-8.

MATHYS, H., BASQUIN, J., OZGUR, S., CZARNOCKI-CIECIURA, M., BONNEAU, F., AARTSE, A., DZIEMBOWSKI, A., NOWOTNY, M., CONTI, E. & FILIPOWICZ, W. 2014. Structural and biochemical insights to the role of the CCR4-NOT complex and DDX6 ATPase in microRNA repression. Mol Cell, 54, 751-65.

MAUXION, F., PREVE, B. & SERAPHIN, B. 2013. C2ORF29/CNOT11 and CNOT10 form a new module of the CCR4-NOT complex. RNA Biol, 10, 267-76.

MEIJER, H. A., KONG, Y. W., LU, W. T., WILCZYNSKA, A., SPRIGGS, R. V., ROBINSON, S. W., GODFREY, J. D., WILLIS, A. E. & BUSHELL, M. 2013. Translational repression and eIF4A2 activity are critical for microRNA-mediated gene regulation. Science, 340, 82-5.

MENO, C., GRITSMAN, K., OHISHI, S., OHFUJI, Y., HECKSCHER, E., MOCHIDA, K., SHIMONO, A., KONDOH, H., TALBOT, W. S., ROBERTSON, E. J., SCHIER, A. F. & HAMADA, H. 1999. Mouse Lefty2 and zebrafish antivin are feedback inhibitors of nodal signaling during vertebrate gastrulation. Mol Cell, 4, 287-98.

MENO, C., SAIJOH, Y., FUJII, H., IKEDA, M., YOKOYAMA, T., YOKOYAMA, M., TOYODA, Y. & HAMADA, H. 1996. Left-right asymmetric expression of the TGF beta-family member lefty in mouse embryos. Nature, 381, 151-5.

MENO, C., SHIMONO, A., SAIJOH, Y., YASHIRO, K., MOCHIDA, K., OHISHI, S., NOJI, S., KONDOH, H. & HAMADA, H. 1998. lefty-1 is required for left-right determination as a regulator of lefty-2 and nodal. Cell, 94, 287-97.

MILLER, J. E. & REESE, J. C. 2012. Ccr4-Not complex: the control freak of eu-

karyotic cells. Crit Rev Biochem Mol Biol, 47, 315-33.

MIYASAKA, T., MORITA, M., ITO, K., SUZUKI, T., FUKUDA, H., TAKEDA, S., INOUE, J., SEMBA, K. & YAMAMOTO, T. 2008. Interaction of antiproliferative protein Tob with the CCR4-NOT deadenylase complex. Cancer Sci, 99, 755-61.

MOLIN, L. & PUISIEUX, A. 2005. C. elegans homologue of the Caf1 gene, which encodes a subunit of the CCR4-NOT complex, is essential for embryonic and larval development and for meiotic progression. Gene, 358, 73-81.

MORITA, M., OIKE, Y., NAGASHIMA, T., KADOMATSU, T., TABATA, M., SUZUKI, T., NAKAMURA, T., YOSHIDA, N., OKADA, M. & YAMAMOTO, T. 2011. Obesity resistance and increased hepatic expression of catabolism-related mRNAs in Cnot3+/- mice. EMBO J, 30, 4678-91.

MORITA, M., SIDDIQUI, N., KATSUMURA, S., ROUYA, C., LARSSON, O., NAGASHIMA, T., HEKMATNEJAD, B., TAKAHASHI, A., KIYONARI, H., ZANG, M., ST-ARNAUD, R., OIKE, Y., GIGUERE, V., TOPISIROVIC, I., OKADA-HATAKEYAMA, M., YAMAMOTO, T. & SONENBERG, N. 2019. Hepatic posttranscriptional network comprised of CCR4-NOT deadenylase and FGF21 maintains systemic metabolic homeostasis. Proc Natl Acad Sci U S A, 116, 7973-7981.

MURRY, C. E. & KELLER, G. 2008. Differentiation of embryonic stem cells to clinically relevant populations: lessons from embryonic development. Cell, 132, 661-80.

NAKAMURA, T., YAO, R., OGAWA, T., SUZUKI, T., ITO, C., TSUNEKAWA, N., INOUE, K., AJIMA, R., MIYASAKA, T., YOSHIDA, Y., OGURA, A., TOSHIMORI, K., NOCE, T., YAMAMOTO, T. & NODA, T. 2004. Oligo-astheno-teratozoospermia in mice lacking Cnot7, a regulator of retinoid X receptor beta. Nat Genet, 36, 528-33.

NEELY, G. G., KUBA, K., CAMMARATO, A., ISOBE, K., AMANN, S., ZHANG, L., MURATA, M., ELMEN, L., GUPTA, V., ARORA, S., SARANGI, R., DAN, D., FUJISAWA, S., USAMI, T., XIA, C. P., KEENE, A. C., ALAYARI, N. N., YAMAKAWA, H., ELLING, U., BERGER, C., NOVATCHKOVA, M., KOGLGRUBER, R., FUKUDA, K., NISHINA, H., ISOBE, M., POSPISILIK, J. A., IMAI, Y., PFEUFER, A., HICKS, A. A., PRAMSTALLER, P. P., SUBRAMANIAM, S., KIMURA, A., OCORR, K., BODMER, R. & PENNINGER, J. M. 2010. A global in vivo Drosophila RNAi screen identifies NOT3 as a conserved regulator of heart function. Cell, 141, 142-53.

NICHOLS, J., SILVA, J., ROODE, M. & SMITH, A. 2009. Suppression of Erk signalling promotes ground state pluripotency in the mouse embryo. Development, 136, 3215-22.

NISHIKAWA, S., JAKT, L. M. & ERA, T. 2007. Embryonic stem-cell culture as a tool for developmental cell biology. Nat Rev Mol Cell Biol, 8, 502-7.

NIWA, H. 2007. How is pluripotency determined and maintained? Development, 134, 635-46.

NIWA, H. 2010. Mouse ES cell culture system as a model of development. Dev Growth Differ, 52, 275-83.

OKADA, Y., UESHIN, Y., ISOTANI, A., SAITO-FUJITA, T., NAKASHIMA, H., KIMURA, K., MIZOGUCHI, A., OH-HORA, M., MORI, Y., OGATA, M., OSHIMA, R. G., OKABE, M. & IKAWA, M. 2007. Complementation of placental defects and embryonic lethality by trophoblast-specific lentiviral gene transfer. Nat Biotechnol, 25, 233-7.

OKAZAKI, N., OKAZAKI, K., WATANABE, Y., KATO-HAYASHI, M., YAMAMOTO, M. & OKAYAMA, H. 1998. Novel factor highly conserved among eukaryotes controls sexual development in fission yeast. Mol Cell Biol, 18, 887-95.

OKOCHI, K., SUZUKI, T., INOUE, J., MATSUDA, S. & YAMAMOTO, T. 2005. Interaction of anti-proliferative protein Tob with poly(A)-binding protein and inducible poly(A)-binding protein: implication of Tob in translational control. Genes Cells, 10, 151-63.

PAVANELLO, L., HALL, B., AIRHIHEN, B. & WINKLER, G. S. 2018. The central region of CNOT1 and CNOT9 stimulates deadenylation by the Ccr4-Not nuclease module. Biochem J, 475, 3437-3450.

PENG, G., SUO, S., CHEN, J., CHEN, W., LIU, C., YU, F., WANG, R., CHEN, S., SUN, N., CUI, G., SONG, L., TAM, P. P., HAN, J. D. & JING, N. 2016. Spatial Transcriptome for the Molecular Annotation of Lineage Fates and Cell Identity in Mid-gastrula Mouse Embryo. Dev Cell, 36, 681-97.

PEREZ-GARCIA, V., FINEBERG, E., WILSON, R., MURRAY, A., MAZZEO, C. I., TUDOR, C., SIENERTH, A., WHITE, J. K., TUCK, E., RYDER, E. J., GLEESON, D., SIRAGHER, E., WARDLE-JONES, H., STAUDT, N., WALI, N., COLLINS, J., GEYER, S., BUSCH-NENTWICH, E. M., GALLI, A., SMITH, J. C., ROBERTSON, E., ADAMS, D. J., WENINGER, W. J., MOHUN, T. & HEMBERGER, M. 2018. Placentation defects are highly prevalent in embryonic lethal mouse mutants. Nature, 555, 463-468.

PETIT, A. P., WOHLBOLD, L., BAWANKAR, P., HUNTZINGER, E., SCHMIDT, S., IZAURRALDE, E. & WEICHENRIEDER, O. 2012. The structural basis for the interaction between the CAF1 nuclease and the NOT1 scaffold of the human CCR4-NOT deadenylase complex. Nucleic Acids Res, 40, 11058-72.

PFENDLER, K. C., CATUAR, C. S., MENESES, J. J. & PEDERSEN, R. A. 2005. Overexpression of Nodal promotes differentiation of mouse embryonic stem cells into

mesoderm and endoderm at the expense of neuroectoderm formation. Stem Cells Dev, 14, 162-72.

PIJUAN-SALA, B., GRIFFITHS, J. A., GUIBENTIF, C., HISCOCK, T. W., JAWAID, W., CALERO-NIETO, F. J., MULAS, C., IBARRA-SORIA, X., TYSER, R. C. V., HO, D. L. L., REIK, W., SRINIVAS, S., SIMONS, B. D., NICHOLS, J., MARIONI, J. C. & GOTTGENS, B. 2019. A single-cell molecular map of mouse gastrulation and early organogenesis. Nature, 566, 490-495.

PINES, J. & HUNTER, T. 1989. Isolation of a human cyclin cDNA: evidence for cyclin mRNA and protein regulation in the cell cycle and for interaction with p34cdc2. Cell, 58, 833-46.

PRELLE, K., ZINK, N. & WOLF, E. 2002. Pluripotent stem cells–model of embryonic development, tool for gene targeting, and basis of cell therapy. Anat Histol Embryol, 31, 169-86.

PREVOT, D., MOREL, A. P., VOELTZEL, T., ROSTAN, M. C., RIMOKH, R., MAGAUD, J. P. & CORBO, L. 2001. Relationships of the antiproliferative proteins BTG1 and BTG2 with CAF1, the human homolog of a component of the yeast CCR4 transcriptional complex: involvement in estrogen receptor alpha signaling pathway. J Biol Chem, 276, 9640-8.

RAISCH, T., CHANG, C. T., LEVDANSKY, Y., MUTHUKUMAR, S., RAUNSER, S. & VALKOV, E. 2019. Reconstitution of recombinant human CCR4-NOT reveals molecular insights into regulated deadenylation. Nat Commun, 10, 3173.

RAMBOUT, X., DETIFFE, C., BRUYR, J., MARIAVELLE, E., CHERKAOUI, M., BROHEE, S., DEMOITIE, P., LEBRUN, M., SOIN, R., LESAGE, B., GUEDRI, K., BEULLENS, M., BOLLEN, M., FARAZI, T. A., KETTMANN, R., STRUMAN, I., HILL, D. E., VIDAL, M., KRUYS, V., SIMONIS, N., TWIZERE, J. C. & DEQUIEDT, F. 2016. The transcription factor ERG recruits CCR4-NOT to control mRNA decay and mitotic progression. Nat Struct Mol Biol, 23, 663-72.

RAN, F. A., HSU, P. D., WRIGHT, J., AGARWALA, V., SCOTT, D. A. & ZHANG, F. 2013. Genome engineering using the CRISPR-Cas9 system. Nat Protoc, 8, 2281-2308.

SABA-EL-LEIL, M. K., FREMIN, C. & MELOCHE, S. 2016. Redundancy in the World of MAP Kinases: All for One. Front Cell Dev Biol, 4, 67.

SAIJOH, Y., ADACHI, H., MOCHIDA, K., OHISHI, S., HIRAO, A. & HAMADA, H. 1999. Distinct transcriptional regulatory mechanisms underlie left-right asymmetric expression of lefty-1 and lefty-2. Genes Dev, 13, 259-69.

SANDLER, H., KRETH, J., TIMMERS, H. T. & STOECKLIN, G. 2011. Not1 me-

diates recruitment of the deadenylase Caf1 to mRNAs targeted for degradation by tristetraprolin. Nucleic Acids Res, 39, 4373-86.

SGROMO, A., RAISCH, T., BACKHAUS, C., KESKENY, C., ALVA, V., WEICHENRIEDER, O. & IZAURRALDE, E. 2018. Drosophila Bag-of-marbles directly interacts with the CAF40 subunit of the CCR4-NOT complex to elicit repression of mRNA targets. RNA, 24, 381-395.

SGROMO, A., RAISCH, T., BAWANKAR, P., BHANDARI, D., CHEN, Y., KUZUOGLU-OZTURK, D., WEICHENRIEDER, O. & IZAURRALDE, E. 2017. A CAF40-binding motif facilitates recruitment of the CCR4-NOT complex to mRNAs targeted by Drosophila Roquin. Nat Commun, 8, 14307.

SHIRAI, Y. T., SUZUKI, T., MORITA, M., TAKAHASHI, A. & YAMAMOTO, T. 2014. Multifunctional roles of the mammalian CCR4-NOT complex in physiological phenomena. Front Genet, 5, 286.

SMITH, A. G., HEATH, J. K., DONALDSON, D. D., WONG, G. G., MOREAU, J., STAHL, M. & ROGERS, D. 1988. Inhibition of pluripotential embryonic stem cell differentiation by purified polypeptides. Nature, 336, 688-90.

SOHN, E. J., JUNG, D. B., LEE, J., YOON, S. W., WON, G. H., KO, H. S. & KIM, S. H. 2015. CCR4-NOT2 Promotes the Differentiation and Lipogenesis of 3T3-L1 Adipocytes via Upregulation of PPARx03B3;, CEBPalpha and Inhibition of P-GSK3alpha/beta and beta-Catenin. Cell Physiol Biochem, 37, 1881-9.

STANFORD, W. L., COHN, J. B. & CORDES, S. P. 2001. Gene-trap mutagenesis: past, present and beyond. Nat Rev Genet, 2, 756-68.

STAVRIDIS, M. P., COLLINS, B. J. & STOREY, K. G. 2010. Retinoic acid orchestrates fibroblast growth factor signalling to drive embryonic stem cell differentiation. Development, 137, 881-90.

STUPFLER, B., BIRCK, C., SERAPHIN, B. & MAUXION, F. 2016. BTG2 bridges PABPC1 RNA-binding domains and CAF1 deadenylase to control cell proliferation. Nat Commun, 7, 10811.

SUGIMOTO, A., IINO, Y., MAEDA, T., WATANABE, Y. & YAMAMOTO, M. 1991. Schizosaccharomyces pombe ste11+ encodes a transcription factor with an HMG motif that is a critical regulator of sexual development. Genes Dev, 5, 1990-9.

SUZUKI, A., IGARASHI, K., AISAKI, K., KANNO, J. & SAGA, Y. 2010. NANOS2 interacts with the CCR4-NOT deadenylation complex and leads to suppression of specific RNAs. Proc Natl Acad Sci U S A, 107, 3594-9.

SUZUKI, A., SABA, R., MIYOSHI, K., MORITA, Y. & SAGA, Y. 2012. Interac-

tion between NANOS2 and the CCR4-NOT deadenylation complex is essential for male germ cell development in mouse. PLoS One, 7, e33558.

SUZUKI, T., KIKUGUCHI, C., SHARMA, S., SASAKI, T., TOKUMASU, M., ADACHI, S., NATSUME, T., KANEGAE, Y. & YAMAMOTO, T. 2015. CNOT3 suppression promotes necroptosis by stabilizing mRNAs for cell death-inducing proteins. Sci Rep, 5, 14779.

TAKAHASHI, A., ADACHI, S., MORITA, M., TOKUMASU, M., NATSUME, T., SUZUKI, T. & YAMAMOTO, T. 2015. Post-transcriptional Stabilization of Ucp1 mRNA Protects Mice from Diet-Induced Obesity. Cell Rep, 13, 2756-67.

TAKAHASHI, A., TAKAOKA, S., KOBORI, S., YAMAGUCHI, T., FERWATI, S., KUBA, K., YAMAMOTO, T. & SUZUKI, T. 2019. The CCR4-NOT Deadenylase Complex Maintains Adipocyte Identity. Int J Mol Sci, 20.

TEMME, C., ZAESSINGER, S., MEYER, S., SIMONELIG, M. & WAHLE, E. 2004. A complex containing the CCR4 and CAF1 proteins is involved in mRNA deadenylation in Drosophila. EMBO J, 23, 2862-71.

TODOKORO, K., WATSON, R. J., HIGO, H., AMANUMA, H., KURAMOCHI, S., YANAGISAWA, H. & IKAWA, Y. 1988. Down-regulation of c-myb gene expression is a prerequisite for erythropoietin-induced erythroid differentiation. Proc Natl Acad Sci U S A, 85, 8900-4.

TUCKER, M., VALENCIA-SANCHEZ, M. A., STAPLES, R. R., CHEN, J., DENIS, C. L. & PARKER, R. 2001. The transcription factor associated Ccr4 and Caf1 proteins are components of the major cytoplasmic mRNA deadenylase in Saccharomyces cerevisiae. Cell, 104, 377-86.

VALENCIA-SANCHEZ, M. A., LIU, J., HANNON, G. J. & PARKER, R. 2006. Control of translation and mRNA degradation by miRNAs and siRNAs. Genes Dev, 20, 515-24.

VAN DER WEYDEN, L., ADAMS, D. J. & BRADLEY, A. 2002. Tools for targeted manipulation of the mouse genome. Physiol Genomics, 11, 133-64.

VOISIN, L., SABA-EL-LEIL, M. K., JULIEN, C., FREMIN, C. & MELOCHE, S. 2010. Genetic demonstration of a redundant role of extracellular signal-regulated kinase 1 (ERK1) and ERK2 mitogen-activated protein kinases in promoting fibroblast proliferation. Mol Cell Biol, 30, 2918-32.

WAHLE, E. & WINKLER, G. S. 2013. RNA decay machines: deadenylation by the Ccr4-not and Pan2-Pan3 complexes. Biochim Biophys Acta, 1829, 561-70.

WASHIO-OIKAWA, K., NAKAMURA, T., USUI, M., YONEDA, M., EZURA, Y.,

ISHIKAWA, I., NAKASHIMA, K., NODA, T., YAMAMOTO, T. & NODA, M. 2007. Cnot7-null mice exhibit high bone mass phenotype and modulation of BMP actions. J Bone Miner Res, 22, 1217-23.

WILLIAMS, R. L., HILTON, D. J., PEASE, S., WILLSON, T. A., STEWART, C. L., GEARING, D. P., WAGNER, E. F., METCALF, D., NICOLA, N. A. & GOUGH, N. M. 1988. Myeloid leukaemia inhibitory factor maintains the developmental potential of embryonic stem cells. Nature, 336, 684-7.

XU, K., BAI, Y., ZHANG, A., ZHANG, Q. & BARTLAM, M. G. 2014. Insights into the structure and architecture of the CCR4-NOT complex. Front Genet, 5, 137.

YAGI, T., TOKUNAGA, T., FURUTA, Y., NADA, S., YOSHIDA, M., TSUKADA, T., SAGA, Y., TAKEDA, N., IKAWA, Y. & AIZAWA, S. 1993. A novel ES cell line, TT2, with high germline-differentiating potency. Anal Biochem, 214, 70-6.

YAMAGUCHI, T., SUZUKI, T., SATO, T., TAKAHASHI, A., WATANABE, H., KADOWAKI, A., NATSUI, M., INAGAKI, H., ARAKAWA, S., NAKAOKA, S., KOIZUMI, Y., SEKI, S., ADACHI, S., FUKAO, A., FUJIWARA, T., NATSUME, T., KIMURA, A., KOMATSU, M., SHIMIZU, S., ITO, H., SUZUKI, Y., PENNINGER, J. M., YAMAMOTO, T., IMAI, Y. & KUBA, K. 2018. The CCR4-NOT deadenylase complex controls Atg7-dependent cell death and heart function. Sci Signal, 11.

YAMAGUCHI, T. P., TAKADA, S., YOSHIKAWA, Y., WU, N. & MCMAHON, A. P. 1999. T (Brachyury) is a direct target of Wnt3a during paraxial mesoderm specification. Genes Dev, 13, 3185-90.

YAMAMOTO, H., TSUKAHARA, K., KANAOKA, Y., JINNO, S. & OKAYAMA, H. 1999. Isolation of a mammalian homologue of a fission yeast differentiation regulator. Mol Cell Biol, 19, 3829-41.

YAMASHITA, A., CHANG, T. C., YAMASHITA, Y., ZHU, W., ZHONG, Z., CHEN, C. Y. & SHYU, A. B. 2005. Concerted action of poly(A) nucleases and decapping enzyme in mammalian mRNA turnover. Nat Struct Mol Biol, 12, 1054-63.

YAN, Y. T., GRITSMAN, K., DING, J., BURDINE, R. D., CORRALES, J. D., PRICE, S. M., TALBOT, W. S., SCHIER, A. F. & SHEN, M. M. 1999. Conserved requirement for EGF-CFC genes in vertebrate left-right axis formation. Genes Dev, 13, 2527-37.

YANG, C. Y., RAMAMOORTHY, S., BOLLER, S., ROSENBAUM, M., RODRIGUEZ GIL, A., MITTLER, G., IMAI, Y., KUBA, K. & GROSSCHEDL, R. 2016. Interaction of CCR4-NOT with EBF1 regulates gene-specific transcription and mRNA stability in B lymphopoiesis. Genes Dev, 30, 2310-2324.

YING, Q. L., WRAY, J., NICHOLS, J., BATLLE-MORERA, L., DOBLE, B., WOOD-

GETT, J., COHEN, P. & SMITH, A. 2008. The ground state of embryonic stem cell self-renewal. Nature, 453, 519-23.

YOUN, J. Y., DUNHAM, W. H., HONG, S. J., KNIGHT, J. D. R., BASHKUROV, M., CHEN, G. I., BAGCI, H., RATHOD, B., MACLEOD, G., ENG, S. W. M., ANGERS, S., MORRIS, Q., FABIAN, M., COTE, J. F. & GINGRAS, A. C. 2018. High-Density Proximity Mapping Reveals the Subcellular Organization of mRNA-Associated Granules and Bodies. Mol Cell, 69, 517-532 e11.

ZHANG, J., GAO, Y., YU, M., WU, H., AI, Z., WU, Y., LIU, H., DU, J., GUO, Z. & ZHANG, Y. 2015. Retinoic Acid Induces Embryonic Stem Cell Differentiation by Altering Both Encoding RNA and microRNA Expression. PLoS One, 10, e0132566.

ZHENG, X., DUMITRU, R., LACKFORD, B. L., FREUDENBERG, J. M., SINGH, A. P., ARCHER, T. K., JOTHI, R. & HU, G. 2012. Cnot1, Cnot2, and Cnot3 maintain mouse and human ESC identity and inhibit extraembryonic differentiation. Stem Cells, 30, 910-22.

ZHOU, B., LIU, J., REN, Z., YAO, F., MA, J., SONG, J., BENNETT, B., ZHEN, Y., WANG, L., HU, G. & HU, S. 2017. Cnot3 enhances human embryonic cardiomyocyte proliferation by promoting cell cycle inhibitor mRNA degradation. Sci Rep, 7, 1500.